

**SOLUTION PROCESSING: FABRICATION AND CHARACTERIZATION OF
POLYMERIC NANOCOMPOSITE FILMS AND POLYSTYRENE NANOPARTICLES**

by
MUSTAFA M. DEMİR

Submitted to the Graduate School of Engineering and Natural Sciences
in partial fulfillment of
the requirements for the degree of
Doctor of Philosophy

Sabanci University
Spring 2004

© MUSTAFA M. DEMİR 2004
All Rights Reserved

to my love
&
to my whole family

SOLUTION PROCESSING: FABRICATION AND CHARACTERIZATION OF
POLYMERIC NANOCOMPOSITE FILMS AND POLYSTYRENE NANOPARTICLES

APPROVED BY:

Assoc. Prof. Dr. Yusuf Z.Menceloğlu
(Dissertation Supervisor)

Prof. Dr. Burak Erman
(Dissertation Co-advisor)

Assoc. Prof. Dr. Canan Baysal

Assoc. Prof. Dr. Mehmet Ali Gülgün

Prof. Dr. Turgut Nugay

DATE OF APPROVAL:3rd May 2004.....

ACKNOWLEDGEMENT

Throughout my graduate years, a number of people have helped and supported me in various ways. At first, I would like to give a sincere gratitude and appreciation to Prof. Burak Erman for suggesting the research topics and for indicating my abilities which I was not aware before. He had non-decreasing patience and support for improving myself in the long and rough pathways of science. I have to extend my appreciation to Assoc. Prof. Yusuf Menciloglu for his guidance and his priceless support for my experiments. He had also presented me a good insight from academic world to industry. I would like to thank to Assoc. Prof. Canan Baysal and Assoc. Prof. Mehmet Ali Gülgün who have presented a creative environment for scientific discussions and have given invaluable advice for my studies. I must also give a special thank to Prof. Turgut Nugay and Prof. Nihan Nugay who initiated my graduate study and have provided endless and careful support throughout my PhD years. I also want to thank all my friends who made this thesis possible.

Finally, I find myself in the pleasurable obligation of expressing my thanks to my love and to my family, whose contributions and supports cannot be assessed enough. To finish, this kind of work is never done by single individual, but by someone who needs, and often receives, the contributions of others. I am grateful to everyone whom I cannot name here.

TABLE OF CONTENTS

Page

LIST OF ABBREVIATIONS.....	viii
LIST OF TABLES.....	ix
LIST OF FIGURES.....	x
ABSTRACT.....	xiii
ÖZET.....	xv
CHAPTER 1. INTRODUCTION.....	1
CHAPTER 2. METALLIZATION OF POLYMERIC ELECTROSPUN NANOFIBERS.....	4
2. 1. Background.....	4
2. 2. Palladium/Poly(acrylonitrile-co-acrylic acid).....	5
2. 2. 1. Experimental.....	6
2. 2. 1. 1. Solution preparation and electrospinning.....	6
2. 2. 1. 2. Characterisation of fibers and metal nanoparticles.....	7
2. 2. 1. 3. Method of hydrogenation.....	8
2. 2. 2. Results.....	8
2. 2. 2. 1. Electrospinning.....	8
2. 2. 2. 2. Characterization of Pd nanoparticles.....	9
2. 2. 2. 3. Electron Microscopy.....	11
2. 2. 2. 4. Energy Dispersive Spectra.....	14
2. 2. 2. 5. Catalytic activity of Pd on electrospun fibers.....	14
2. 2. 3. Discussion.....	16
2. 3. Silver / Poly(acrylonitrile-co-glycidylmethacrylate).....	17
2. 3. 1. Experimental.....	18
2. 3. 1. 1. Polymer synthesis and Metallization of nanofibers.....	18
2. 3. 2. Results and Discussion.....	19

CHAPTER 3. EFFECT OF FILLER AMOUNT ON THERMOELASTIC PROPERTIES OF POLY(DIMETHYLSILOXANE) NETWORKS.....	29
3. 1. Background.....	29
3. 2. Experiments.....	30
3. 2. 1. Materials.....	30
3. 2. 2. Network synthesis.....	31
3. 2. 3. AFM imaging.....	31
3. 2. 4. Sol-Gel Analysis and Swelling Experiments.....	31
3. 2. 5. Thermoelasticity Measurements.....	32
3. 2. 6. Mechanical measurements.....	33
3. 3. Thermoelasticity Theory.....	34
3. 4. Results.....	34
3. 4. 1. AFM imaging and particle size.....	34
3. 4. 2. Swelling Measurements and Sol-Gel Analysis.....	36
3. 4. 3. Elastomeric Force and Temperature coefficient.....	37
3. 4. 4. Thermoelasticity Measurements.....	37
3. 5. Discussion.....	43
CHAPTER 4. DIMENSIONS OF POLYSTYRENE PARTICLES DEPOSITED ON MICA FROM DILUTE CYCLOHEXANE SOLUTION AT DIFFERENT TEMPERATURES.....	41
4. 1. Background.....	41
4. 2. Experimental.....	42
4. 2. 1. Materials.....	42
4. 2. 2. Sample preparation.....	43
4. 2. 3. AFM imaging.....	43
4. 3. Results and Discussion.....	44
4. 3. 1. The single chain per particle scenario.....	48
4. 3. 2. Several chains per particle scenario.....	48
4. 3. 3. Morphology of PS structures - Round versus Flat.....	50
4. 3. 4. Conformational change of PS chains in coil-to-globule transition.....	51
APPENDIX I. CALCULATION OF DEGREE OF END-LINKING AND MODULUS FROM SWELLING DATA.....	53
CHAPTER 5. CONCLUSION.....	54
REFERENCES.....	56

LIST OF ABBREVIATIONS

AA	Acrylic acid
AFD	Average Fiber Diameter
AFM	Atomic Force Microscopy
Ag	Silver
AgNO ₃	Silver nitrate
AN	Acrylonitrile
CH	Cyclohexane
DMF	Dimethyl formamide
EDS	Energy Dispersive Spectra
GMA	Glycidylmethacrylate
NMR	Nuclear Magnetic Resonance
P(AN-GMA)	Poly(acrylonitrile-co-glycidylmethacrylate)
PAN-AA	Poly(acrylonitrile-co-acrylic acid)
Pd	Palladium
PdCl ₂	Palladium chloride
PDMS	Poly(dimethylsiloxane)
PS	Polystyrene
SEM	Scanning Electron Microscopy
TEM	Transmission Electron Microscopy
TGA	Thermogravimetric analysis
XRD	X ray diffraction

LIST OF TABLES

<u>Table</u>		<u>Page</u>
Table 2.1.	Compositions of PAN-AA copolymer solutions.....	7
Table 2.2.	Dimensions of electrospun PAN-AA fibers and Pd particles.....	13
Table 3.1.	Density and Diameter of silica particles.....	33
Table 3.2.	Swelling measurements on end-linked PDMS.....	34
Table 4.1.	Experimentally measured particle dimensions on mica at four different temperatures.....	46
Table 4.2.	Maximum possible number of chains in a particle on mica at four different temperatures.....	49

LIST OF FIGURES

<u>Figure</u>	<u>Page</u>
Figure 2.1.	Hydrogenation reaction of dehydrolinalool (3,7-dimethyloctaen-6-in-1-ol-3).....8
Figure 2.2.	Electron microscope images of nanofibers electrospun from 8 %wt. PAN with (a) 5.4 % mol AA (b) 8.1 % mol AA under 1.8 kV/cm.....9
Figure 2.3.	X-ray diffraction peaks of mat PAN with 11 (□) 5.4 mol % AA and 1.25% PdCl ₂ before the reduction process (•) 5.4 mol % AA and 0.63% PdCl ₂ after the reduction process (■) 5.4 mol % AA and 1.25% PdCl ₂ after the reduction process (▼) 8.1 mol % AA and 1.25% PdCl ₂ after the reduction process (▲) 5.4 mol % AA and 8.3% PdCl ₂ after the reduction process.
Figure 2.4.	Electron microscope images of PAN-AA fibers with generated Pd nanoparticles, (a) Sample <i>A'</i> (b) Sample <i>B'</i> (c) Sample <i>C'</i> (d) Sample <i>D'</i> . Sample A is magnified 300k times, the others 50k times.....12
Figure 2.5.	Distribution of palladium particle size for samples <i>A'</i> , <i>B'</i> , <i>C'</i> and <i>D'</i>13
Figure 2.6.	Pd particle size as a function of PdCl ₂ concentration inside spinning solution.....14
Figure 2.7.	EDS of electrospun mats on showing the presence of Pd. The analyses were performed on regions where there was (a) no particle (b) particle.....15
Figure 2.8.	¹ H spectrum of poly(glycidyl methacrylate) recorded at 25°C. (Solvent: CDCl ₃)..19
Figure 2.9.	The electron microscope image of P(AN-GMA) nanofibers obtained from 30 wt% solution in DMF at 1.53 kV/cm.....20
Figure 2.10.	Surface modification and metallization reactions of P(AN-GMA) nanofibers.....20
Figure 2.11.	IR spectra of (a) P(AN-GMA) and (b) hydrazine treated P(AN-GMA).....21
Figure 2.12.	Electron microscope images of poly(glycidymethacrylate) nanofibers (a) and hydrazine treated nanofibers (b).....21
Figure 2.13.	XRD of P(AN-GMA) nanofibers after 24 hours coating time. Particle distribution of silver nanoparticles is shown in the inset. The bin size of the distribution is 15 nm. Coating time is 2 minute.....22

Figure 2.14.	Electron microscope images of Ag coated P(AN-GMA) nanofibers. Coating time is 2 minutes.....	23
Figure 2.15.	Thermogravimetric curve of the electrospun fibers and Ag coated electrospun fibers, and DTA curve of the Ag coated electrospun fibers.....	24
Figure 2.16.	Diameter distributions of silver particles obtained five different coating times.....	24
Figure 2.17.	Agglomeration of nanofibers and nanoparticles.....	25
Figure 3.1.	Schematic view of experimental apparatus.....	30
Figure 3.2.	AFM tapping mode phase image of silica particles in PDMS matrix, (a) 1% wt. (b) 3 % wt. (c) 5% wt. Silica.....	32
Figure 3.3.	Equilibrium swelling degree of PDMS networks for unfilled and filled with 1%, 3%, 5% wt. fumed silica in benzene and toluene.....	34
Figure 3.4.	Thermoelasticity plot of end-linked PDMS with 5% wt. silica. The equations of the best-fitting lines are: $\ln (f/T) = -8.7 \times 10^{-4} T - 6.1$ ($\alpha = 1.81$), $\ln (f/T) = -7.0 \times 10^{-4} T - 6.3$ ($\alpha = 1.56$) and $\ln (f/T) = -8.3 \times 10^{-4} T - 6.7$ ($\alpha = 1.44$).....	35
Figure 3.5.	(I) Force map for 5% wt silica filled PDMS network at 1.41 loading (8859 data points). (II) Detailed force map for segment I, loading at room temperature (80 data points). (III) Detailed force map for segment II; relaxation upon loading at room temperature, shrinkage and relaxation at 120°C. (426 data points) (IV) The force recorded between 104°C to 83 °C during the experiment for segment IV (945 data points); detailed force map for segment IV including only the equilibrium plateau regions at different temperatures are shown in the inset.....	36
Figure 3.6.	f_e/f values as a function of silica concentration. Open circles represent results from Reference [52] and close circles show our experimental data.....	38
Figure 3.7.	$\ln \langle r^2 \rangle_0 / dT$ of PDMS chains as a function of silica concentration.....	38
Figure 3.8.	Typical force-temperature curves at various elongations at constant length. The equations of the best-fitting lines are: $\sigma = 8.4 \times 10^{-4} T + 0.29$, $\sigma = 6.1 \times 10^{-4} T + 0.23$, and $\sigma = 4.4 \times 10^{-4} T + 0.23$. Slopes of the lines decrease with decreasing the extension ratio.....	39

Figure 3.9.	Elastic modulus of the unfilled and silica filled PDMS networks obtained by mechanical and by swelling in toluene and benzene.....	40
Figure 4.1.	AFM images of polystyrene particles deposited from a very dilute solution of PS in CH onto a mica substrate at (a) 25 °C (b) 35°C (c) 50 °C (d) 80 °C. All images have 5 x 5 μm^2 scan area.....	46
Figure 4.2.	AFM height images captured from (a) center (b) perimeter of the drop after solvent evaporation.....	47
Figure 4.3.	Volume distributions of polystyrene particles at 25°C, 35°C, 50°C, 80°C. Bin sizes are 3500, 10000, 40000, and 50000 m^3	47
Figure 4.4.	Diameter distribution of polystyrene particles at 25, 35, 50, and 80°C.....	49
Figure 4.5.	Height distribution of polystyrene particles at 25, 35,50, and 80°C.....	50
Figure 4.6.	Section analysis of two different morphologies of PS (a) round (b) flat.....	51
Figure 4.7.	a) Time dependence of hydrodynamic radius of a single polystyrene chain in cyclohexane during the transition [61] b) AFM image of polystyrene chain deposit on mica from cyclohexane 35°C.....	52

ABSTRACT

An approach to bottom-up design of new materials was developed starting from homogenous solutions. Solution processing techniques were used to fabricate advanced solid state materials, and processing parameters were identified and characterized. Three studies related to this work are reported herein:

i) Polymeric electrospun nanofibers were metallized with transition metals for potential use as catalysts in organic reactions or sensing elements. Two different polymer-metal systems, which were palladium/poly(acrylonitrile-co-acrylic acid) and silver/poly(acrylonitrile-co-glycidylmethacrylate), were employed. Polyacrylonitrile based copolymers were chosen as carrier material in view of their facile spinnability and established utility as precursor materials of carbon fibers. Nanofibers, in both cases, were obtained by electrospinning of homogeneous solutions in dimethylformamide. Metals were deposited on electrospun films starting from the metal salts by following two different procedures. In one route, palladium-II-chloride and the polymer were dissolved in dimethylformamide and subjected to electrospinning. Salt molecules were homogeneously distributed into nanofibers. Palladium cations were reduced after the electrospun film was immersed into an aqueous solution of hydrazine. The parameters affecting and tuning the particle size were determined. In particular, the amount of acrylic acid on the polymer backbone and palladium salt concentration in solution described two key factors. Palladium particles, called clusters, were afforded as polycrystalline structures consisting of smaller crystal units. Catalytic activity of palladium produced on electrospun film was investigated in a hydrogenation reaction of unsaturated alcohols. It was found that electrospun-supported palladium particles displayed 4.5 times higher catalytic activity than alumina-supported palladium. In the second route, silver was coated on poly(acrylonitrile-co-glycidylmethacrylate) nanofibers by use of electroless plating techniques. Reagent-accessible oxirane groups supported on the nanofibers were modified with a reducing agent, hydrazine. Surface-modified electrospun nanofibers were allowed to react with an ammoniac solution of silver nitrate. A redox reaction took place during which time metallic silver was nucleated along the fiber surface, affording silver nanoparticles of 40 nm diameter. These particles featured typical separation distances of 5-50 nm.

ii) Thermoelasticity of silica reinforced poly(dimethylsiloxane) networks was examined. Poly(dimethylsiloxane) networks exhibit rubber-like elasticity; that is, they recover their original

state following deformation. Elasticity is an entropy driven phenomena for polymers. Uniaxial stretching of a network elongates the chains, resulting in a decreased conformational entropy due to the restricted number of low energy conformations that the extended chains can adopt. When the stress is removed, the chains recoil into the relaxed state with higher entropy. Elastomeric force, f , applied in uniaxial extension has an entropic and an energetic component affecting the network chains at the molecular level. The entropic component, f_s , is used in changing the configurations of the chains into less disordered state. The rest of the force, f_e , is used in changing the conformations of the chains. The ratio of f_e/f can be determined by thermoelasticity experiments which are based on stress-strain measurements at constant volume. An ideal network was prepared from hydroxyl-ended poly(dimethylsiloxane) chains. They were dissolved in toluene. Fumed silica was introduced into the polymer solution prior to end-linking. A tetrafunctional crosslinker, tetraethoxysilane, was added into the homogenous solution and end-linked in the presence of Tin(II) 2-ethylhexanoate as a catalyst. The thickness of the nanocomposite film is on the order of 2 mm. The filler content was varied in the range 0-5 wt%. Tapping mode Atomic Force Microscopy was performed to characterize the silica particles, which become larger as the silica concentration increases. The temperature coefficient and the energetic part of the force in uniaxial extension are found to increase with increasing silica content. The elastic modulus of the reinforced networks was determined by mechanical experiments and swelling measurements. The modulus increases linearly with increasing silica concentration.

iii) Amorphous polystyrene molecules/clusters were isolated and investigated. Erman and Flory showed that long polystyrene molecules undergo large dimensional changes in cyclohexane at 35°C. This event is known as coil-globule transition. Here the dimensional changes at dry state after the transition takes place were imaged and measured. Dilute solution of cyclohexane was cast on mica by the drop deposition technique. Solvent evaporation left behind a discontinuous film consisting of separated polystyrene islands. Atomic Force Microscopy was employed to determine the morphology and dimensions (volume, height and diameter) of the polystyrene particles. The experiment was performed at four different temperatures. It is found that the dimensions are strongly temperature dependent and exhibit a Gaussian-like distribution. Polystyrene chains tend to form clusters as the temperature increases. Two scenarios were discussed for whether the particles contain single or several chains.

ÖZET

POLİMERİK NANOKOMPOZİT FİLMLEİN VE POLİSTİREN NANOPARÇACIKLARIN ÇÖZELTİ İŞLEME, ÜRETİM, VE NİTELENDİRME TEKNİKLERİ

Çözelti işleme yöntemleri kullanılarak nanoyapıda parçacık içeren yeni malzemeler üretilmiştir. İşleme parametreleri tanımlanmış ve nitelendirilmiştir. Bu tezde üç çalışma raporlanmıştır:

i) Elektrodokuma metodu ile elde edilen nanolif yüzeyi geçiş elementleri ile kaplanmıştır. İki farklı metal polimer sistemi, paladyum/poli(akrilonitril-ko-akrilik asit) ve gümüş/poli(akrilonitril-ko-glisidilmetakrilat), çalışılmıştır. Elektrodokunabilirliği ve karbon fiber öncüsü olması sebebiyle, poliakrilonitril kimyası, taşıyıcı olarak düşünülmüştür. Her iki sistemde de metal parçacıkları metal kationlarının indirgenmesi sonucu elde edilmiştir. Birinci sistemde paladyum (II) klorür ve poli (akrilonitril akrilik asit) dimethylformamide içerisinde çözülmüş ve elektrodokuma metoduna tabi tutulmuştur. Tuz molekülleri nanolif içerisinde homojen olarak dağıldığı düşünülmektedir. Elektrodokunan kumaş sulu hidrazin çözeltisi içerine konularak ve paladyum kasyonu paladyum metale dönüşürülmüştür. Paladyum parçacıklarının büyüklüğünü etkileyen değişkenler tanımlanmıştır. Polimer zinciri üzerindeki akrilik asit miktarı ve çözelti içerisindeki paladyum tuz konsantrasyonu parçacık büyüklüğünü etkileyen iki önemli değişkendir. X ışını kırılım spektroskopisi ve elektron mikrosopi tetkikleri sonucu paladyum parçacıkların polikristal kümeler oluşturduğu gözlemlenmiştir. Elektrodokunan lifler üzerindeki paladyum parçacıklarının katalitik aktivitesi doymamış bir alkolün hidrojenlenme reaksiyonunda incelenmiştir. Sonuçlar göstermiştir ki, oluşturduğumuz paladyum parçacıkları standart paladyum katalizöründen (Alumina destekli katalizör) 4.5 kat daha hızlıdır. İkinci sistemde, gümüş parçacıkları poli(akrilonitril-ko-glisidilmetakrilat) nanolifler üzerinde elektrotsuz kaplama metodu ile üretilmiştir. Nanolif yüzeyinde bulunan oksiran grupları indirgeyici ajan molekülleri (hidrazin) ile açılmıştır. Yüzeyi değiştirilmiş elektrodokunan lifler sulu gümüş nitrat çözeltisi içerisine konmuştur. İndirgenme hidrazin molekülleri ile gümüş kationları arasında gerçekleşen redoks reaksiyonu sonucu metalik gümüş parçacıkları oluşmuştur. Gümüş parçacıkları ortalama 40 nanometre çapa sahiptir ve birbirlerinden 5-50 nanometre uzaklıktadır.

ii) Silica dolgulu poly(dimetilsiloksan) kauçuk nanokompozitleri hazırlanıp ve bu malzemelerin termoelastik özellikleri incelenmiştir. Termoelastisite madde esnekliğinin sıcaklığa karşı değişimi olarak tanımlanır. Hidroksil uçlu zincirler, tetraetoksi silan molekülleri ile reaksiyona sokulmuş ve ağsı bir yapı elde edilmiştir. Poly(dimetilsiloksan) zincirleri esnek özelliğe sahip olduklarından, reaksiyon sonucu oluşan ağsı yapı da elastik özelliğe sahiptir. Kauçularda elastikiyet hem entropik hem de enerjetik kökene sahiptir. Kauçuk bir malzeme boyuna paralel doğrultuda uzatılırsa, uygulanan kuvvet molekuler düzeyde iki iş yapar. Kuvvetin bir bölümü polimer zincirlerin uçlarını birbirinden uzaklaştırırken, bu etki sistemin entropisini azalttığı için biz buna entropik bileşen diyeceğiz, geriye kalan kuvvet ise zincirlerin konformasyonunu değiştirmeye harcanır, bu etki ise enerjetik bileşen olarak adlandırılır. Entropik bileşen deneysel olarak ölçülebilir bir büyüklüktür. Bizim bu çalışmadaki amacımız değişik miktarlarda dolgu malzemesi ile hazırladığımız PDMS elastomerlerinin elastik kuvvetini oluşturan entropik ve enerjetik bileşenlerini bulmaktır. Termoelastisite ölçüm sonuçları göstermiştir ki, elastik kuvvetin enerjetik bileşeni sisteme yüklenen silica dolgu malzemesi ile doğrusal bir biçimde artmıştır.

iii) Amorf polistiren molekülleri ve molekül kümeleri çözelti içerisinde birbirinden ayrılmış ve kuru ortamda incelenmiştir. Uzun polistiren moleküllerinin sikloheksan içerisinde 25-50°C arasında boyutsal bir değişim gösterdikleri Erman ve Flory tarafından hem deneysel olarak hem de hesapsal olarak gösterilmişti. Bu boyutsal değişim polimerlerde açık-derlenmiş (coil-globule transition) dönüşümü olarak adlandırılır. Bu çalışmadaki hedef polistiren moleküllerini dört farklı sıcaklıkta kaplamış oldukları hacmi bulmak ve sözkonusu geçişi Atomik Kuvvet Mikroskopu ile görüntülemektir. Polistiren zincirlerini birbirinden ayırmak amacıyla çok seyreltik polistiren-sikloheksan çözeltisi hazırlanmıştır. Çözelti düz bir yüzey üzerine dökülüp çözücü tamamen buharlaştıktan sonra yüzey mikroskop ile taranmıştır. Yüzey üzerinde kalan polimer zincirleri ve kümeleri görüntülenmiştir. Parçacıkların yükseklik, uzunluk, ve hacimleri ölçülmüş, tek bir küme içerisinde bulunan ortalama zincir sayısı hesaplanmıştır. Sıcaklık artışı ile parçacık boyutunun artışı tek bir zincir dönüşümü mü yoksa zincirlerin kümelenmesi sonucu mu oluştuğu tartışılmıştır.

**SOLUTION PROCESSING: FABRICATION AND CHARACTERIZATION OF
POLYMERIC NANOCOMPOSITE FILMS AND POLYSTYRENE NANOPARTICLES**

by
MUSTAFA M. DEMİR

Submitted to the Graduate School of Engineering and Natural Sciences
in partial fulfillment of
the requirements for the degree of
Doctor of Philosophy

Sabanci University
Spring 2004

© MUSTAFA M. DEMİR 2004

All Rights Reserved

to my love

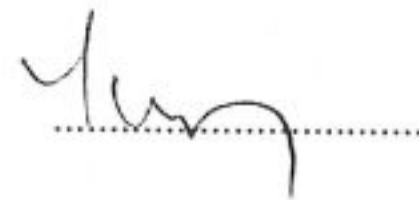
&

to my whole family

SOLUTION PROCESSING: FABRICATION AND CHARACTERIZATION OF
POLYMERIC NANOCOMPOSITE FILMS AND POLYSTYRENE NANOPARTICLES

APPROVED BY:

Assoc. Prof. Dr. Yusuf Z. Menceloğlu
(Dissertation Supervisor)



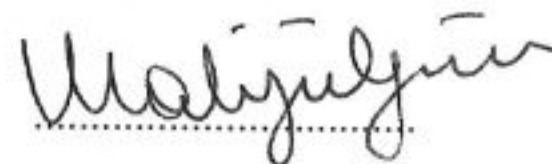
Prof. Dr. Burak Erman
(Dissertation Co-advisor)



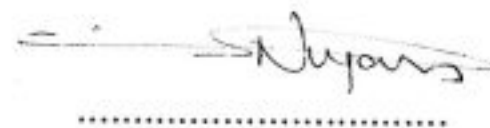
Assoc. Prof. Dr. Canan Baysal



Assoc. Prof. Dr. Mehmet Ali Gülgün



Prof. Dr. Turgut Nugay



DATE OF APPROVAL:3rd May 2004.....

ACKNOWLEDGEMENT

Throughout my graduate years, a number of people have helped and supported me in various ways. At first, I would like to give a sincere gratitude and appreciation to Prof. Burak Erman for suggesting the research topics and for indicating my abilities which I was not aware before. He had non-decreasing patience and support for improving myself in the long and rough pathways of science. I have to extend my appreciation to Assoc. Prof. Yusuf Mencilođlu for his guidance and his priceless support for my experiments. He had also presented me a good insight from academic world to industry. I would like to thank to Assoc. Prof. Canan Baysal and Assoc. Prof. Mehmet Ali Gülgün who have presented a creative environment for scientific discussions and have given invaluable advice for my studies. I must also give a special thank to Prof. Turgut Nugay and Prof. Nihan Nugay who initiated my graduate study and have provided endless and careful support throughout my PhD works. I also want to thank all my friends who made this thesis possible.

Finally, I find myself in the pleasurable obligation of expressing my thanks to my love and to my family, whose contributions and supports cannot be assessed enough. To finish, this kind of work is never done by single individual, but by someone who needs, and often receives, the contributions of others. I am grateful to everyone whom I cannot name here.

TABLE OF CONTENTS

	<u>Page</u>
LIST OF ABBREVIATIONS.....	viii
LIST OF TABLES.....	ix
LIST OF FIGURES.....	x
ABSTRACT.....	xiii
ÖZET.....	xv
CHAPTER 1. INTRODUCTION.....	1
CHAPTER 2. METALLIZATION OF POLYMERIC ELECTROSPUN NANOFIBERS.....	4
2. 1. Background.....	4
2. 2. Palladium/Poly(acrylonitrile-co-acrylic acid).....	5
2. 2. 1. Experimental.....	6
2. 2. 1. 1. Solution preparation and electrospinning.....	6
2. 2. 1. 2. Characterisation of fibers and metal nanoparticles.....	7
2. 2. 1. 3. Method of hydrogenation.....	8
2. 2. 2. Results.....	8
2. 2. 2. 1. Electrospinning.....	8
2. 2. 2. 2. Characterization of Pd nanoparticles.....	9
2. 2. 2. 3. Electron Microscopy.....	11
2. 2. 2. 4. Energy Dispersive Spectra.....	14
2. 2. 2. 5. Catalytic activity of Pd on electrospun fibers.....	14
2. 2. 3. Discussion.....	16
2. 3. Silver / Poly(acrylonitrile-co-glycidylmethacrylate).....	17
2. 3. 1. Experimental.....	18
2. 3. 1. 1. Polymer synthesis and Metallization of nanofibers.....	18
2. 3. 2. Results and Discussion.....	19

CHAPTER 3. EFFECT OF FILLER AMOUNT ON THERMOELASTIC PROPERTIES OF POLY(DIMETHYLSILOXANE) NETWORKS.....	29
3. 1. Background.....	29
3. 2. Experiments.....	30
3. 2. 1. Materials.....	30
3. 2. 2. Network synthesis.....	31
3. 2. 3. AFM imaging.....	31
3. 2. 4. Sol-Gel Analysis and Swelling Experiments.....	31
3. 2. 5. Thermoelasticity Measurements.....	32
3. 2. 6. Mechanical measurements.....	33
3. 3. Thermoelasticity Theory.....	34
3. 4. Results.....	34
3. 4. 1. AFM imaging and particle size.....	34
3. 4. 2. Swelling Measurements and Sol-Gel Analysis.....	36
3. 4. 3. Elastomeric Force and Temperature coefficient.....	37
3. 4. 4. Thermoelasticity Measurements.....	37
3. 5. Discussion.....	43
CHAPTER 4. DIMENSIONS OF POLYSTYRENE PARTICLES DEPOSITED ON MICA FROM DILUTE CYCLOHEXANE SOLUTION AT DIFFERENT TEMPERATURES.....	41
4. 1. Background.....	41
4. 2. Experimental.....	42
4. 2. 1. Materials.....	42
4. 2. 2. Sample preparation.....	43
4. 2. 3. AFM imaging.....	43
4. 3. Results and Discussion.....	44
4. 3. 1. The single chain per particle scenario.....	48
4. 3. 2. Several chains per particle scenario.....	48
4. 3. 3. Morphology of PS structures - Round versus Flat.....	50
4. 3. 4. Conformational change of PS chains in coil-to-globule transition.....	51
APPENDIX I. CALCULATION OF DEGREE OF END-LINKING AND MODULUS FROM SWELLING DATA.....	53
CHAPTER 5. CONCLUSION.....	54
REFERENCES.....	56

LIST OF ABBREVIATIONS

AA	Acrylic acid
AFD	Average Fiber Diameter
AFM	Atomic Force Microscopy
Ag	Silver
AgNO ₃	Silver nitrate
AN	Acrylonitrile
CH	Cyclohexane
DMF	Dimethyl formamide
EDS	Energy Dispersive Spectra
GMA	Glycidylmethacrylate
NMR	Nuclear Magnetic Resonance
P(AN-GMA)	Poly(acrylonitrile-co-glycidylmethacrylate)
PAN-AA	Poly(acrylonitrile-co-acrylic acid)
Pd	Palladium
PdCl ₂	Palladium chloride
PDMS	Poly(dimethylsiloxane)
PS	Polystyrene
SEM	Scanning Electron Microscopy
TEM	Transmission Electron Microscopy
TGA	Thermogravimetric analysis
XRD	X ray diffraction

LIST OF TABLES

<u>Table</u>	<u>Page</u>
Table 2.1. Compositions of PAN-AA copolymer solutions.....	7
Table 2.2. Dimensions of electrospun PAN-AA fibers and Pd particles.....	13
Table 3.1. Density and Diameter of silica particles.....	33
Table 3.2. Swelling measurements on end-linked PDMS.....	34
Table 4.1. Experimentally measured particle dimensions on mica at four different temperatures.....	46
Table 4.2. Maximum possible number of chains in a particle on mica at four different temperatures.....	49

LIST OF FIGURES

<u>Figure</u>		<u>Page</u>
Figure 2.1.	Hydrogenation reaction of dehydrolinalool (3,7-dimethyloktaen-6-in-1-ol-3).....	8
Figure 2.2.	Electron microscope images of nanofibers electrospun from 8 %wt. PAN with (a) 5.4 % mol AA (b) 8.1 % mol AA under 1.8 kV/cm.....	9
Figure 2.3.	X-ray diffraction peaks of mat PAN with (□) 5.4 mol % AA and 1.25% PdCl ₂ before the reduction process (•) 5.4 mol % AA and 0.63% PdCl ₂ after the reduction process (■) 5.4 mol % AA and 1.25% PdCl ₂ after the reduction process (▼) 8.1 mol % AA and 1.25% PdCl ₂ after the reduction process (▲) 5.4 mol % AA and 8.3% PdCl ₂ after the reduction process.	11
Figure 2.4.	Electron microscope images of PAN-AA fibers with generated Pd nanoparticles, (a) Sample A' (b) Sample B' (c) Sample C' (d) Sample D'. Sample A is magnified 300k times, the others 50k times.....	12
Figure 2.5.	Distribution of palladium particle size for samples A', B', C' and D'.....	13
Figure 2.6.	Pd particle size as a function of PdCl ₂ concentration inside spinning solution.....	14
Figure 2.7.	EDS of electrospun mats on showing the presence of Pd. The analyses were performed on regions where there was (a) no particle (b) particle.....	15
Figure 2.8.	¹ H spectrum of poly(glycidyl methacrylate) recorded at 25°C. (Solvent: CDCl ₃)...	19
Figure 2.9.	The electron microscope image of P(AN-GMA) nanofibers obtained from 30 wt% solution in DMF at 1.53 kV/cm.....	20
Figure 2.10.	Surface modification and metallization reactions of P(AN-GMA) nanofibers.....	20
Figure 2.11.	IR spectra of (a) P(AN-GMA) and (b) hydrazine treated P(AN-GMA).....	21
Figure 2.12.	Electron microscope images of poly(glycidymethacrylate) nanofibers (a) and hydrazine treated nanofibers (b).....	21
Figure 2.13.	XRD of P(AN-GMA) nanofibers after 24 hours coating time. Particle distribution of silver nanoparticles is shown in the inset. The bin size of the distribution is 15 nm. Coating time is 2 minute.....	22

Figure 2.14.	Electron microscope images of Ag coated P(AN-GMA) nanofibers. Coating time is 2 minutes.....	23
Figure 2.15.	Thermogravimetric curve of the electrospun fibers and Ag coated electrospun fibers, and DTA curve of the Ag coated electrospun fibers.....	24
Figure 2.16.	Diameter distributions of silver particles obtained five different coating times.....	24
Figure 2.17.	Agglomeration of nanofibers and nanoparticles.....	25
Figure 3.1.	Schematic view of experimental apparatus.....	30
Figure 3.2.	AFM tapping mode phase image of silica particles in PDMS matrix, (a) 1% wt. (b) 3 % wt. (c) 5% wt. Silica.....	32
Figure 3.3.	Equilibrium swelling degree of PDMS networks for unfilled and filled with 1%, 3%, 5% wt. fumed silica in benzene and toluene.....	34
Figure 3.4.	Thermoelasticity plot of end-linked PDMS with 5% wt. silica. The equations of the best-fitting lines are: $\ln(f/T) = -8.7 \times 10^{-4} T - 6.1$ ($\alpha = 1.81$), $\ln(f/T) = -7.0 \times 10^{-4} T - 6.3$ ($\alpha = 1.56$) and $\ln(f/T) = -8.3 \times 10^{-4} T - 6.7$ ($\alpha = 1.44$).....	35
Figure 3.5.	(I) Force map for 5% wt silica filled PDMS network at 1.41 loading (8859 data points). (II) Detailed force map for segment I, loading at room temperature (80 data points). (III) Detailed force map for segment II; relaxation upon loading at room temperature, shrinkage and relaxation at 120°C. (426 data points) (IV) The force recorded between 104°C to 83 °C during the experiment for segment IV (945 data points); detailed force map for segment IV including only the equilibrium plateau regions at different temperatures are shown in the inset.....	36
Figure 3.6.	f/f values as a function of silica concentration. Open circles represent results from Reference [52] and close circles show our experimental data.....	38
Figure 3.7.	$\ln\langle r^2 \rangle_0 / dT$ of PDMS chains as a function of silica concentration.....	38
Figure 3.8.	Typical force-temperature curves at various elongations at constant length. The equations of the best-fitting lines are: $\sigma = 8.4 \times 10^{-4} T + 0.29$, $\sigma = 6.1 \times 10^{-4} T + 0.23$, and $\sigma = 4.4 \times 10^{-4} T + 0.23$. Slopes of the lines decrease with decreasing the extension ratio.....	39

Figure 3.9.	Elastic modulus of the unfilled and silica filled PDMS networks obtained by mechanical and by swelling in toluene and benzene.....	40
Figure 4.1.	AFM images of polystyrene particles deposited from a very dilute solution of PS in CH onto a mica substrate at (a) 25 °C (b) 35°C (c) 50 °C (d) 80 °C. All images have 5 x 5 μm^2 scan area.....	46
Figure 4.2.	AFM height images captured from (a) center (b) perimeter of the drop after solvent evaporation.....	47
Figure 4.3.	Volume distributions of polystyrene particles at 25°C, 35°C, 50°C, 80°C. Bin sizes are 3500, 10000, 40000, and 50000 m^3	47
Figure 4.4.	Diameter distribution of polystyrene particles at 25, 35, 50, and 80°C.....	49
Figure 4.5.	Height distribution of polystyrene particles at 25, 35,50, and 80°C.....	50
Figure 4.6.	Section analysis of two different morphologies of PS (a) round (b) flat.....	51
Figure 4.7.	a) Time dependence of hydrodynamic radius of a single polystyrene chain in cyclohexane during the transition [61] b) AFM image of polystyrene chain deposit on mica from cyclohexane 35°C.....	52

ABSTRACT

An approach to bottom-up design of new materials was developed starting from homogenous solutions. Solution processing techniques were used to fabricate advanced solid state materials, and processing parameters were identified and characterized. Three studies related to this work are reported herein:

i) Polymeric electrospun nanofibers were metallized with transition metals for potential use as catalysts in organic reactions or sensing elements. Two different polymer-metal systems, which were palladium/poly(acrylonitrile-co-acrylic acid) and silver/poly(acrylonitrile-co-glycidylmethacrylate), were employed. Polyacrylonitrile based copolymers were chosen as carrier material in view of their facile spinnability and established utility as precursor materials of carbon fibers. Nanofibers, in both cases, were obtained by electrospinning of homogeneous solutions in dimethylformamide. Metals were deposited on electrospun films starting from the metal salts by following two different procedures. In one route, palladium-II-chloride and the polymer were dissolved in dimethylformamide and subjected to electrospinning. Salt molecules were homogeneously distributed into nanofibers. Palladium cations were reduced after the electrospun film was immersed into an aqueous solution of hydrazine. The parameters affecting and tuning the particle size were determined. In particular, the amount of acrylic acid on the polymer backbone and palladium salt concentration in solution described two key factors. Palladium particles, called clusters, were afforded as polycrystalline structures consisting of smaller crystal units. Catalytic activity of palladium produced on electrospun film was investigated in a hydrogenation reaction of unsaturated alcohols. It was found that electrospun-supported palladium particles displayed 4.5 times higher catalytic activity than alumina-supported palladium. In the second route, silver was coated on poly(acrylonitrile-co-glycidylmethacrylate) nanofibers by use of electroless plating techniques. Reagent-accessible oxirane groups supported on the nanofibers were modified with a reducing agent, hydrazine. Surface-modified electrospun nanofibers were allowed to react with an ammoniac solution of silver nitrate. A redox reaction took place during which time metallic silver was nucleated along the fiber surface, affording silver nanoparticles of 40 nm diameter. These particles featured typical separation distances of 5-50 nm.

ii) Thermoelasticity of silica reinforced poly(dimethylsiloxane) networks was examined. Poly(dimethylsiloxane) networks exhibit rubber-like elasticity; that is, they recover their original

state following deformation. Elasticity is an entropy driven phenomena for polymers. Uniaxial stretching of a network elongates the chains, resulting in a decreased conformational entropy due to the restricted number of low energy conformations that the extended chains can adopt. When the stress is removed, the chains recoil into the relaxed state with higher entropy. Elastomeric force, f , applied in uniaxial extension has an entropic and an energetic component affecting the network chains at the molecular level. The entropic component, f_s , is used in changing the configurations of the chains into less disordered state. The rest of the force, f_e , is used in changing the conformations of the chains. The ratio of f_s/f can be determined by thermoelasticity experiments which are based on stress-strain measurements at constant volume. An ideal network was prepared from hydroxyl-ended poly(dimethylsiloxane) chains. They were dissolved in toluene. Fumed silica was introduced into the polymer solution prior to end-linking. A tetrafunctional crosslinker, tetraethoxysilane, was added into the homogenous solution and end-linked in the presence of Tin(II) 2-ethylhexanoate as a catalyst. The thickness of the nanocomposite film is on the order of 2 mm. The filler content was varied in the range 0-5 wt%. Tapping mode Atomic Force Microscopy was performed to characterize the silica particles, which become larger as the silica concentration increases. The temperature coefficient and the energetic part of the force in uniaxial extension are found to increase with increasing silica content. The elastic modulus of the reinforced networks was determined by mechanical experiments and swelling measurements. The modulus increases linearly with increasing silica concentration.

iii) Amorphous polystyrene molecules/clusters were isolated and investigated. Erman and Flory showed that long polystyrene molecules undergo large dimensional changes in cyclohexane at 35°C. This event is known as coil-globule transition. Here the dimensional changes at dry state after the transition takes place were imaged and measured. Dilute solution of cyclohexane was cast on mica by the drop deposition technique. Solvent evaporation left behind a discontinuous film consisting of separated polystyrene islands. Atomic Force Microscopy was employed to determine the morphology and dimensions (volume, height and diameter) of the polystyrene particles. The experiment was performed at four different temperatures. It is found that the dimensions are strongly temperature dependent and exhibit a Gaussian-like distribution. Polystyrene chains tend to form clusters as the temperature increases. Two scenarios were discussed for whether the particles contain single or several chains.

ÖZET

POLİMERİK NANOKOMPOZİT FİLMLEİN VE POLİSTİREN NANOPARÇACIKLARIN ÇÖZELTİ İŞLEME, ÜRETİM, VE NİTELENDİRME TEKNİKLERİ

Çözelti işleme yöntemleri kullanılarak nanoyapıda parçacık içeren yeni malzemeler üretilmiştir. İşleme parametreleri tanımlanmış ve nitelendirilmiştir. Bu tezde üç çalışma raporlanmıştır:

i) Elektrodokuma metodu ile elde edilen nanolif yüzeyi geçiş elementleri ile kaplanmıştır. İki farklı metal polimer sistemi, paladyum/poli(akrilonitril-ko-akrilik asit) ve gümüş/poli(akrilonitril-ko-glisidilmetakrilat), çalışılmıştır. Elektrodokunabilirliği ve karbon fiber öncüsü olması sebebiyle, poliakrilonitril kimyası, taşıyıcı olarak düşünülmüştür. Her iki sistemde de metal parçacıkları metal katyonlarının indirgenmesi sonucu elde edilmiştir. Birinci sistemde paladyum (II) klorür ve poli(akrilonitril akrilik asit) dimethylformamide içerisinde çözülmüş ve elektrodokuma metoduna tabi tutulmuştur. Tuz molekülleri nanolif içerisinde homojen olarak dağıldığı düşünülmektedir. Elektrodokunan kumaş sulu hidrazin çözeltisi içerine konularak ve paladyum katyonu paladyum metaline dönüştürülmüştür. Paladyum parçacıklarının büyüklüğünü etkileyen değişkenler tanımlanmıştır. Polimer zinciri üzerindeki akrilik asit miktarı ve çözelti içerisindeki paladyum tuz konsantrasyonu parçacık büyüklüğünü etkileyen iki önemli değişkendir. X ışını kırılım spektroskopisi ve elektron mikroskopi tetkikleri sonucu paladyum parçacıkların polikristal kümeler oluşturduğu gözlemlenmiştir. Elektrodokunan lifler üzerindeki paladyum parçacıklarının katalitik aktivitesi doymamış bir alkolün hidrojenlenme reaksiyonunda incelenmiştir. Sonuçlar göstermiştir ki, oluşturduğumuz paladyum parçacıkları standart paladyum katalizöründen (Alumina destekli katalizör) 4.5 kat daha hızlıdır. İkinci sistemde, gümüş parçacıkları poli(akrilonitril-ko-glisidilmetakrilat) nanolifler üzerinde elektrotsuz kaplama metodu ile üretilmiştir. Nanolif yüzeyinde bulunan oksiran grupları indirgeyici ajan molekülleri (hidrazin) ile açılmıştır. Yüzeyi değiştirilmiş elektrodokunan lifler sulu gümüş nitrat çözeltisi içerisine konmuştur. İndirgenme hidrazin molekülleri ile gümüş katyonları arasında gerçekleşen redoks reaksiyonu sonucu metalik gümüş parçacıkları oluşmuştur. Gümüş parçacıkları ortalama 40 nanometre çapa sahiptir ve

birbirlerinden 5-50 nanometre uzaklıktadır.

ii) Silica dolgulu poly(dimetilsiloksan) kauçuk nanokompozitleri hazırlanıp ve bu malzemelerin termoelastik özellikleri incelenmiştir. Termoelastisite madde esnekliğinin sıcaklığa karşı değişimi olarak tanımlanır. Hidroksil uçlu zincirler, tetraetoksi silan molekülleri ile reaksiyona sokulmuş ve ağsı bir yapı elde edilmiştir. Poly(dimetilsiloksan) zincirleri esnek özelliğe sahip olduklarından, reaksiyon sonucu oluşan ağsı yapı da elastik özelliğe sahiptir. Kauçularda elastikiyet hem entropik hem de enerjetik kökene sahiptir. Kauçuk bir malzeme boyuna paralel doğrultuda uzatılırsa, uygulanan kuvvet molekuler düzeyde iki iş yapar. Kuvvetin bir bölümü polimer zincirlerin uçlarını birbirinden uzaklaştırırken, bu etki sistemin entropisini azalttığı için biz buna entropik bileşen diyeceğiz, geriye kalan kuvvet ise zincilerin konformasyonunu değiştirmeye harcanır, bu etki ise enerjetik bileşen olarak adlandırılır. Entropik bileşen deneysel olarak ölçülebilir bir büyüklüktür. Bizim bu çalışmadaki amacımız değişik miktarlarda dolgu malzemesi ile hazırladığımız PDMS elastomerlerinin elastik kuvvetini oluşturan entropik ve enerjetik bileşenlerini bulmaktır. Termoelastisite ölçüm sonuçları göstermiştir ki, elastik kuvvetin enerjetik bileşeni sisteme yüklenen silica dolgu malzemesi ile doğrusal bir biçimde artmıştır.

iii) Amorf polistiren molekülleri ve molekül kümeleri çözelti içerisinde birbirinden ayrılmış ve kuru ortamda incelenmiştir. Uzun polistiren moleküllerinin sikloheksan içerisinde 25-50°C arasında boyutsal bir değişim gösterdikleri Erman ve Flory tarafından hem deneysel olarak hem de hesapsal olarak gösterilmişti. Bu boyutsal değişim polimerlerde açık-derlenmiş (coil-globule transition) dönüşümü olarak adlandırılır. Bu çalışmadaki hedef polistiren moleküllerini dört farklı sıcaklıkta kaplamış oldukları hacmi bulmak ve sözkonusu geçişi Atomik Kuvvet Mikroskopu ile görüntülemektir. Polistiren zincirlerini birbirinden ayırmak amacıyla çok seyreltik polistiren-sikloheksan çözeltisi hazırlanmıştır. Çözelti düz bir yüzey üzerine dökülüp çözücü tamamen buharlaştıktan sonra yüzey mikroskop ile taranmıştır. Yüzey üzerinde kalan polimer zincirleri ve kümeleri görüntülenmiştir. Parçacıkların yükseklik, uzunluk, ve hacimleri ölçülmüş, tek bir küme içerisinde bulunan ortalama zincir sayısı hesaplanmıştır. Sıcaklık artışı ile parçacık boyutunun artışı tek bir zincir dönüşümü mü yoksa zincirlerin kümelenmesi sonucu mu oluştuğu tartışılmıştır.

CHAPTER 1. INTRODUCTION

A nanometer, one billionth of a meter, is about the length of seven carbon-carbon bonds. One tenth of this length, furthermore, is equal to the size of an atom. A carbon atom, for example, is ca. 0.15 nm in diameter. A single atom has no function alone; however, when atoms adhere to become the size of a nanometer such as the Buckyball, carbon nanotube, or nanoparticle, they suddenly acquire properties of functions such as conductivity or mechanical property etc. A nanometer, thus, is the size of the smallest functional unit [1]. Feynman defines atomic size in relative terms: "if an apple is magnified to the size of the earth, then the atoms in the apple are approximately the size of the original apple" [2]. The materials at this scale display unusual electronic and mechanical properties because of intermediate size and large surface area to volume ratios. The nanometer sized materials exhibit unique electronic, optical, and catalytic properties [3]. The percentage of surface atoms increases when the materials become smaller. The increasing proportion of the surface atoms makes small materials highly reactive due to their large surface area. For nanomaterials, unlike the conventional solids, almost every atom participate in the mechanism. Hence, nanomaterials provide cost benefits because of obtaining required surface area by using small amount of material.

The origin of the current scientific activity on the nanoscale dates back to 1861. The term colloid was used by the British chemist Thomas Graham to describe a solution which has sub-micron particles in suspension. The concept of nanotechnology is attributed to the Nobel prize laureate Richard Feynman in a 1959 lecture [4]. In 1930, Langmuir-Blodgett developed monolayer films of organic molecules and Formhals reported the electrostatic spinning of continuous polymeric nanofibers in 1934. Uyeda demonstrated the formation of diffraction patterns of nanosize crystals by electron microscope in 1960; twenty years later, clustering phenomena was defined as the aggregation of less than 100 molecules [5]. New characterization equipments have played central role in the improvement of nanoscience and nanotechnology. The ability to characterize nanomaterials has been increased greatly by the invention of (Scanning Tunneling Microscopy) STM and (Atomic Force Microscopy) AFM. In 1986, Binnig developed the STM, the father of the AFM. This invention allows probing nanoscale objects and 'seeing' atoms, hence making

nanotechnology possible. Exploring C_{60} clusters in 1985 [6] and carbon nanotubes in 1991 [7] have opened the age of carbon nanotechnology.

Nanomaterials are not new. As a matter of fact, nature has been utilizing nanomaterials for millions of years. For example, several species of aquatic bacteria use the Earth's magnetic field to orient themselves. All magnetotactic bacteria contain magnetosomes [8], which are magnetic mineral particles enclosed in membranes. The magnetosome mineral particles are magnetite, Fe_3O_4 , [9] and are characterized by a narrow size distribution, and species-specific crystals [10]. They are arranged in one or several chains. The particle sizes range from 40 to 100 nm, which are within the permanent single-magnetic-domain size range for magnetite.

Three independent studies were presented in this thesis. The main theme of all three concentrate is the preparation of polymer based nanoscale materials by using solution processing techniques. The systems, sample preparation, and characterization techniques are presented separately in the following three chapters. A brief background of the studies covered in the text is as follows:

(i) The first project we focused on is the metallization of polyacrylonitrile based nanofibers with transition metals, palladium and silver. The growing interest of metal nanoparticles stems from the various applications that metallized nanofibers can be used for as catalyst, electronic and optical sensors, solar energy absorbers and light weight mirrors [11]. Electrospinning is a fiber fabrication technique that produces continuous polymer fibers with submicron diameters by using a uniform electrical field. As a result, a porous film, namely fiber mat, composed of nanoscale thin fibers is obtained. Such thin fibers provide very high surface area to volume ratios and are of interest for many applications in nanofiber textiles, composite reinforcement, sensors, biomaterials and membrane technology. Since polyacrylonitrile fibers are the precursor of carbon nanofibers, polyacrylonitrile based copolymers were electrospun and used as substrates in our experiments. Two different routes have been developed for depositing metallic nanoparticle onto electrospun nanofiber surfaces: One is the electrospinning of metal salt with polymer solution and then reducing metal cations in a reducing media; the other route is the modification of the nanofiber surface with a reducing agent and nucleating the metal particles on the fiber surface with electroless plating technique. The diameter of the nanofibers can be precisely controlled by the viscosity of the solution subjected to electrospinning [12]. The size of particles deposited on the electrospun fibers can also be tuned by changing the content of comonomer on the backbone. Electrospun mat coated with metal nanoparticles falls well within the definition of nanomaterials. The large surface area provides a greater potential as a catalyst. Pd is a well known highly selective and active

hydrogenation catalyst. The electrospun mats supported Pd nanoparticles have been investigated in the hydrogenation of the unsaturated alcohol (dehydrolinool 3,7-dimethyl oct-6-ene-1-yne-3-ol, DHL).

(ii) The second project deals with thermoelasticity study of silica filled, poly(dimethylsiloxane) (PDMS), networks. Nanometer sized silica particles are mixed into the hydroxyl ended PDMS chains which are end-linked with tetrafunctional crosslinker. PDMS chains cover the silica particles and form a thin layer of immobilized chains adsorbed to their surface [13]. Chain immobilization is caused by a loss of configurational entropy due to chain anchoring to the silica surface [14]. The chains in the bulk amorphous elastomer have the full freedom of taking all possible configurations between two cross-link points. However, the presence of nanometer size fillers results in a mobility gradient of the chains that play an important role in thermal properties such as heat capacity and glass transition temperature [14-16]. We claim that chains situated at the interface alter the elastic property of the materials as a function of temperature.

(iii) The third project is the AFM study of the dimensional change of high molecular weight PS (polystyrene) molecules in (cyclohexane) CH solution at different temperatures. Long PS molecules undergo a large dimensional change, called transition, in the range of 25 to 50°C [17]. The observation of large dimensional changes in single chains at easily accessible temperatures is especially important for technological applications at the molecular scale. Identification of the morphology of the PS clusters is of interest due to its direct applications in biological molecules such as DNA packing and protein folding. The morphology of the clusters is determined with the scattering technique when all details of morphology cannot be easily extracted. AFM has proved a powerful tool for the visualization of single polymer molecules [18]. Scattering studies suggest that long PS molecules show slow phase transition and clustering in CH solution [19]. In the present work, AFM operating in tapping mode was employed to obtain structural information of PS molecules at different temperatures in the dry state.

The one is capable of preparing advance materials with tailored properties by employing solution processing techniques [20]. The films mentioned above were prepared by means of homogenous polymer solutions at ambient conditions without using high technology equipment and high energy consumption. The processibility of the polymeric molecules in solution allows better control over nanoscale structure and facility in preparation steps. Metals (Pd and Ag) and ceramic (SiO_2) are used as complementary materials in the nanocomposite films. The ability to process nanocomposite films provides new tailor-made materials and technological opportunities.

CHAPTER 2. METALLIZATION OF POLYMERIC ELECTROSPUN NANOFIBERS

2. 1. Background

Metal nanoparticles have been gaining importance in fields of physics (quantum optics), chemistry (catalysts), and nanotechnology. Chemical and physical properties of nanoscale metal clusters are quite different from those of bulk metals [1]. The major difficulty in working with nanoparticles is their undesirable agglomeration to form larger particles. To prevent formation of such agglomerates, surfactants [21-22], ligand exchange materials [23-24] and polymeric carriers [25] have been used extensively. One new approach can be the deposition of nanoparticles directly on electrospun fibers from metal ion solution. A large surface area substrate, fiber mat, is produced by electrospinning in the first step and then well-separated nanoparticles are produced on the fiber mat by employing bottom-up approaches.

Electrospinning is a fiber fabrication technique producing continuous submicron diameter polymer fibers by using an electrical field [26]. In the process, a polymer solution is placed into a container that has a millimetre diameter nozzle. An electrical field of several kilovolts is applied between the nozzle and the substrate that also serves as the ground. Under applied electrical force, a thin jet is ejected from the nozzle through to the grounded sheet. Solvent evaporation leaves behind randomly coated nanofibers. Eventually, a porous film, namely fiber mat composed of nanoscale thin fibers, is obtained on the grounded sheet. Such thin fibers provide very high surface area to volume ratios and are of interest for many applications in textiles, composite reinforcement, sensors, biomaterials and membrane technology.

This work presents the fabrication of nanofibers with well-separated nanometer sized metal particles. Two recipes are used to synthesize Pd and Ag particles on poly(acrylonitrile-co-acrylic acid) (PAN-AA) and poly(acrylonitrile-co-

glycidylmethacrylate) (PAN-GMA) nanofibers, respectively. In both recipes, metal cations are directly reduced in an aqueous media. In both systems, polyacrylonitrile (PAN) based copolymer is chosen as the substrate material because of its good electrospinnability. The comonomers are incorporated into the chains to functionalize the PAN backbone. The metals, incorporated into electrospun fibers, are selected from transition elements due to their possession of high catalytic activity in organic reactions such as hydrogenation of unsaturated hydrocarbons, and epoxidation of butadiene. Silver and palladium also find applications in solar energy absorption, and light weight mirrors.

2. 2. Palladium / Poly(acrylonitrile-co-acrylic acid) system

Catalytic Palladium (Pd) nanoparticles on electrospun copolymers of (PAN-AA) mats were produced via reduction of PdCl_2 with hydrazine. Fiber mats were electrospun from homogenous solutions of PAN-AA and PdCl_2 in dimethylformamide (DMF). Pd cations were reduced to metallic Pd when fiber mats were treated in an aqueous hydrazine solution at room temperature. Previously, hydrothermal reduction [27], aqueous solution of alkali borohydrides and hydrazine media [28] were used to reduce metallic salts to metal particles. Recently, Gui et. al reported on the reduction of first row [3d] transition metal complexes in aqueous hydrazine solution [28]. A number of studies were performed to synthesize noble metal particles of different elements starting from micellization of polymeric templates in an aqueous medium [29, 30]. The key factor of this method is to synthesize a soluble copolymer making micellar [30] or dendritic [29] structures which have enough space at the core for smaller metal salt molecules. Following the reduction process of the metal salt, uniform sized stable metal nanoparticles were formed. This is a result of fine control over micelle morphology. Various parameters like type of reducing agent and pH of solution and type of copolymer (diblock, branched or star) [31] affect the nanoparticle size as well.

Palladium is known for its selective catalytic activity in hydrogenation of dienes and olefins [25], enamine synthesis [32] and amination of halopyridines [33]. Ledoux et al. observed that carbon nanotube supported Pd accelerates selective hydrogenation of cinnamaldehyde significantly [34]. Reneker and his co-workers

utilized electrospun fibers for catalytic purposes [35]. In the present work we also report on the catalytic activity of Pd nanoparticles on nanofibers for the hydrogenation reaction of unsaturated alcohols.

2. 2. 1. Experimental

2. 2. 1. 1. Solution preparation and electrospinning

The synthesis of PAN-AA copolymers was accomplished in dimethylformamide at 68°C in argon atmosphere. Azo-bis-iso-butyronitrile (AIBN) was used as an initiator. Monomer concentration was 35 wt %. Polymerisation reaction was completed in 11 hours. The polymers used in the experiments have viscosity molecular weight (M_n) in the range of $100 \pm 20 \text{ kg mol}^{-1}$. The molecular weights of the synthesized copolymers were characterized by viscosimetry. Two different compositions of copolymers were prepared (i) 5.4 % mol AA (ii) 8.1% mol AA. 500 Mhz NMR (Varian 500 MHz) was employed to determine the AA content on the copolymer backbone by peak integration technique. The composition of the AA monomer in solution is approximately equal to the composition of AA on the backbone. The solutions were prepared at room temperature by stirring to facilitate the dissolution of PdCl_2 . The compositions of solutions which were subjected to electrospinning are given in Table 2.1. Since the solutions are water sensitive, preparations were carefully carried out in dry environment. The electrospun fiber mat deposited on the cathode was removed easily and immersed into dilute hydrazine water solution. A dilute aqueous solution of hydrazine was prepared in the ratio of 1:200 ($V_{\text{hydrazine}}:V_{\text{water}}$). Aqueous hydrazine solution is a nonsolvent for both PdCl_2 and PAN-AA copolymer and a reducing agent for PdCl_2 . Metallic Pd atoms appear after several hours of reaction time in the immersed state. The colour of the film turns dark grey, indicating that the Pd^{+2} ions are reduced to Pd^0 metal particles. The intensity of the colour depends on the amount of PdCl_2 used. The electrospun mats were then washed with distilled water 8 times and were dried.

The samples prepared from the solutions of A, B, C, and D are illustrated as A', B', C', and D' respectively.

Table 2.1. Compositions of PAN-AA copolymer solutions.

Solutions	AA, mol%	Poly. Conc.(% wt)	PdCl ₂ (%wt)*	Pd(% wt)†
A	5.4	8	0.63	0.4
B	5.4	8	1.25	0.75
C	8.1	8	1.25	0.75
D	5.4	8	8.3	5

* Weight of PdCl₂ divided by weight of polymer

† Weight of Pd atom divided by weight of polymer.

2. 2. 1. 2. Characterisation of fibers and metal nanoparticles

The morphology of the fiber mats, fiber diameters, and the distribution and size of the palladium particles/agglomerates were investigated using conventional (JSM 840-A, JEOL, Tokyo, Japan) and low voltage-high resolution FEG-SEMs (field emission gun scanning electron microscopes, ESEM-FEG, FEI, Eindhoven, Holland). Samples were either spun onto aluminium foils for SEM investigations or on copper grids for investigations with a transmission electron microscope (TEM) (JEM 2000FX, JEOL, Tokyo, Japan). The SEM resolution was adequate to determine the diameter of the fibers and the size of the palladium agglomerates. The primary particle and crystallite sizes of the Pd-particles were determined using a TEM. The small subunits are defined as the primary particles. A particle may consist of several subunits. Energy dispersive spectroscopy (EDS) attached to the TEM was employed to determine the chemical composition of the polymer fibers as well as the chemistry of the particles on them. For TEM and high voltage SEM investigations, samples were coated with carbon. Several samples were studied with the low voltage SEM (at 0.8 to 2 kV) without coating, to determine if the Pd particles are on or in the polymer fibers. X-ray analyses were performed using a powder diffractometer (Bruker AXS, D8 Advance, AXS, Karlsruhe, Germany). A piece of mat was placed on to the sample holder and was scanned over more than 20 times to improve the signal to noise ratio of the data. Scans were made from 30° to 90° (2 θ) with the speed of 0.02° per second. The size of the Pd particles was estimated from X-ray peak broadening in the diffractograms and from the TEM and SEM images. Fiber diameters were determined

from TEM and SEM micrographs. Average Fiber Diameter (AFD) and size of Pd particles were measured for all samples by using at least 40 representative data points.

2. 2. 1. 3. Method of hydrogenation

Catalytic properties of PAN-AA copolymer containing Pd were investigated via hydrogenation of dehydrolinalool (3,7-dimethyloctaen-6-in-1-ol-3) (DHL). The procedure for determining catalytic activity measurements were described elsewhere [36,37]. Figure 2.1 shows the hydrogenation reaction of acetylene alcohol (DHL), which is a heavily used intermediate product of vitamin A, E, and K synthesis. A selective hydrogenation of dehydrolinalool leads to the formation of linalool (3,7-dimethyl-1,6-octadien-3-ol) (LN). In contrast, a non-selective process yields 3,7-dimethylokten-6-ol-3 (DiLH). Copolymers of PAN-AA with 5.4 and 8.1 mol % AA, containing 0.75 % Pd were analysed (Sample *B'* and *C'*) in terms of catalytic activity.

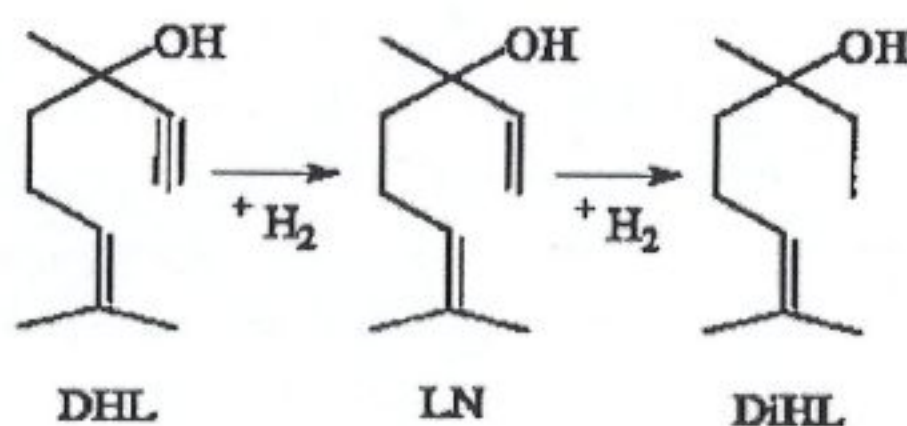


Figure 2.1. Hydrogenation reaction of dehydrolinalool (3,7-dimethyloctaen-6-in-1-ol-3) (DHL).

2. 2. 2. Results

2. 2. 2. 1. Electrospinning

PAN based fibers, the precursors of carbon fibers, having diameters 165 ± 35 nm were obtained by applying an electrical field of 1.8 kV/cm to the polymer solutions. Precise measurements of fiber diameters were performed on 20 test fibers. PAN was chosen with its comonomer AA as a model system. Copolymers with (a) 5.4% wt. and (b) 8.1% wt. AA were successfully electrospun from DMF. Figure 2.2 displays representative electron microscope images of PAN-AA nanofibers,

electrospun from these two copolymer solutions, (a) 5.4 % mol and (b) 8.1 % mol, respectively. Electrospun mats were easily detached from the grounded Al foil with a size of 3 x 5 cm² and their specific surface area was estimated from their diameter to be on the order of 25 m² per gram of polymer.

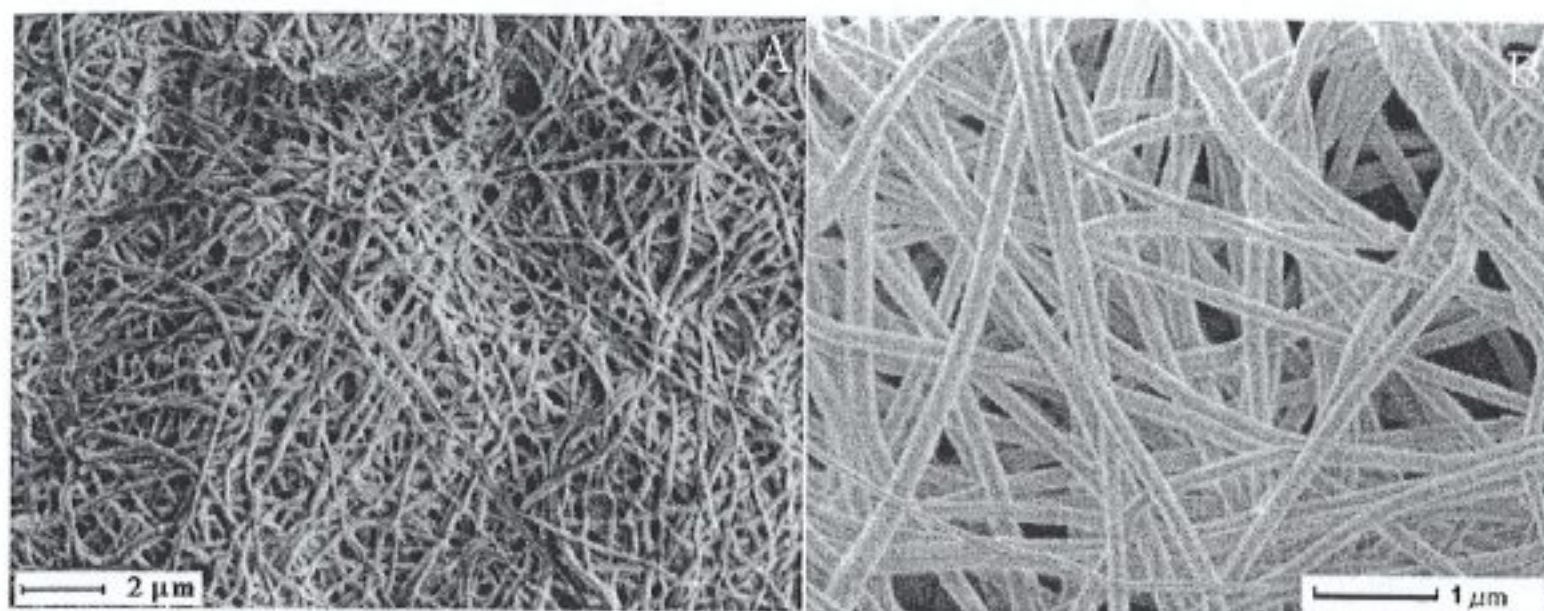
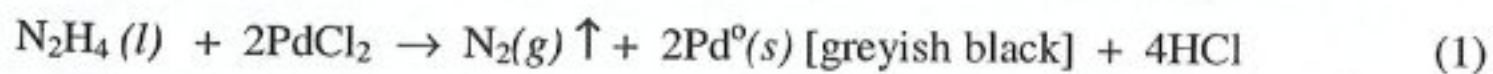


Figure 2.2. Electron microscope images of nanofibers electrospun from 8 % wt. PAN with (a) 5.4 % mol AA (b) 8.1 % mol AA under 1.8 kV/cm.

2. 2. 2. 2. Characterisation of Pd nanoparticles

Characterisation of Pd particles was performed mainly on four samples which are obtained from electrospinning of solutions A, B, C and D. Pd particles were produced inside the electrospun mats by reducing PdCl₂ with hydrazine hydrate. Pd particles were detected by XRD, imaged by electron microscopy and identified by EDS. Particle agglomeration was determined by X-ray peak broadening, and high resolution SEM and TEM techniques. Aqueous hydrazine in a basic solution is a powerful reducing agent, i.e. an electron donor [38]. The redox reaction of PdCl₂ in hydrazine solution is illustrated as follows:



The oxidation-reduction reaction proceeds with the appearance of bubbles on the electrospun fibers. These bubbles are the N₂ gas according to Eq.1.

Figure 2.3 illustrates the X-ray diffraction pattern for PAN-AA with different amounts of comonomer and PdCl₂ before and after the reduction process of Pd cation.

Five peaks were detected on the X-ray diffraction pattern between 30–90°. The main peak appeared around $2\Theta = 40.1^\circ$ corresponding to the (111) peak of Pd. The other four peaks were at 46.6°, 68.1°, 82.1°, 86.6°. The bars in the graph are from the JCPDS (Joint Committee on Powder Diffraction Standards) reference diffraction data file for Pd. The diffraction peaks from the fiber mats with Pd matches the reference for synthetic Pd. The curve labelled with the open square shows the XRD spectrum of the electrospun mat before the reduction process. The difference between this curve and other X-ray diffraction curves shown in the Figure 2.3 indicates the commence of the reduction process from Pd cation to Pd metal in aqueous hydrazine solution. The full width at half maximum (FWHM) of the spectra indicates different particle sizes. The dimensions of the Pd particles were estimated by using Debye-Scherrer formula ($\beta = 0.9 \times \lambda / (\text{FWHM} \times \cos \theta)$) [39]. β is the size of the Pd crystals, presented in the fifth column of Table 2.2. The FWHM values of the diffraction peaks are given in the fourth column of Table 2.2. The calculated average size of Pd particles was 11.5 nm when acrylic acid content of copolymer is 5.4% mol and 14.5 nm when acrylic acid content is 8.1% mol. The sixth column of Table 2.2 corresponds to the approximate number of crystallites in average agglomerate whose size is determined by electron microscopy. In Table 2.2, dimensions of PAN-AA fibers and Pd particles are presented. Four samples were electrospun from solutions of equal polymer concentration including two different constituents. Solutions A, B and D contain same copolymer, which has 5.4% AA, but PdCl₂ concentrations were different. Solutions B and C have equal amounts of PdCl₂, in contrast to solutions A and D, they include polymers with different AA contents. Results of measurements on fiber diameters are presented in the second column of Table 2. Peak values of the size distributions of Pd particles are presented in columns 3 of Table 2.2.

Möller and Spatz [40] pointed out that using micellar diblock copolymer template which is poly(styrene-*b*-2-vinylpyridine), a regular arrangement of 6 nm gold particles with an 30 nm interparticle distance can be obtained. Toluene dissolves preferentially the polystyrene block while polyvinylpyridine is almost insoluble. The solubility difference drives the formation of the micelles. Forster and Keane [41] further made stable gold nanoparticles prepared by reduction of HAuCl₄ in polyvinylpyridine and metallopolymer composite. Particle size can be precisely tuned by the amount of the metallopolymer mixed into polymer matrix

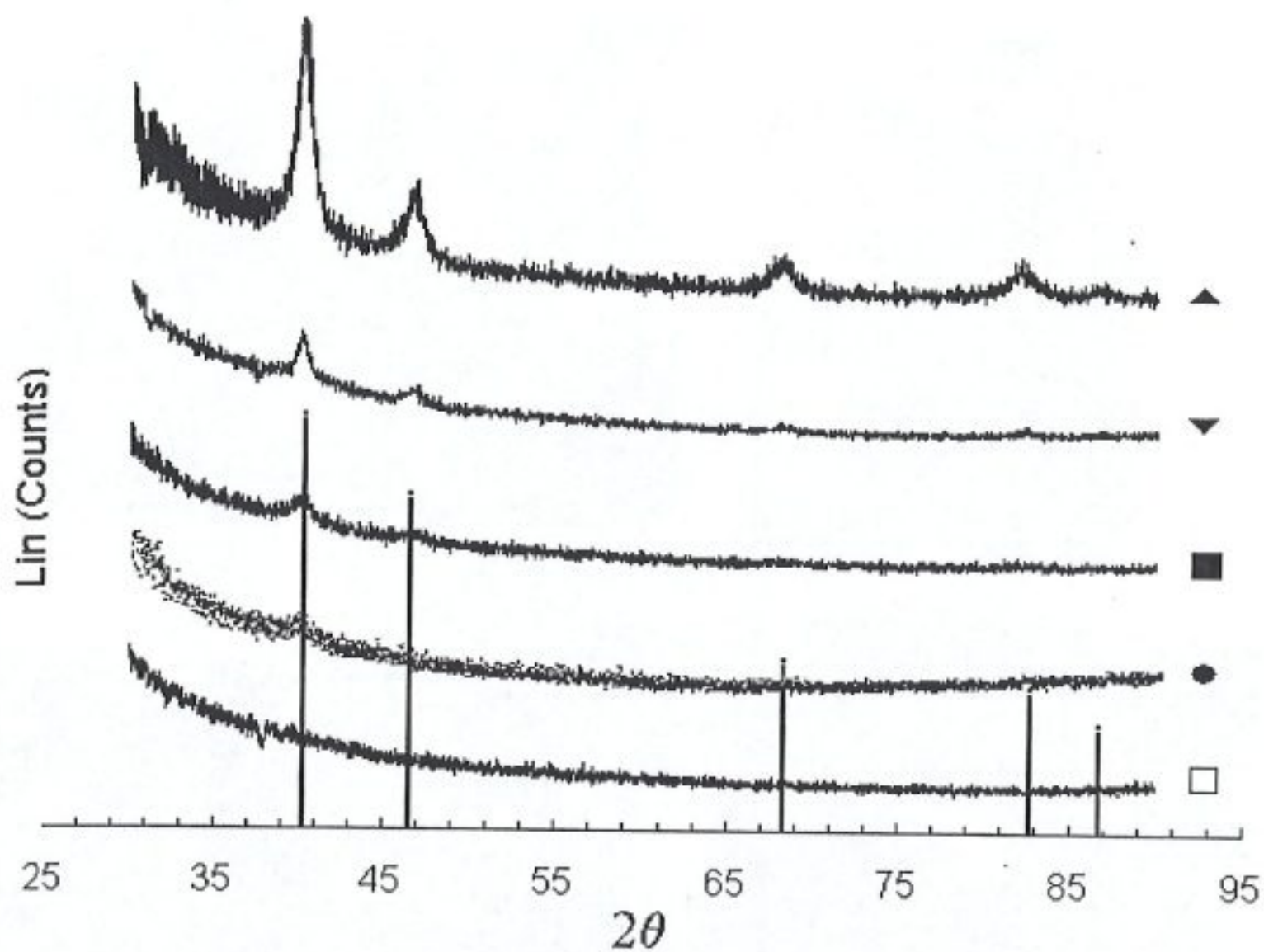


Figure 2.3. X-ray diffraction peaks of mat PAN with

- (□) B before the reduction process
- (●) A after the reduction process
- (■) B after the reduction process
- (▼) C after the reduction process
- (▲) D after the reduction process.

2. 2. 2. 3. Electron Microscopy

Figure 2.4 shows the electron micrograph of mats with Pd nanoparticles in bright contrast. The particles appear to be spherical at this magnification. The atomic number difference between Pd and carbon facilitates imaging of the metal particles.

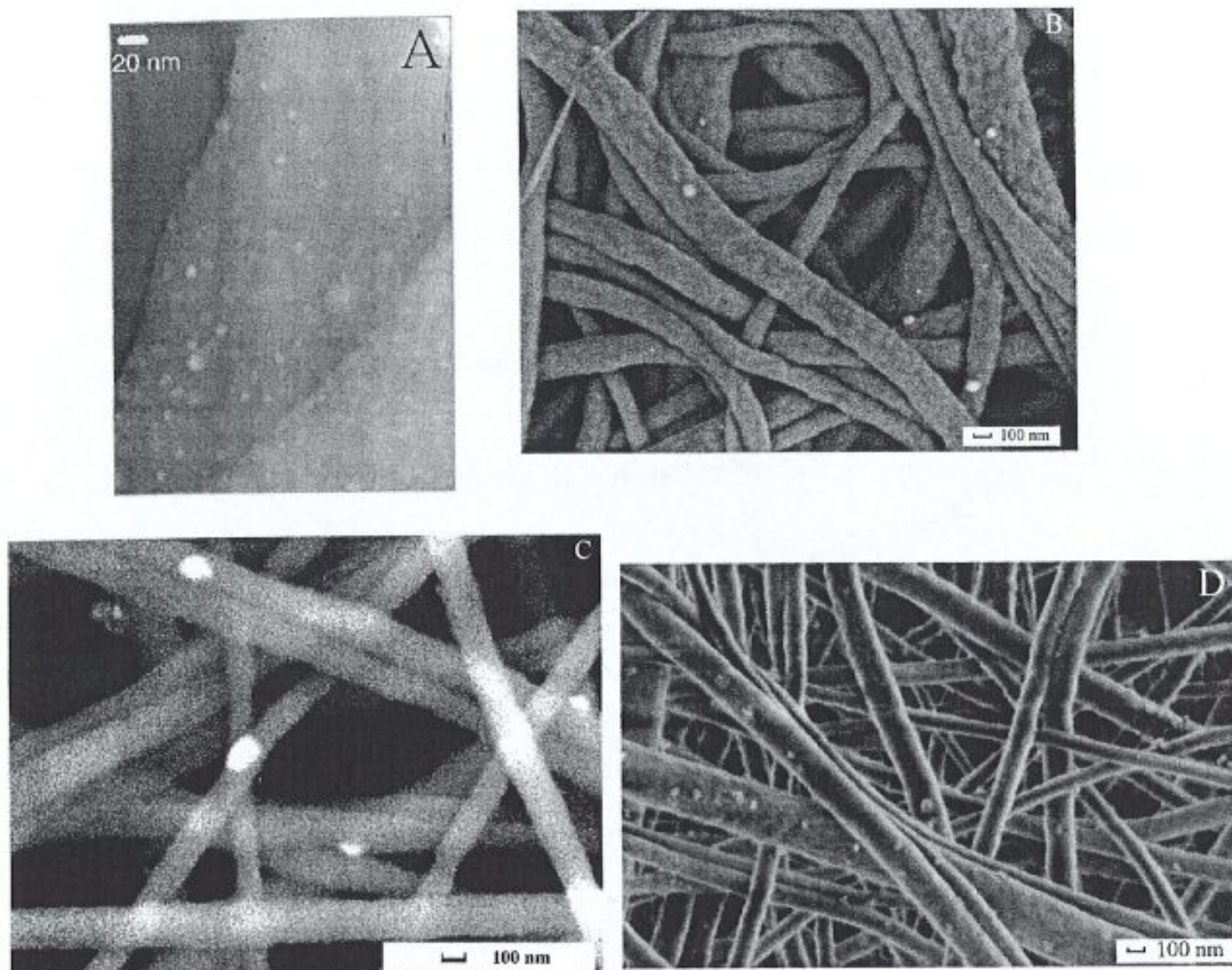


Figure 2.4. Electron microscope images of PAN-AA fibers with generated Pd nanoparticles, (a) Sample A' (b) Sample B' (c) Sample C' (d) Sample D'. Sample A' is magnified 300k times, the others 50k times.

Figure 2.5 illustrates the normalized size distribution of the Pd particles inside electrospun mats for different samples. Precise measurements of particle diameter were performed on 20 test particles. Particle size is larger when the AA amount is higher on polymer chains at constant PdCl_2 concentration in the spinning solution. Increasing the salt concentration (PdCl_2) also leads to larger particles, but the effect is not as dominant as that of the AA concentration. Figure 2.6 shows the particle size observed on electron microscope as a function of PdCl_2 concentration inside the spinning solution, keeping the AA content on the polymer chain constant. Particle size increases as the PdCl_2 concentration increases.

Table 2.2. Dimensions of electrospun PAN-AA fibers and Pd particles

Sample	Peak of AFD distributions (nm) ^a	Peak of Pd particle diameter distributions (nm) ^a	FWHM (°)	Pd crystallite diameter (nm) ^b	Average number of crystallites in particles (agglomerates) ^c
A'	100	10	0.741	14	1
B'	180	20	0.904	11	2
C'	150	60	0.721	14	4
D'	165	30	0.973	11	3

^a Measured and calculated from TEM images.

^b Calculated from X-ray peak broadening.

^c Column 3 divided by column 5.

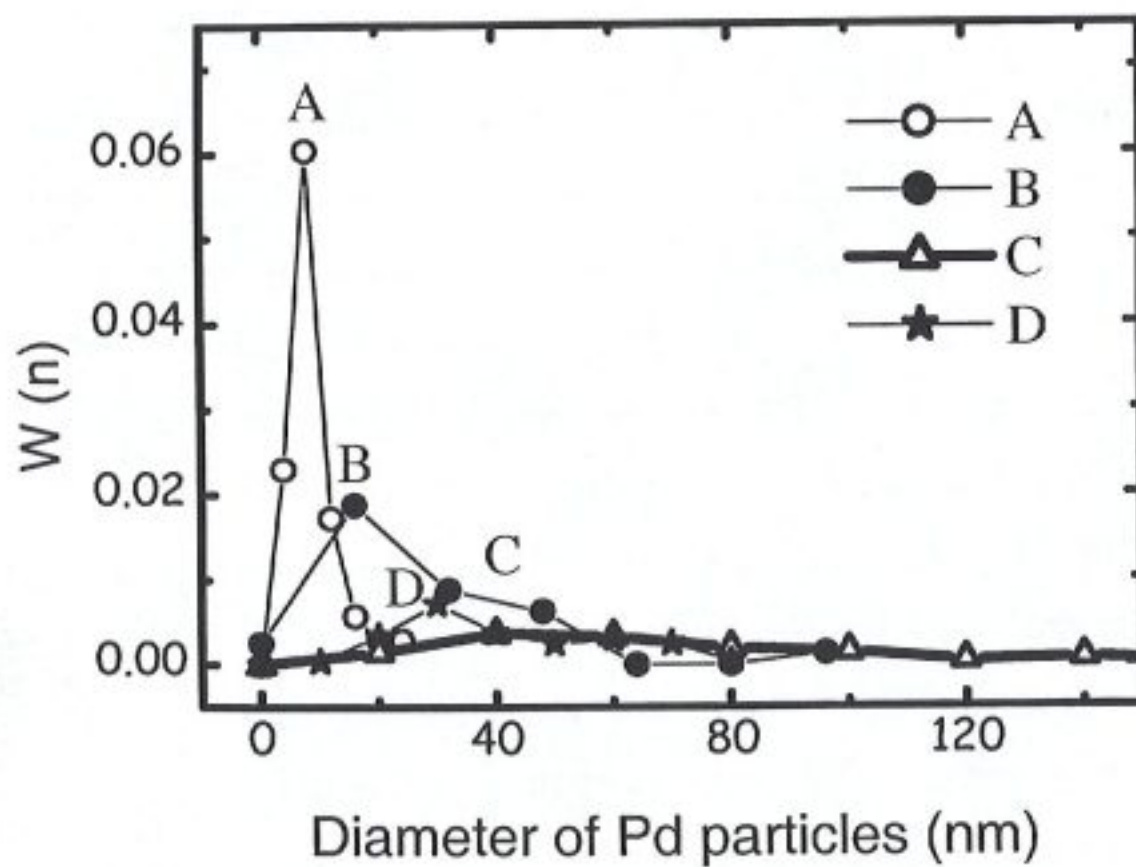


Figure 2.5. Distribution of palladium particle size for samples A', B', C' and D'.

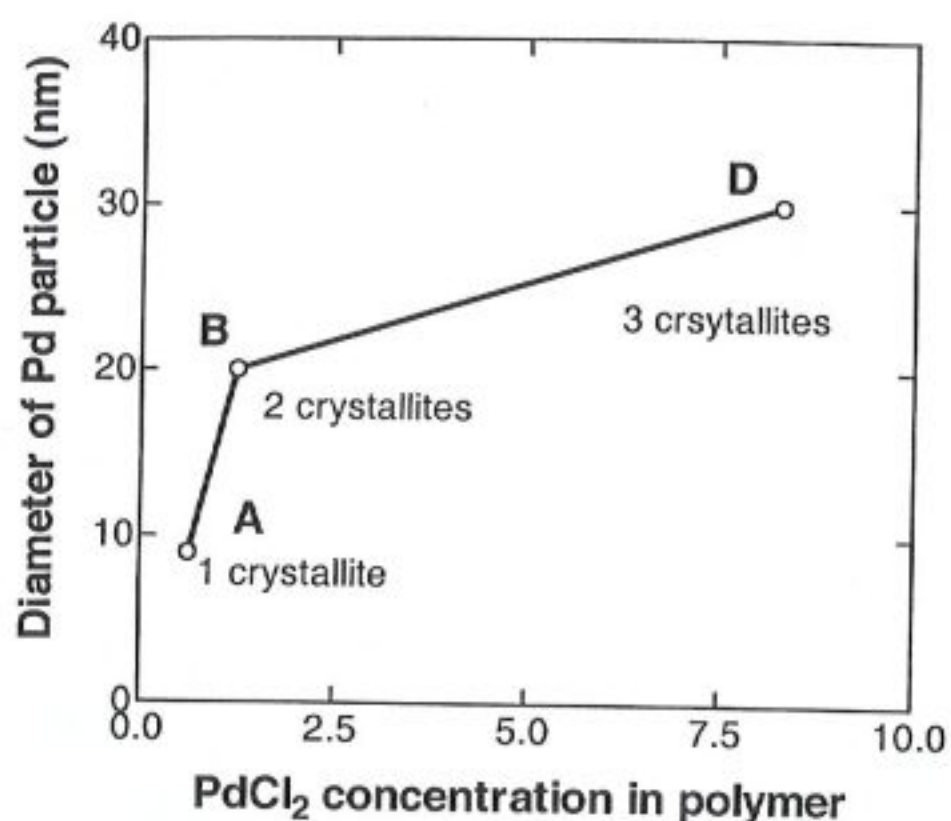


Figure 2.6. Pd particle size as a function of PdCl₂ concentration inside the spinning solutions.

2. 2. 2. 4. Energy Dispersive Spectra

EDS attached to the TEM was employed to identify Pd metal particles. Figure 2.7 illustrates the EDS collected from two regions which are shown at inset on electrospun mats: a) region without and b) region with Pd particles, respectively, for sample B' (see Table 2.1). Along with the presence of Pd peak, Ca and Cu peaks are also seen on the spectrum. The source of Ca may be the tap water used for precipitation of the polymer after finishing the polymerisation reaction. The copper peak comes from the TEM grid. Absence of the Cl peak on the spectra indicates that Pd cations are almost completely reduced. The proposed mechanism is as follows: First, hydrazine molecules penetrate inside the nanofibers and reduce the Pd cations; then the Pd atoms move to the perimeter of the fibers and agglomerate. In fact, high resolution electron microscope images demonstrate that the particles are on the surface of the nanofibers. Cl anions of the salt are removed during washing.

2. 2. 2. 5. Catalytic activity of Pd on electrospun fibers

Catalytic activity of PAN-AA fibers, containing 5.4 and 8.1% of AA and variable content of Pd were studied in the reaction given in Figure 2.1. When

compared to the widely employed catalyst, i.e. Pd particles on Al_2O_3 supports, the catalytic activity of the Pd nanoparticles in electrospun fibers was found to be 4.5 times higher than that of $\text{Pd}/\text{Al}_2\text{O}_3$. This difference is due to the diverse chemical structure of the supporting materials. Organic supports, like polymeric fibers, work better than inorganic supports in organic reactions.

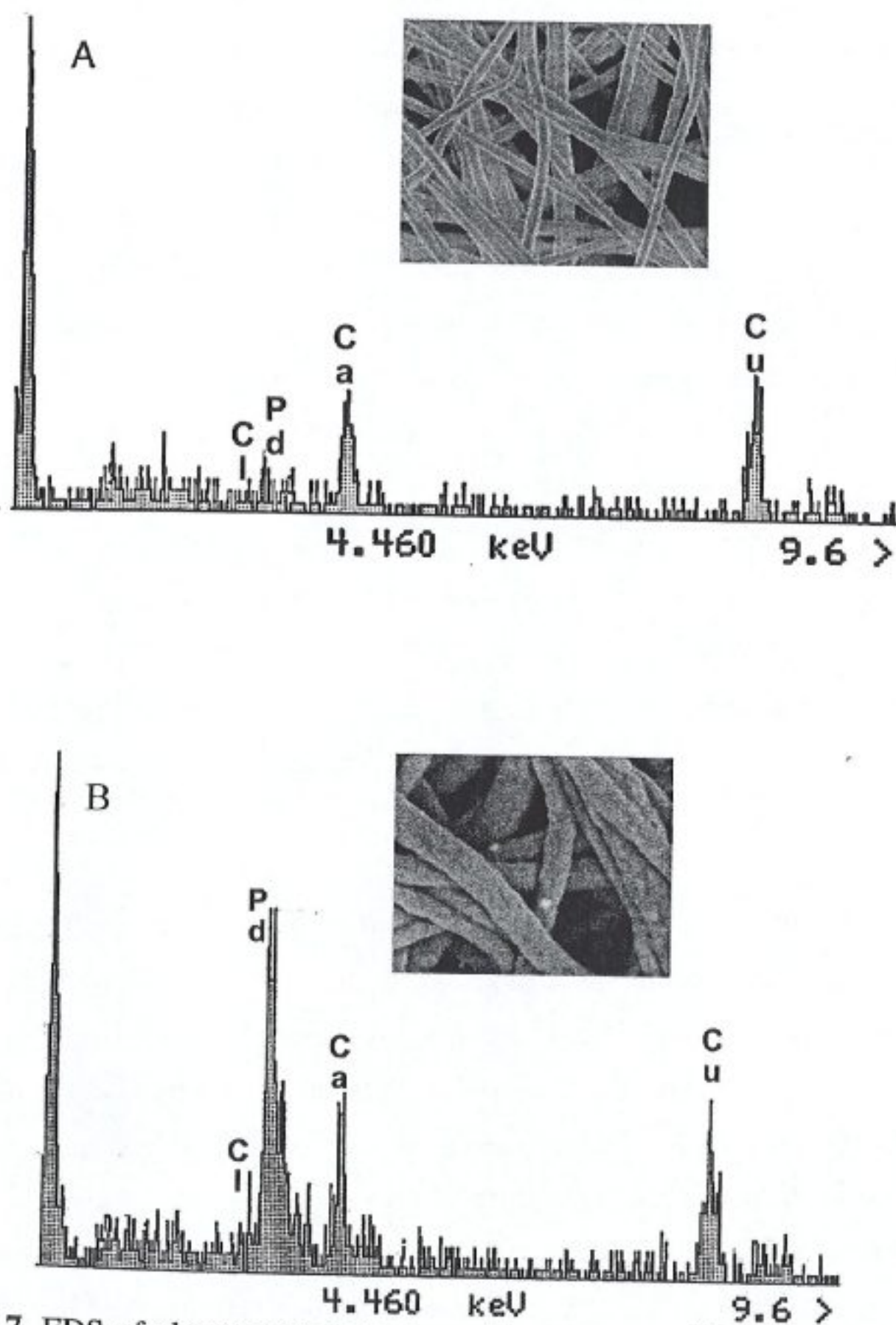


Figure 2.7. EDS of electrospun mats shows the presence of Pd. The analyses were performed on regions (a) without particles (b) with particles for sample B' . The locations of the expected Cl, Pd, Ca, and Cu peaks are indicated.

2. 2. 3. Discussion

Control of particle size and its dispersion is one of the main goals of nanocomposite preparation technology. There are two different levels of particle sizes in our experiments. Comparison of columns 3 and 5 of Table 2.2 shows that the size of Pd crystallites estimated from X-ray diffraction data differs from the data obtained for Pd particle sizes from electron microscopy images. Several primary particles (single crystallites) whose sizes were determined by X-ray, agglomerate and form a cluster that is imaged in SEM. The small subunits are defined as primary particles. They are single grains (crystallites) that form the clusters. Several high-resolution images indicated that the Pd particles were clusters of smaller crystallites. It is possible to estimate the average number of primary particles (crystallites) in such clusters. Two or four primary particles constitute each cluster when the AA concentrations are 5.4 % and 8.1 %, respectively (Sample *B'*, *C'*). In the case of sample *A'*, the size of the particles observed with an electron microscope is less than or equal to the crystallite size detected by X ray diffractograms. Small crystals imaged by the electron microscope may not be detected by XRD due to small crystal effect alone [39]. Most of Pd the particles are single crystallites when PdCl₂ concentration in the initial solution is 0.6 wt % and AA content is 5.4 wt %. When PdCl₂ concentration was increased six times on the same polymer (sample *D'*), an average of three crystallites form an agglomerate.

The amount of acrylic acid on the polymer backbone is the dominant parameter affecting the size of the primary Pd particles. As the comonomer amount increases, the shape of the main peak on the X-ray spectra becomes narrower and the crystallite size becomes larger. A possible explanation of this observation is as follows: The comonomer, acrylic acid, serves as a host for the Pd cation because the latter is attracted to the acrylic acid group due to an electrostatic interaction. During the reduction process, the Pd ion becomes neutral (Pd atom) which can dissociate easily from the acid groups. The Pd atoms come together and nucleate as primary Pd particles whose size can be estimated from the X-ray spectra. Since nucleation of metal particles takes place around acrylic acid groups, the amount and dispersion of acrylic acid on the polymer chain can directly determine the size and dispersion of the Pd crystallites formed. Electrostatic interaction of carboxyl anions and Pd cations cannot be considered as a driving force determining the particle size. When

electrostatic attraction disappears, secondary forces become dominant and particles adsorb on the fibers. The radii of the Pd particles are several times the contour length of the macromolecule. The molecular weight of the copolymer is in the order of 100 kg/mol [29]. Increasing salt concentration increases the number of nucleation sites, namely particle density on the fibers. Consequently, particle size and dispersion can be tuned by the amount of PdCl₂ and composition of the copolymer (i.e. AN to AA ratio). For catalyst applications, the size of the Pd particles produced plays an important role. Smaller particles have larger surface area and accelerate the reaction rate. The area of Pd particles inside per gram of polymer is estimated approximately as 0.1 m² (sample B'). The amount of Pd on the electrospun fiber mat is in the order of 50 mg/g. The present experimental technique does not allow for the determination of the amount of Pd particles lost from the surface during the rigorous washing.

The amount of Pd is a maximum of 5 wt% on the electrospun mat (Sample D'). It is well known that the presence of metal in polymer matrix makes the material conductive. However, this level of metal on fiber mat is not enough for conductivity or any other functionality such as reflectivity. To make use of large surface area metal particles and to increase the amount of metal on electrospun mat, the following project was developed.

2. 3. Silver / Poly(acrylonitrile-co-glycidylmethacrylate) system

Electrospun poly(acrylonitrile-co-glycidylmethacrylate) (PAN-GMA) nanofibers were coated with monodisperse silver nanoparticles by an electroless plating technique, which relies on the direct deposition of metal atoms from metal ion solutions. In the earliest methods of metal plating, a polymeric surface was first activated by reducing agents and then treated with the metal ion solution. In the present method, the reducing agent is immobilized on the nanofiber surface and the metal atoms nucleate on the fibers in the aqueous solution of the metal ion. Electroless plating is applicable to silver plating because silver is a metal on which an autocatalytic reaction can occur [42]. Although many methods are available for coating, such as baking, chemical vapour deposition, and ion-sputtering, the electroless plating method is very effective because the mechanism is simple, can be done on a complex shaped substrate, and is suitable for mass production. Silver is an

efficient catalyst for the following reactions: Oxidative conversion of methanol to formaldehyde [43], and selective and butadiene epoxidation [44].

The novel approach of this work is to produce metal nanoparticles on nanometer size fibers in solution at ambient conditions. The modification of the fiber surface with the reducing agent provides binding sites for nucleation of metal atoms. Glycidyl methacrylate monomer is rather useful, since the pendant oxirane ring can be opened and a range of functionalities can be introduced to the polymer backbone.

2. 3. 1. Experimental

2. 3. 1. 1. Polymer synthesis and metallization of nanofibers

Acrylonitrile (AN) and glycidyl methacrylate (GMA) monomers were polymerised by radical polymerization in dimethylformamide (DMF) using 1 wt% ammonium persulphate initiator, carried out over a period of 24 h at 50°C. P(AN-GMA) was then electrospun from solution in DMF under an electrical field. The details of the electrospinning process were explained in the section 2.2. The spinning process was maintained for nearly 6 hours to obtain a thick electrospun mat that detaches easily from the grounded foil. The electrospun polymer web was immersed into aqueous hydrazine in a 250-mL solution stirred overnight, then filtered and washed with an excess of distilled water that had been deoxygenized with a flow of nitrogen gas. The product was dried at 50°C for 24 hours in vacuum. The hydrazine modified electrospun mat was introduced into a mixture of 25 ml of a 0.1 M AgNO₃ solution, 2.5 ml of a 1 M KOH solution, and 5 ml concentrated NH₃ solution in a closed glass bottle. The mat was kept in metal ion solution for 1 minute, 10 minutes, 1 hour, 3 hours, and then 24 hours to investigate the effect of deposition time on particle size. Thermogravimetric analysis (TGA) was performed using Netzch STA449C under an oxidative media to examine the weight percent of the silver loaded into the electrospun mat. The deposited Ag particles were identified by X-ray diffraction (XRD) and imaged by using scanning (LEO Supra 35) and transmission electron microscopes (JEM 2000FX, JEOL, Tokyo, Japan).

2. 3. 2. Results and Discussion

Copolymer composition was determined by using ^1H NMR. Figure 2.8 shows the ^1H NMR spectrum of the polymer. The proton resonance for the oxirane ring was assigned to the peaks at 3.26 ppm (d), 2.88 ppm, and 2.95 ppm (e). GMA content of the polymer was estimated from the NMR spectra via the integration of the characteristic peaks of oxirane over those of acrylonitrile. The amount of GMA is found as 58%wt on the chain.

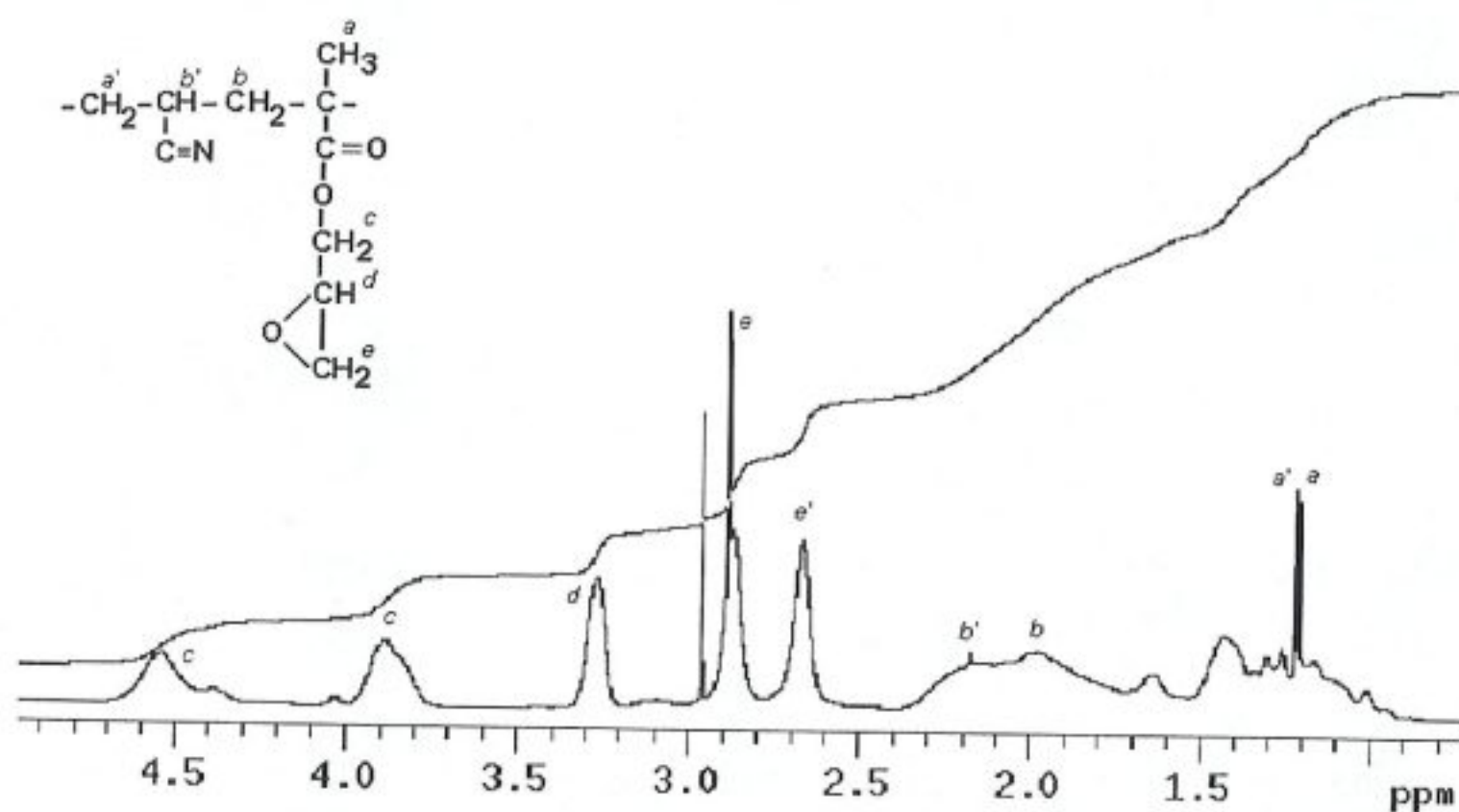


Figure 2.8. ^1H spectrum of poly(glycidyl methacrylate) recorded at 25°C (Solvent : CDCl_3).

The P(AN-GMA) solution, having 30 % wt solid content in DMF, was subjected to 1.53 kV/cm electrical field, and fibers having 274 ± 19 nm diameter on average were obtained. Figure 2.9 shows SEM images of electrospun nanofibers of P(AN-GMA).

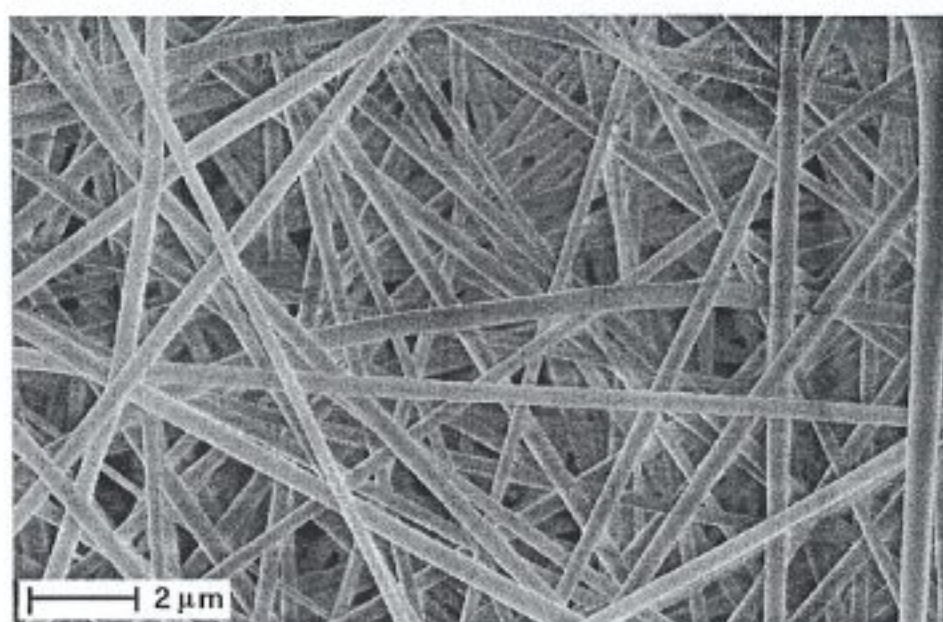


Figure 2.9. The electron microscope image of P(AN-GMA) nanofibers obtained from 30 wt% solution in DMF at 1.53 kV/cm.

A two-step procedure was followed during the preparation of metal-coated polymer nanofibers as illustrated in Figure 2.10.

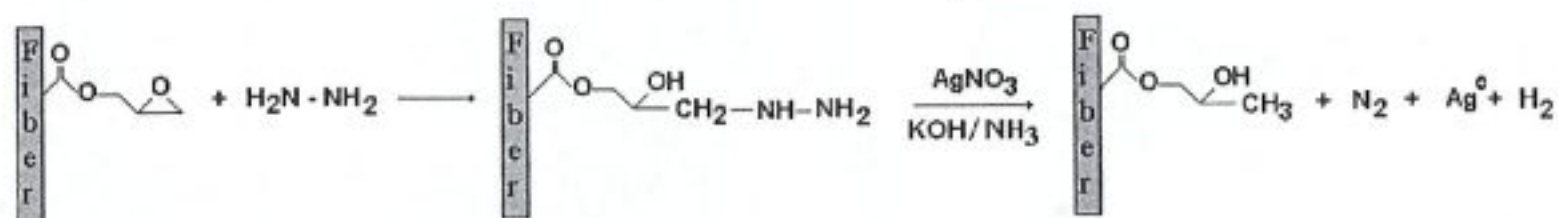


Figure 2.10. Surface modification and metallization reactions of P(AN-GMA) nanofibers.

In the first step, hydrazine, electron donor is attached to polymer fiber surface through the above described reaction. Hydrazine as a strong nucleophile attacks the highly strained three member ring of glycidylmethacrylate. Hydrazination of the oxirane ring was monitored by IR spectroscopy through the disappearance of the bands of asymmetric stretching of oxirane group at 1129 cm^{-1} and appearance of the bands of symmetric stretching of the $-\text{NH}_2$ (primary amine) group at 3216 cm^{-1} , as shown in Figure 2.11 [45].

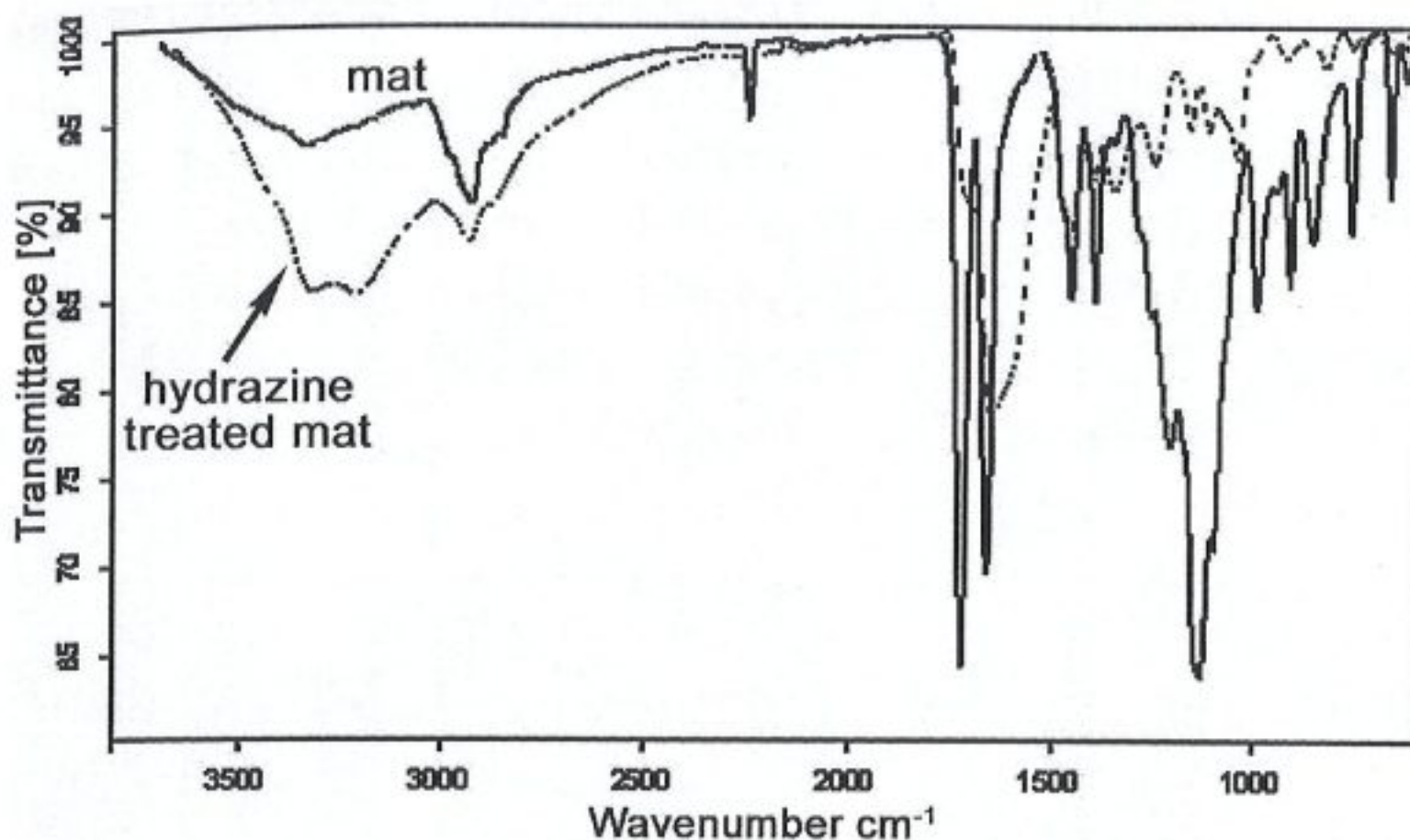


Figure 2.11. IR spectra of P(AN-GMA), (solid line) and hydrazine treated P(AN-GMA), (dashed line).

The morphology of the nanofibers was investigated before and after the hydrazination process. As Figure 2.12 illustrates, the morphology and diameter of fibers remain unchanged after this surface modification.

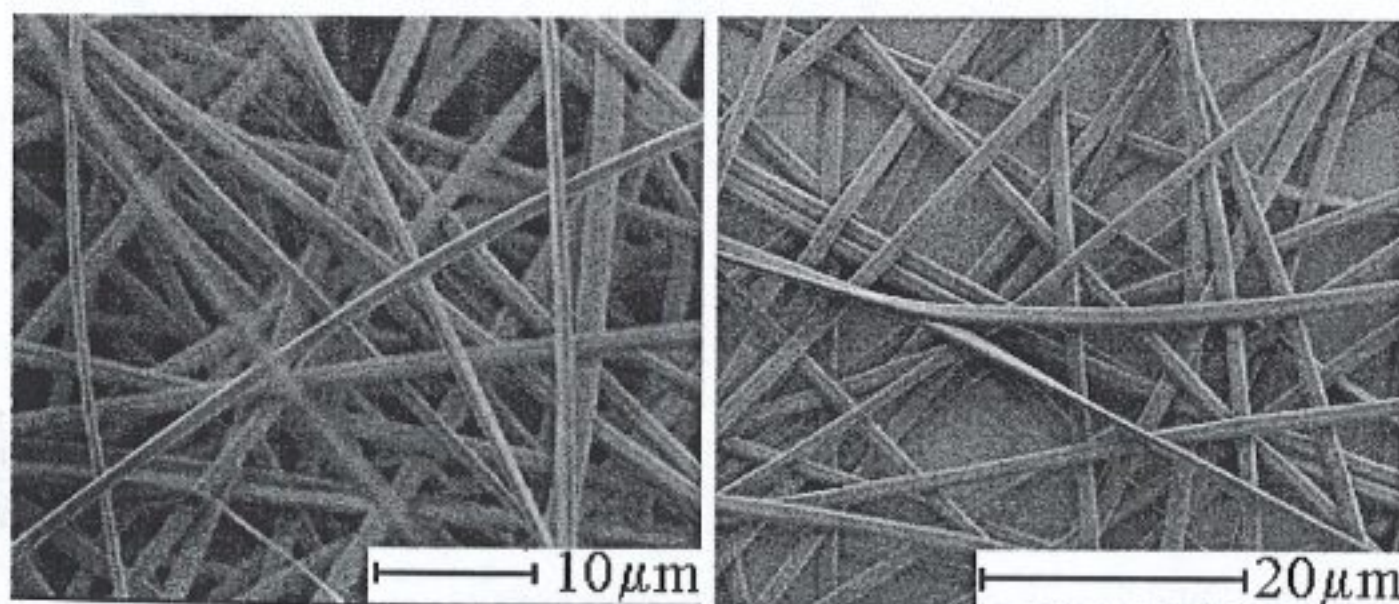


Figure 2.12. Electron microscope images of poly(glycidymethacrylate) nanofibers (a) and hydrazine treated nanofibers (b).

Hydrazine modified electrospun mat was introduced into a solution of aqueous alkaline AgNO_3 . A redox reaction occurs between hydrazine attached electrospun fibers and Ag cations such that the oxidation of hydrazine reduces the silver atoms and deposits them on fibers surface under aqueous alkaline media. Hydrazine is

efficiently used on the fiber surface for metal reductions. In contrast to other deposition techniques (physical or chemical), this method takes place with redox reaction. Figure 2.13 illustrates the XRD curve for (PAN-GMA) after the metallization process. Four peaks were detected on the X-ray spectra between 30–90°. The main peak appeared around $2\Theta = 38.1^\circ$ corresponding to the (111) peak of Ag. The dimensions of the Ag particles were estimated by using Debye-Scherer formula [39]. The estimated average size of Ag particles is 40 ± 3 nm.

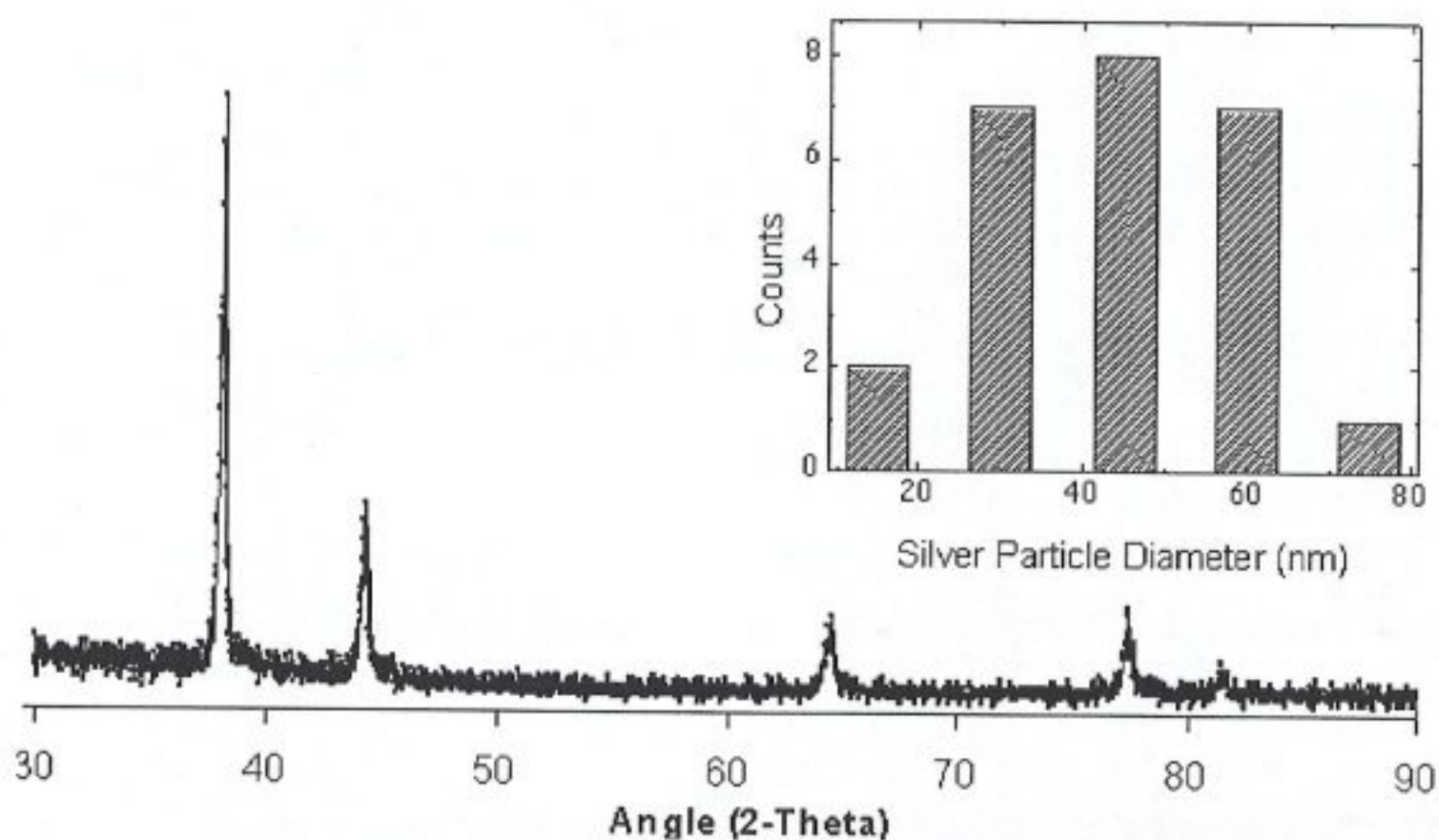


Figure 2.13. XRD of P(AN-GMA) nanofibers. Particle distribution of silver nanoparticles is shown in the inset. The bin size of the distribution is 15 nm.

Figure 2.14 shows the spherical silver nanoparticles on the electrospun nanofibers after the reduction of silver cations. Silver nanoparticles were heterogeneously distributed on the fiber surface. The average diameter of the particles measured from the graphs is 37 ± 5 nm. The particle diameter calculated from peak broadening of X-ray spectra matches with the diameter measured from the electron microscope images (40 ± 3). This result indicates that silver atoms are single crystals.

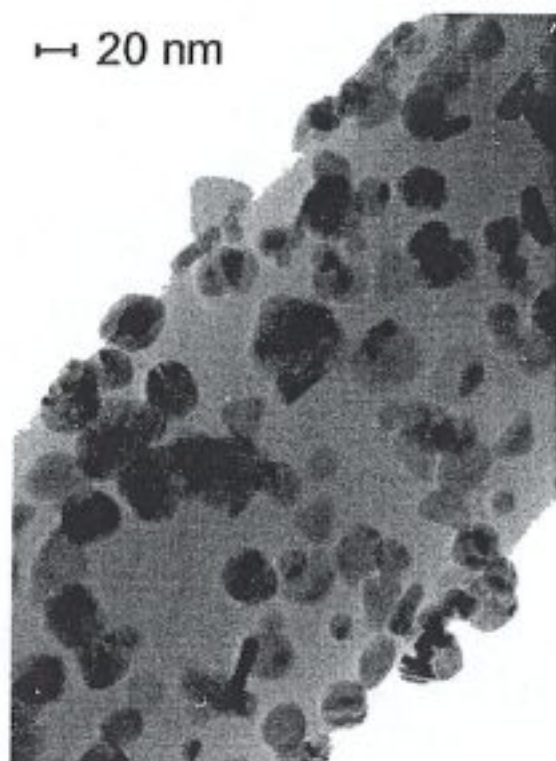


Figure 2.14. Electron microscope images of Ag coated P(AN-GMA) nanofibers. Coating time is 2 minutes.

The P(AN-GMA) electrospun mats were heated in oxidative media to remove the polymer and to determine the amount of metal on the electrospun mat. Thermo analytical curves of P(AN-GMA) and Ag coated P(AN-GMA) are presented in Figure 2.15. Degradation occurs and mass decreases as the temperature increases from room temperature to 1000°C with a 10°C increase per minute. While only 2% of polymer moiety remains beyond 750°C under the thermoxidative environment for electrospun mat of P(AN-GMA), 55% of the total mass was measured at the end of the thermal analysis for a metal deposited sample. Mass difference between the samples before and after the metallization procedure is attributed to the amount of Ag deposited on the electrospun mat. The melting point of Ag is 961°C is observed as an endothermic peak, in the inset of Figure 2.15.

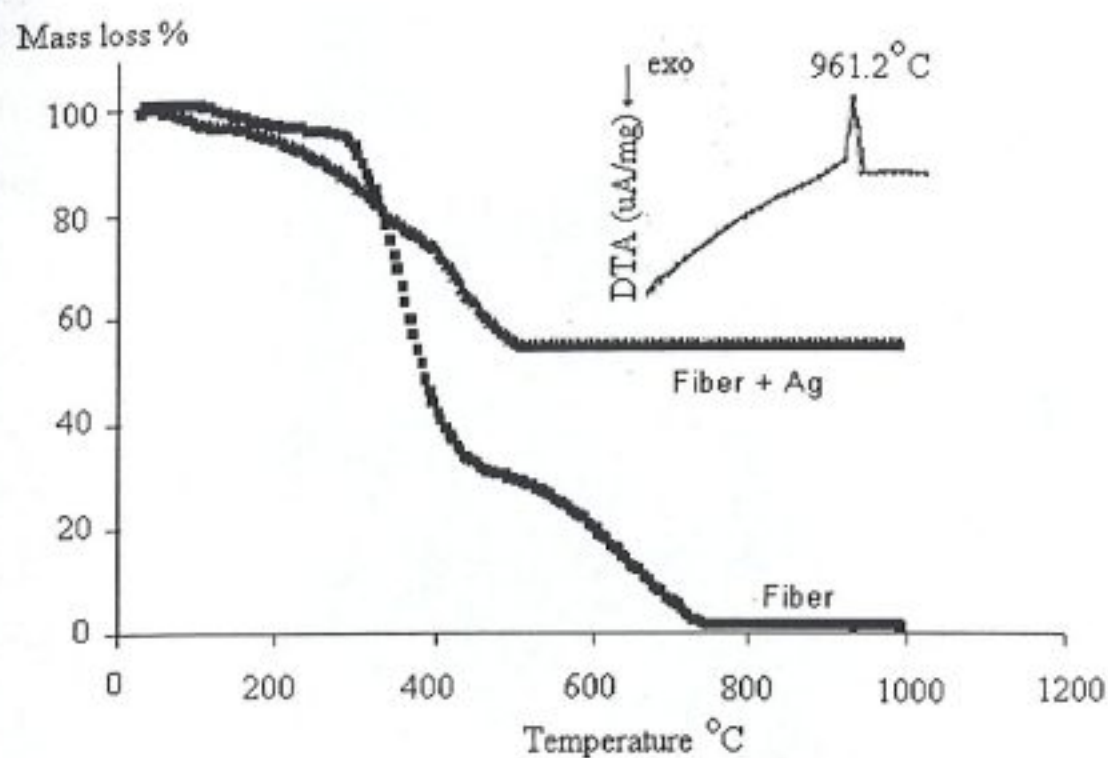


Figure 2.15. Thermogravimetric curve of the electrospun fibers and Ag coated electrospun fibers, and DTA curve of the Ag coated electrospun fibers.

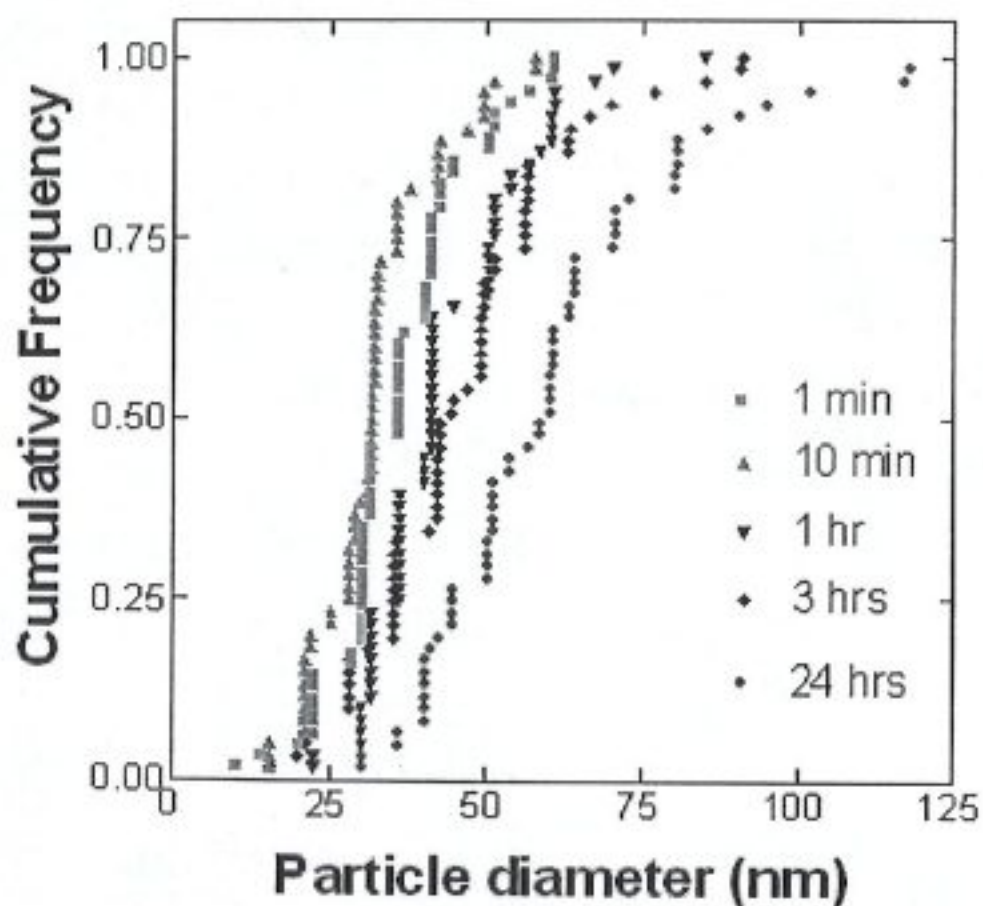


Figure 2.16. Diameter distributions of silver particles obtained in five different coating times.

The particle size was investigated as a function of coating time, i.e. the time duration for the electrospun mat in the metal ion solution. Figure 2.16 illustrates the cumulative frequency of the particle diameters obtained from five different deposition times. Increasing deposition time broadens the distributions and the particle size grows with the deposition time. The size of silver particles is in the range of 35-55

nm. The resistance of the electrospun film was measured before and after the metallization process at room temperature. The electrospun P(AN-GMA) mat was found infinitely resistant, which means that it is insulator, whereas the metallized mat has resistance on the order of 50 M Ω .

The area occupied by the metal particles on fibers surface was measured using an image analysis program. The metal particles cover 35% of the fiber surface on average. The coating is not uniform on a nanometer level. The centre of crystal nucleation is the hydrazinated oxirane molecules on the fibers surface. The density of particle attachment is derived by the formation of reactive sites on the surface. Successful hydrazination reaction may increase nucleation centres and therefore the particles become denser. Well-dispersed silver nanoparticles deposited on several nanofibers are seen on the inset of Figure 2.17. Silver atoms nucleate not only on the fibers but also in the space between the nanofibers.

The uncontrollable crystal growth raises the particle agglomerations which unite fibers together to make nanobundles as can be seen in Figure 2.17. As a result, the pores between electrospun fibers become larger. The actual mechanism of undesirable crystal growth is not fully understood, but it is speculated that the nucleation centres of the two neighbouring fibers which are close to each other adhere and crystal growth makes a bridge among the two fibers. The agglomeration of fibers and nanoparticles reduces surface area to volume ratio of both electrospun fibers and metal nanoparticles.

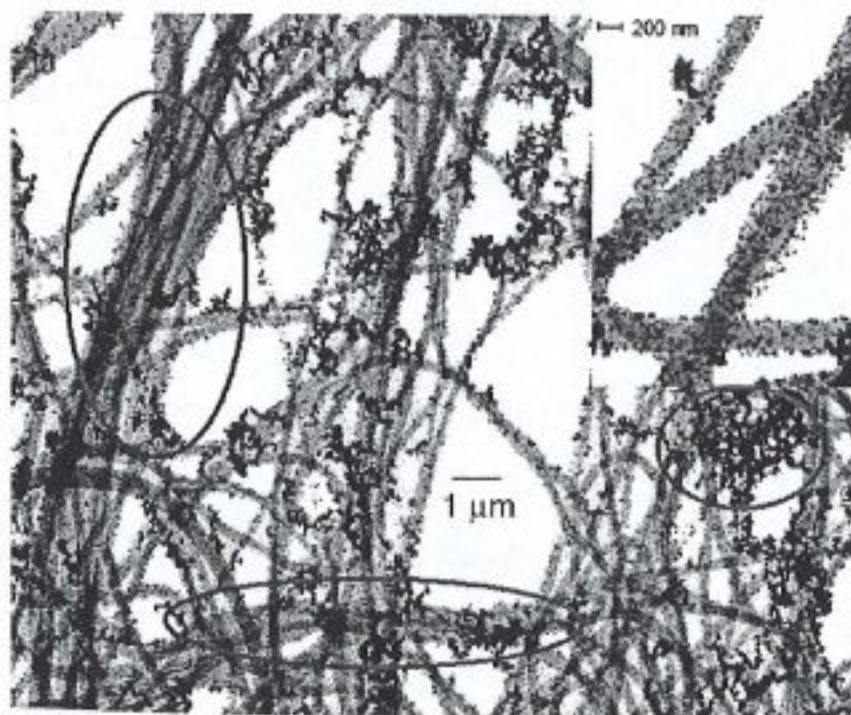


Figure 2.17. Agglomeration of nanofibers and nanoparticles.

CHAPTER 3. EFFECT OF FILLER AMOUNT ON THERMOELASTIC PROPERTIES OF POLY(DIMETHYLSILOXANE) NETWORKS

3. 1. Background

Poly(dimethylsiloxane) (PDMS) is a well-known member of the siloxane family, which is heavily used in the industry. The importance of PDMS comes from its good electrical properties, optical clarity, weather resistance and very low glass transition temperature, T_g ($\sim -120^\circ\text{C}$). Its elastic properties cover a large range of temperatures. However, its mechanical properties are very poor. Additives, particularly silica, are used to improve its mechanical properties and also to protect the optical clarity. There are very few applications of the PDMS elastomers used in the unfilled state. Filler morphology, which is described as particle size and structure, plays a significant role on the degree of elastomer reinforcement [46]. Good dispersion of particles in the elastomer is crucial for achieving high quality. Yuan and Mark reported that precipitation of the silica particles in-situ provides better dispersion of the filler and enhances reinforcement [47]. The statistical properties of PDMS chains are markedly different than other common elastomeric chains. Since the Si-O bond is rotationally flexible, PDMS shows an unusually high degree of chain flexibility. Alternating bond angles in the PDMS chain and the ionic nature of the Si-O bond leads to highly variable conformational behavior.

The reinforcement of PDMS elastomers by fillers has been the subject of numerous studies [48,49]. Earlier work on filled PDMS concentrated on the effects of fillers on macroscopic properties, several examples of which are given in [50]. Effects of molecular structure at the polymer-filler interface and its effects on network properties began to be emphasized only in recent years. Notably, Litvinov et al. studied, by NMR, the structure and behavior of grafted PDMS chains on silica and found that the layer consists of immobilized chain segments at the PDMS-silica interface and mobile chain portions outside the interface [14]. Chains at the

interface exhibit substantial decrease in heat capacity at the glass transition temperature. Some of the PDMS chain units were immobilized as a result of physical adsorption at the silica surface, the amount being proportional to the number of silanol groups at the silica surface. Gussoni et al. also used NMR spectroscopy to investigate silica filled PDMS rubbers, and observed the decrease of segmental mobility of the PDMS chains in the vicinity of the filler surface [15]. Berriot et al. employed ^1H NMR experiments on filled rubbers and observed a layer of immobilized segments at the particle surface [16]. In the case of chains chemically grafted to the silica surface, they observed immobile layers, which they described as a glassy shell around the filler surface. Cosgrove et al. used differential scanning calorimetry and NMR measurements, and showed that the reduction in the mobility of the PDMS chains corresponded to a shift in the glass transition to higher temperatures [51]. These shifts are relatively small; nevertheless, they indicate the presence of a gradient of segmental mobility in going from the rubber towards the silica surface.

Thermoelasticity of filled cross-linked PDMS was studied earlier by Galanti and Sperling who obtained a strong increase in the energetic contribution to the elastic force with increasing filler content [52]. Nanocomposites of fumed silica and PDMS chains were prepared in different levels of composition and thermoelasticity of the samples were performed. Our results qualitatively agree with their results, with the quantitative difference that the energetic contribution in our measurements increases more strongly than theirs with filler amount. A precise quantitative characterization of the filler effect in PDMS networks is important due to their use in technological applications. Sperling's results and ours thus set two different levels of thermoelasticity which should further be investigated. Galanti and Sperling interpreted their results in terms of a semi-quantitative equation of state and attributed the increase in energetic contributions to filler-rubber interface. Their interpretation is now validated by the precise NMR observations, which we discuss further in the discussion section.

3. 2. Experiments

3. 2. 1. Materials

Untreated fumed silica, provided from CAB-O-SIL, was used. The specifications and typical properties of the filler are as follows: The particle size of the silica is 14 nm and surface area is $200 \pm 25 \text{ m}^2/\text{g}$. For surface chemistry, hydroxyl groups cover approximately 45 percent of the surface of the silica making the surface hydrophilic. Elastic modulus and thermal expansion coefficient of bulk amorphous silica are $72.4 \times 10^9 \text{ m}^{-1}\text{kgs}^{-2}$ and $0.5 \times 10^{-6}/^\circ\text{C}$ respectively [53].

3. 2. 2. Network synthesis

The hydroxyl terminated PDMS was end-linked into a network by reacting with an excess amount of the crosslinking agent, tetraethoxysilane (TEOS). The molecular weight of the PDMS is 53 kDa ($n_w = 675$), where n_w is the weight average degree of polymerization. Polydispersity was close to 1.62. The end-linking reaction was performed in solution to facilitate the mixing process and the samples were sonicated to obtain better dispersion of silica particles. The hydroxyl ended PDMS was dissolved in toluene. The desired amount (unfilled, 1, 3, 5 % wt) of silica particles was added to the solution. The mixtures were stirred and later sonicated for two minutes to obtain a homogeneous dispersion. The favorable dispersion effects of sonication were observed by comparing with the atomic force microscope images of samples prepared without sonication. 600 μl TEOS and the catalyst, Tin(II) 2-ethylhexanoate, were added to the dispersion while stirring. The crosslinking reactions were carried out overnight in a teflon mold at room temperature for 24 hours and at 80°C . The thickness of the resulting film was on the order of 1.5-2 mm. The amount of solvent during the end-linking process is not constant due to the evaporation of toluene. An average value of 0.50 is estimated for the volume fraction of polymer during the end-linking process. Higher silica concentration ($>5\%$ wt) in PDMS films could not be prepared due to silica agglomeration. This issue will be discussed further in the Results section.

3. 2. 3. AFM imaging

Tapping mode in air Atomic Force Microscopy (AFM) (Nanoscope IIIa, Digital Instruments) imaging was carried out with oxide sharpened Si tips. Sample surfaces were

scanned without any surface preparation. Dimensions of the silica particles were measured by the image analysis options of the Nanoscope software. AFM images are recorded in the height and phase modes.

3. 2. 4. Sol-Gel Analysis and Swelling Experiments

Sol-Gel analysis was performed to determine the cross-linking degree in two different solvents, toluene and benzene. A small piece of the unfilled end-linked PDMS film was placed in a 30 ml of reagent grade toluene or benzene. The sample was allowed to remain in the solvent for two days at room temperature. The swollen gel was taken from the solvent and dried in a vacuum oven at room temperature. The sol fraction in the end-linked sample was calculated from

$$\% \text{ sol fraction} = [(m_o - m_e / m_o) \times 100] \quad (1)$$

where m_e is the dry mass of the extracted sample and m_o is the initial mass of the sample. Swelling experiments of the end-linked PDMS samples were carried out in the same two solvents. The polymer films were allowed to remain in the solvent for 24 hrs at room temperature and the dimensions of the swollen films were measured as soon as they were taken out of the solvent. Swelling ratios, q_v , of networks at equilibrium were determined.

$$q_v = \text{Volume of swollen network} / \text{Volume of dry network} \quad (2)$$

3. 2. 5. Thermoelasticity Measurements

The dimensions of the samples on which the thermoelasticity measurements were performed are $40 \times 2 \times 2.5 \text{ mm}^3$. The ends of the sample were mounted between two metal clamps. The lower clamp was fixed and the upper one was connected to a movable force transducer. A short condenser was designed as a temperature chamber. Hot silicone oil was circulated with a temperature-regulated pump (Haake DC 30). Two small points were marked on the sample with a permanent marker. A JVC TK-C 1381 camera attached to an Olympus SZ-STUZ optical microscope was used to image the points. Displacements of the marked points were followed via an image analysis program by which the distance between the centers of points was measured in pixels. A sensitive force transducer (TSD125F, Biopac systems, Inc.) was employed

for force measurement. The length between the two centers was kept constant with the help of a tension adjuster (HDW100A) that provides micron-scale control. The stress on the film was read out from the multimeter (Agilent 34401A) in terms of the potential difference in volts. A schematic view of the experimental apparatus is presented in Figure 3.1. The transducer was calibrated by relating the potential difference into a force unit, by applying a set of dead weights on the transducer. Potential differences corresponding to the masses were recorded and plotted as a function of force. A linear calibration curve was obtained with a good regression value ($R^2 = 0.968$). The sample was loaded and heated in a glass chamber. $120 \pm 1^\circ\text{C}$ was the highest temperature employed, and 16 hrs were allowed for chain relaxation. Next, a stepwise cooling was performed on the system at 20°C intervals down to room temperature. A sufficient time, more than two hours, was allowed to bring the system to equilibrium between two successive measurements. Force data were recorded by the help of a HP-GPIB data acquisition card. The cross-sectional area of the undeformed sample was determined by measuring the thickness and the width of each sample with a micrometer of $100 \mu\text{m}$ precision.

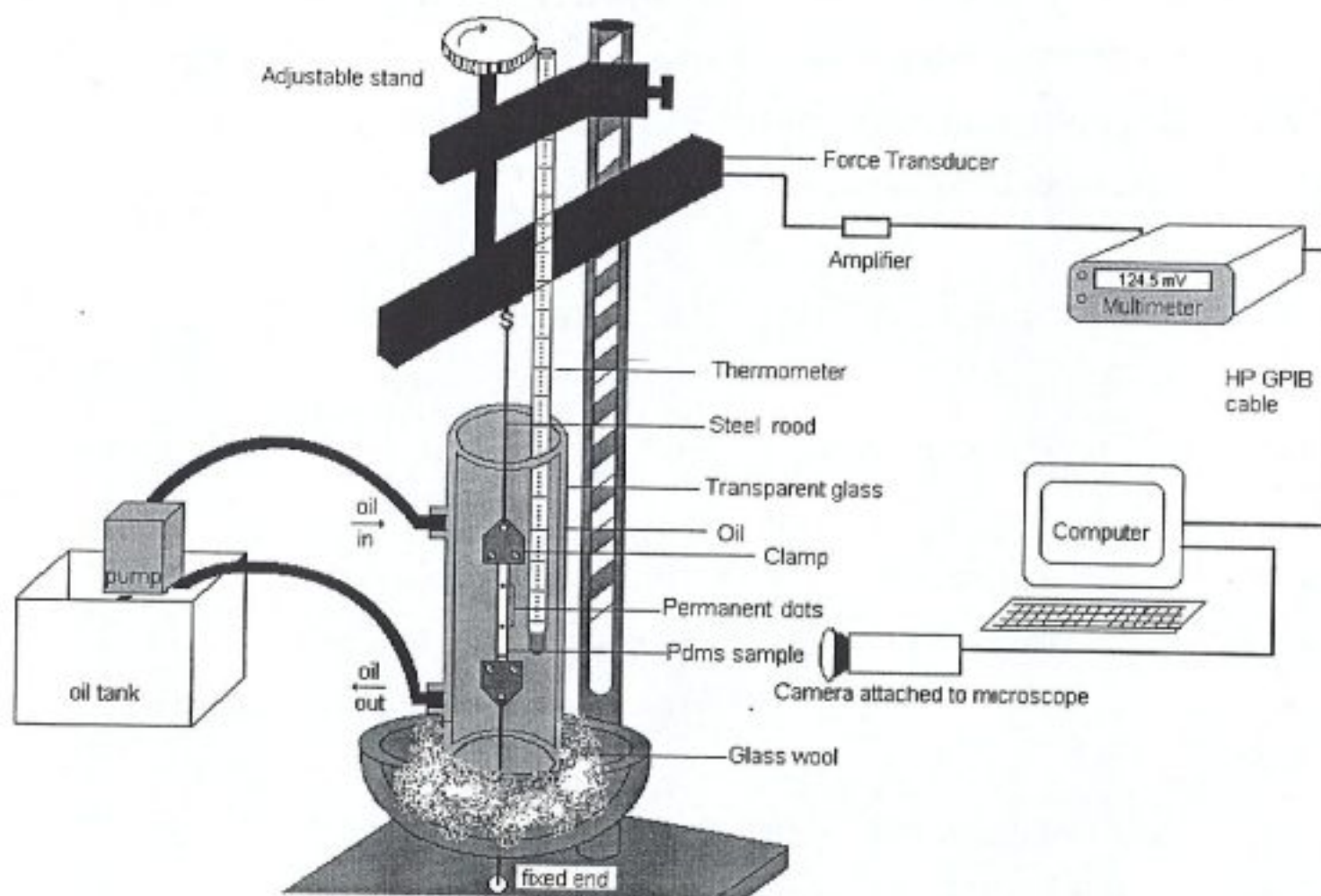


Figure 3.1. Schematic view of experimental apparatus.

3. 2. 6. Mechanical measurements

Stress-strain measurements were obtained at room temperature in uniaxial extension and along the direction of increasing elongations. Stress is calculated as $\sigma = f/A_0$; where, f and A_0 are the measured force and the undeformed cross-sectional area, respectively.

3. 3. Thermoelasticity Theory

The elastic force (f) has two components, an internal energy component (f_e) and an entropic component (f_s). The latter is defined as the change in the conformational entropy arising from the deformation of the polymer chains to a less probable state. The end-linked PDMS samples are stretched to a fixed length (L) and the force (f) is measured as a function of temperature. The energetic origin of the applied force is calculated according to [49]

$$f_e/f = -T [\partial \ln (f/T) / \partial T]_{L,p} - (\beta T / (\alpha^3 - 1)) \quad (3)$$

Here, β is the thermal expansion coefficient taken as $15 \times 10^{-6} \text{ K}^{-1}$ for unfilled samples [54]. β of filled elastomers were calculated according to the following formula: wt% silica \times β of silica + (1 - wt% silica) \times β of PDMS. α is the extension ratio L/L_0 , f is the force and T is the absolute temperature. Dividing through by T , and using the relation $f_e/f = T d \ln \langle r^2 \rangle_0 / dT$, we get

$$d \ln \langle r^2 \rangle_0 / dT = - [\partial \ln (f/T) / \partial T]_{L,p} - (\beta / (\alpha^3 - 1)) \quad (4)$$

Eq. (4) relates microscopic information carried in the left hand side to macroscopic measurements given by the right hand side. The derivation of this equation is described in the original references [55-57]. The unperturbed end-to-end distance, $\langle r^2 \rangle_0$, can be estimated from $\langle r^2 \rangle_0 = C_M n l^2$. C_M is the characteristic ratio at finite molecular weight, which was estimated by Flory for PDMS [58] using the rotational isomeric state theory to be in the range 5.85 - 7.60. n is the number of repeat units (675) and $l = 0.167 \text{ nm}$ is the Si-O bond length. Thus, the end-to-end distance is estimated as 10.6 nm.

3. 4. Results

3. 4. 1. AFM imaging and particle size

The morphology of silica filled PDMS is presented in Figure 3.2. The background of the image is the PDMS matrix and the bright objects are the silica fillers. Particle density and mean particle diameter were measured for each sample. Results of the measurements are given in Table 3. 1. Dispersion of the silica particles becomes relatively poor as silica concentration increases. When the silica concentration is higher, the number of silica particles per unit area becomes markedly less and mean particle diameter increases. The primary silica particles have 14 nm diameters, but they tend to aggregate, and to form larger agglomerates to reduce the total surface energy. Figure 3.2 (a) is for the 1% silica sample. It shows that the filler is uniformly distributed in the PDMS matrix. The tendency of the filler particles to agglomerate is enhanced as the silica concentration increases as shown in Figure 3.2 (b) for the 3% and Figure 3.2 (c) for the 5% silica samples.

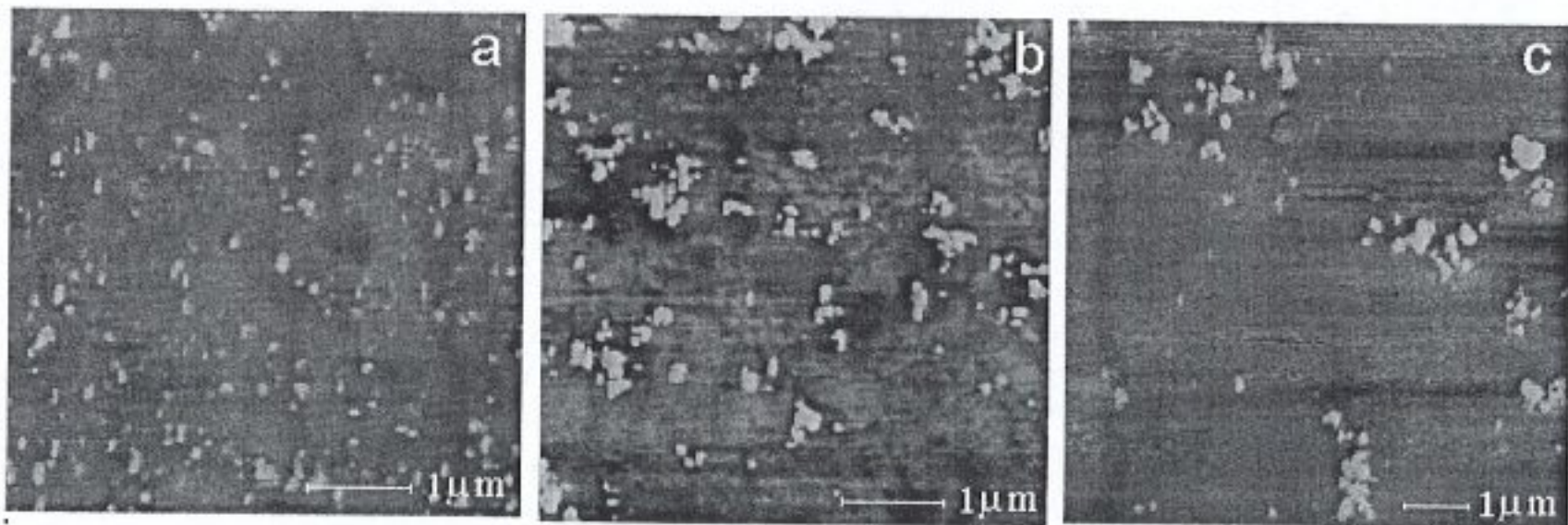


Figure 3.2. AFM tapping mode phase image of silica particles in PDMS matrix, (a) 1% wt. (b) 3% wt. (c) 5% wt. silica.

Table 3.1. Density and Diameter of silica particles

Silica conc. (%wt)	Particle density / μm^2	Mean Particle Diameter (nm)
1	7.83	76
3	3.91	101
5	0.62	201

Fillers with smaller particle size, i.e. higher effective surface area are favored for rubber reinforcement. Better reinforcement is achieved by increasing the effective surface area, which enhances the contact area between the polymer and filler. At higher concentrations, the particles become larger and form both aggregates and agglomerates. Thus, it is difficult to control the particle size and degree of dispersion due to agglomeration.

3. 4. 2. Swelling Measurements and Sol-Gel Analysis

Results of equilibrium swelling measurements are presented in Table 3.2. The second and third columns give the swelling degrees for toluene and benzene, respectively. The last three columns give the molecular weight of network chains, M_c , and the corresponding small deformation elastic moduli (in parenthesis) from swelling in toluene, benzene and from mechanical measurements, respectively. The amount of material extracted is small for swelling in both benzene and toluene, varying in the range 2-4.2 % by weight. Swelling degrees of the end-linked PDMS in the two solvents are presented in Figure 3.3 as a function of the amount of silica filler.

Table 3.2. Swelling measurements on end-linked PDMS.

Silica conc.	q_v		$M_c \times 10^3 \text{ g}$ ($E \times 10^6 \text{ m}^{-1} \text{ kgs}^{-2}$)		
	Toluene	Benzene	Toluene	Benzene	Mechanical
Unfilled	4.4	5.2	28.4 (0.26)	58.4 (0.13)	39.4 (0.19)
1	4.2	3.6	25.3 (0.30)	19.1 (0.39)	26.8 (0.28)
3	3.5	3.1	15.1 (0.50)	10.5 (0.71)	18.8 (0.40)
5	3.3	2.6	12.2 (0.62)	5.5 (1.36)	12.1 (0.62)

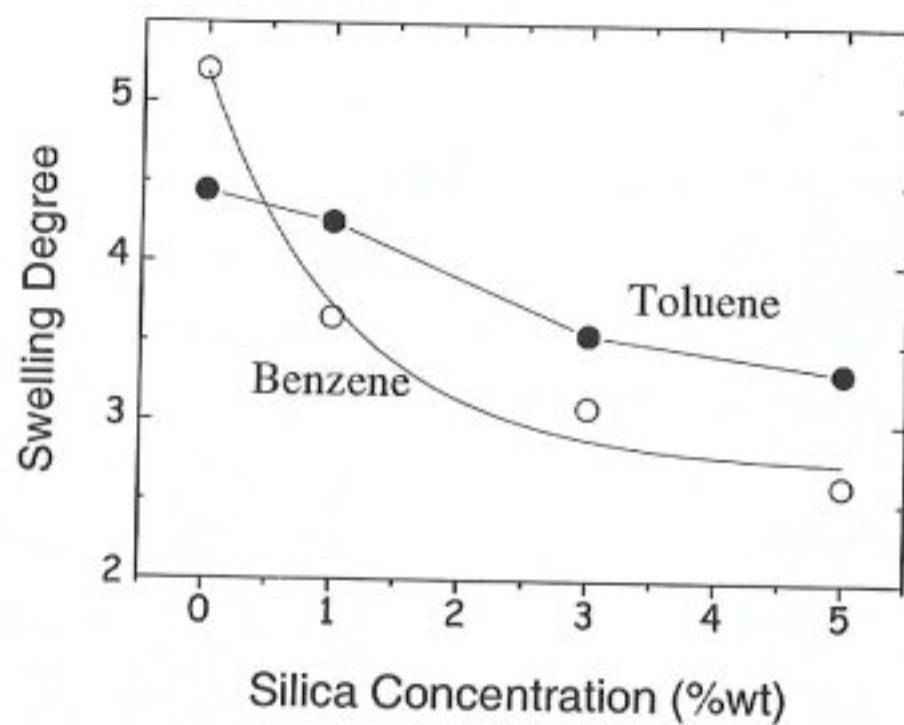


Figure 3.3. Equilibrium swelling degree of PDMS networks for unfilled and filled with 1%, 3%, 5% wt. fumed silica in benzene and toluene.

3. 4. 3. Elastomeric Force and Temperature coefficient

$\ln(f/T)$ vs. T was plotted to obtain the slope $\partial \ln(f/T)/\partial T$ for each sample. Figure 3.4 is given as a representative plot among the other samples (unfilled, 1%, 3% wt silica). All samples exhibit similar behavior, $\ln(f/T)$ decreases linearly as temperature increases. The slopes of the curves are critical in determining the f_e/f value, Eq. (3).

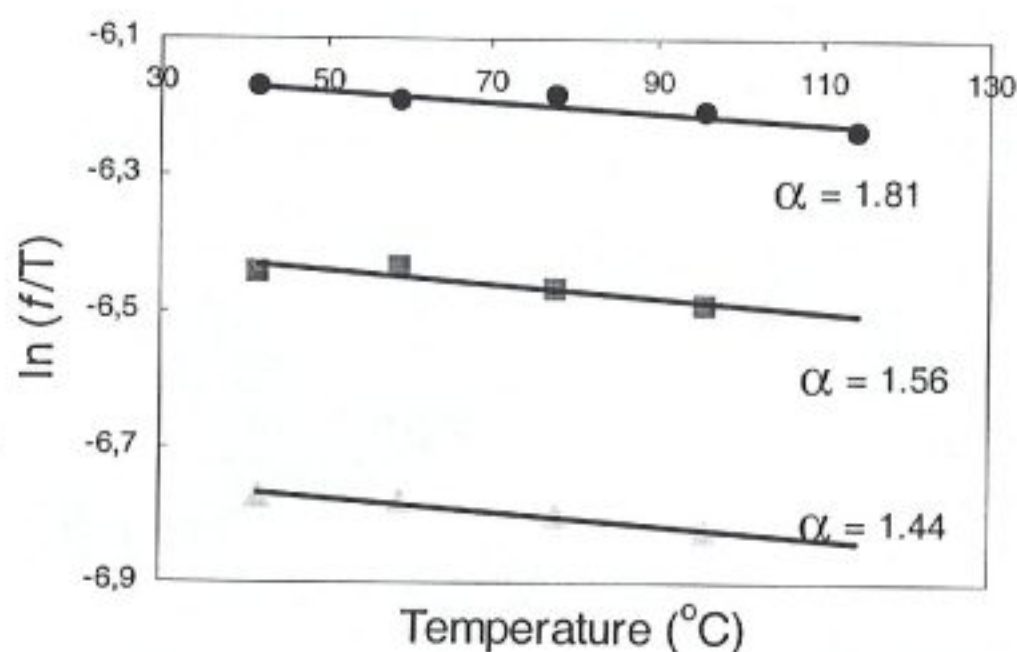


Figure 3.4. Thermoelasticity plot of end-linked PDMS with 5% wt. silica. The equations of the best-fitting lines are: $\ln(f/T) = -8.7 \times 10^{-4} T - 6.1$ ($\alpha = 1.81$), $\ln(f/T) = -7.0 \times 10^{-4} T - 6.3$ ($\alpha = 1.56$) and $\ln(f/T) = -8.3 \times 10^{-4} T - 6.7$ ($\alpha = 1.44$).

3. 4. 4. Thermoelasticity Measurements

Uniaxial tension between the two ends of the sample was recorded in 10 second intervals via the HP-GPIB software. Figure 3.5 (I) presents over 8,000 data points obtained during the thermoelasticity measurement of 5% wt silica filled PDMS network at 1.41-extension ratio. The force map is divided into four segments (I, II, III, IV) and they will be discussed in detail (Figure 3.5 I-IV). The number of data illustrated on the graph is given as 'Data points' in figure captions. The first segment, I, includes loading. At the beginning of the segment, the distance between two points on the sample was ca. 36 pixels and the force is zero. Uniaxial loading extended the distance to ca. 51 pixels and increased force was recorded (Figure 3.5-II). In the second segment, II, the sample was allowed to relax at room temperature for 15 minutes. Force difference upon

the relaxation process is on the order of 20 mN. Note that stress relaxation was found to be higher at high extension ratios such as 78 mN and 165 mN for extension ratios 1.56 and 1.81, respectively (data not shown).

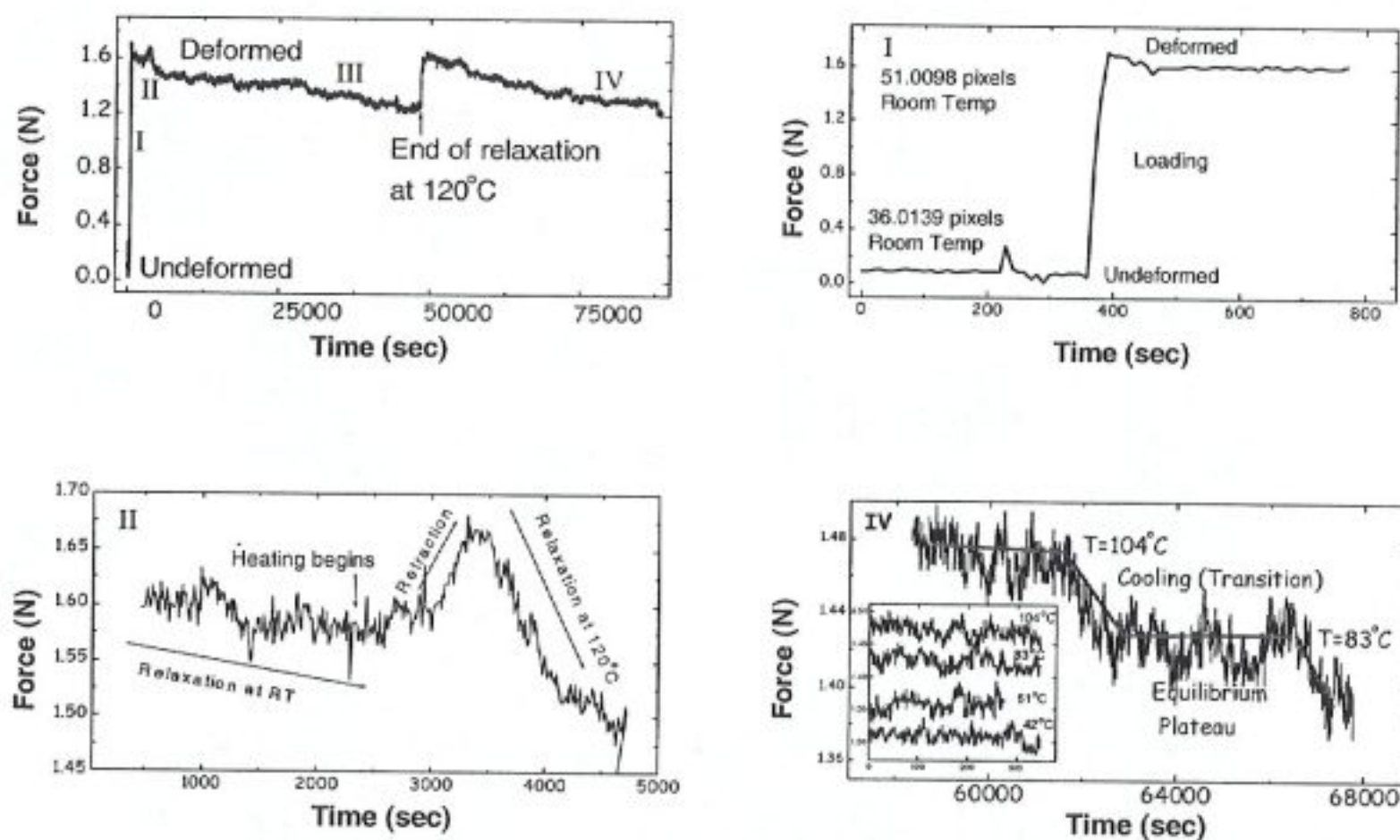


Figure 3.5. (I) Force map for 5% wt silica filled PDMS network at 1.41 loading (8859 data points). (II) Detailed force map for segment I, loading at room temperature (80 data points). (III) Detailed force map for segment II; relaxation upon loading at room temperature, shrinkage and relaxation at 120°C. (426 data points) (IV) The force recorded between 104°C to 83 °C during the experiment for segment IV (945 data points); detailed force map for segment IV including only the equilibrium plateau regions at different temperatures are shown in the inset.

Next, the temperature was gradually raised inside the chamber and heating rate inside the condenser was monitored. The temperature reaches 120°C within 1100 seconds and the force reaches its maximum value within 1000 seconds. Immediate response of the sample to temperature change can be seen if the ordinate of the force map is adjusted, Figure 3.5 (III). Force increases dramatically due to retraction of the chains upon heating. Temperature of the chamber at the peak is 120°C. Stress relaxation takes place upon heating. The sample was kept under load at 120°C overnight to achieve a complete relaxation (Segment III in Figure 3.5).

Relaxation at 120°C under 1.41 extension ratio is 200 mN. The distance between two points was found to be shortened by approximately 6%. Shrinkage degree was similar for all other samples at different extension ratios. The sample was elongated to its initial length by a tension adjuster. Finally, the force was captured at different temperatures during step-wise cooling of the sample while keeping the distance between the points constant. As illustrated in Figure 3.5 (IV), a step-like force map, consisting of plateau and transition regions, is recorded during measurement. At plateau regions, temperature does not change and the system is allowed to equilibrate. However, at transition regions the system is cooled down. Equilibrium points corresponding to different temperatures appear at plateau regions. In the inset of Figure 3.5 (IV), transition regions are removed from segment IV (Figure 3.5-I) and only the equilibrium plateau regions at different temperatures are illustrated for clarity. At high temperatures, the force needed to keep the distance constant is high. The fluctuations in the force are on the order of 10 mN. The causes for fluctuation may arise from the ambient factors such as airflow, humidity and change of the sensitivity of the force transducer at different temperatures.

Figure 3.6 illustrates f_e/f values as a function of silica concentration. The filled circles are from the present work and the empty circles denote the results of Galanti and Sperling [52]. The filled points are determined by averaging f_e/f values of a sample for the three different extension ratios. The error bar corresponds to the standard deviation in the data. Recall that the AFM analysis of the filled polymers indicates that aggregation of fillers increases significantly with filler content (Figure 3.2). For this reason, filler amounts larger than 5% were not considered. Comparison of our data with that of Galanti and Sperling shows that the contribution to the energetic component of the elastic force f_e/f and the rate of increase of f_e/f are both larger in our measurements. It is also found that f_e/f values are approximately independent of extension ratios (not shown as a separate figure). Values of $d \ln \langle r^2 \rangle_0 / dT$, obtained by substituting the measured forces and extension ratios in Eq. (4) are displayed in Figure 3.7 as a function of silica concentration. Figure 3.8 illustrates Force-Temperature data for 3% silica filled PDMS networks in elongation at constant length. Elastic moduli of the samples obtained by mechanical experiments and by swelling measurements in toluene and benzene are presented as a function of filler content in Figure 3.9.

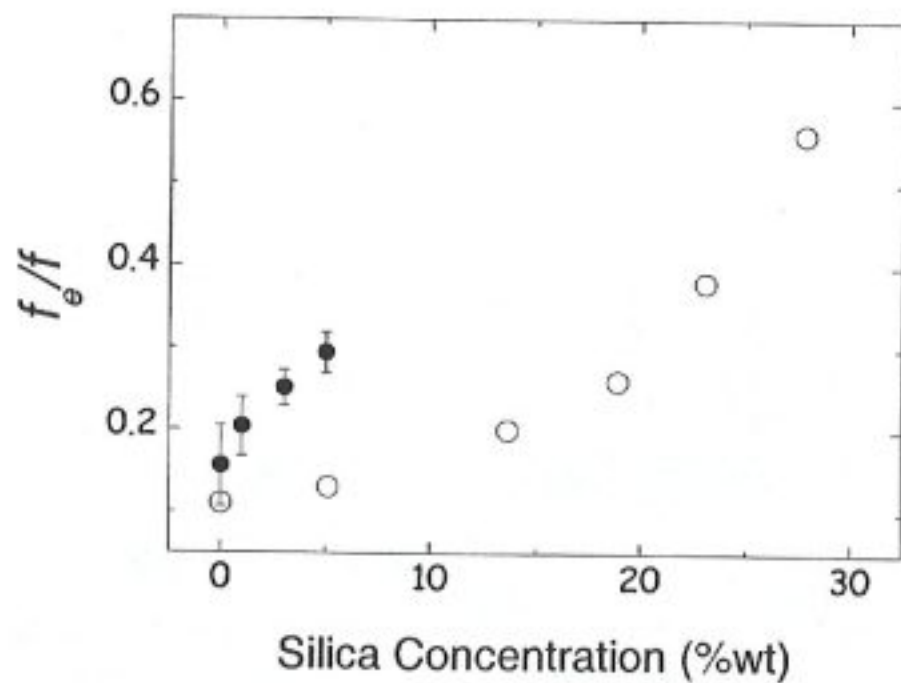


Figure 3.6. f_e/f values as a function of silica concentration. Open circles represent results from Reference [52] and closed circles show our experimental data.

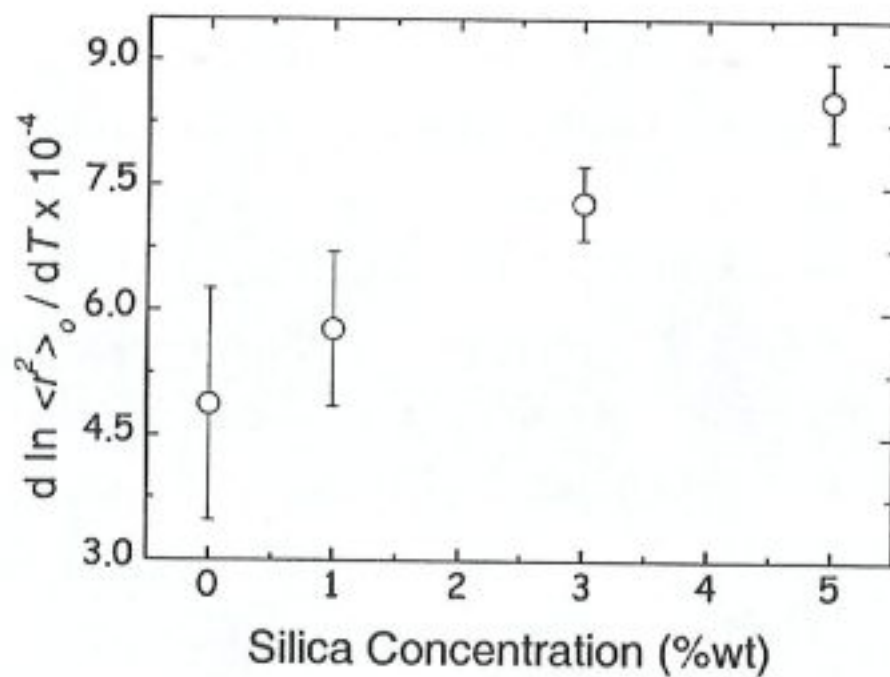


Figure 3.7. $d \ln \langle r^2 \rangle_0 / dT$ of PDMS chains as a function of silica concentration.

The calculations leading to the points in the figure are described in Appendix I. The empty circles are obtained from the initial slopes of stress-strain curves of the samples and indicate the small deformation moduli. The modulus increases linearly with increasing silica concentration. Results from swelling in toluene show approximate agreement with the mechanical data. Swelling in benzene yields larger values in higher silica concentration samples.

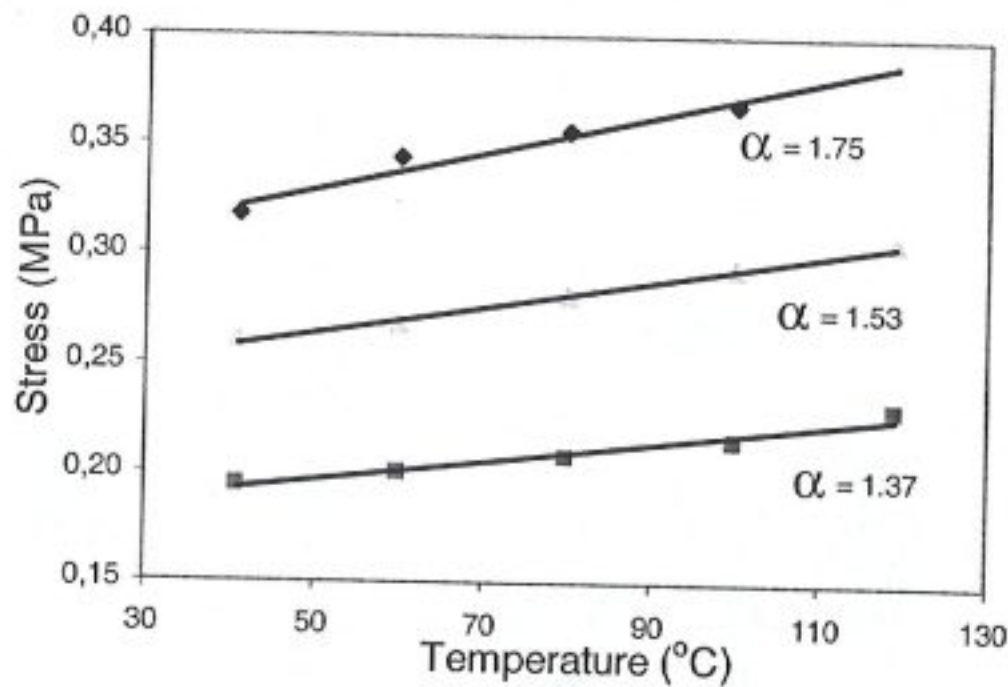


Figure 3.8. Typical force-temperature curves at various elongations at constant length. The equations of the best-fitting lines are: $\sigma = 8.4 \times 10^{-4} T + 0.29$, $\sigma = 6.1 \times 10^{-4} T + 0.23$, and $\sigma = 4.4 \times 10^{-4} T + 0.23$. Slopes of the lines decrease with decreasing the extension ratio.

3. 5. Discussion

The temperature coefficient of PDMS chains are positive with an experimental value of $f/f = 0.2$ and $d \ln \langle r^2 \rangle / dT = 0.67 \times 10^{-3}$ [49,59]. The present results which agree with those of Galanti and Sperling are lower, lying in the range $f/f = 0.11-0.15$ and $d \ln \langle r^2 \rangle / dT = 0.32-0.45 \times 10^{-3}$. The observed increase in f/f and $d \ln \langle r^2 \rangle / dT$ with filler content results from the presence of the filler, or more specifically from the filler polymer interface. As suggested by the recent NMR, DSC and AFM measurements, the presence of a mobility gradient of the chains play important role in the observed temperature dependence [14,16]. The chains in a bulk amorphous elastomer have the full freedom of taking all possible configurations, subject to the constraints imposed by the cross-links at their two ends only.

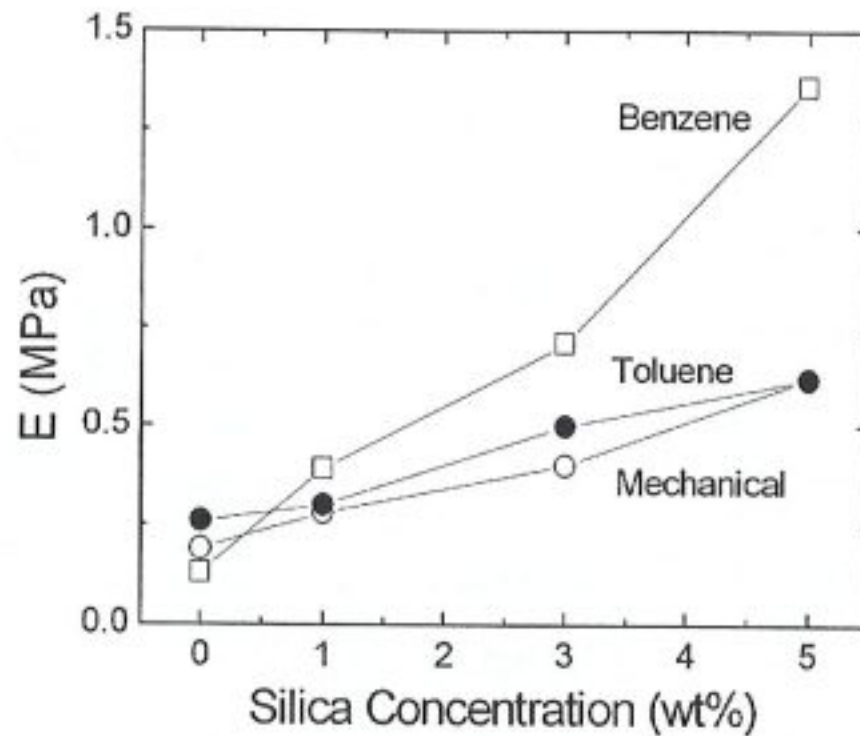


Figure 3.9. Elastic modulus of the unfilled and silica filled PDMS networks obtained by mechanical experiments and by swelling in toluene and benzene.

However, the presence of nanometer size fillers results in adsorption and immobilization of a significant fraction of these chains on the walls of the filler. There is a permanent chemical bonding between the silanol of the silica surface and the ethoxy group of the TEOS. The interaction is known as chemisorption which severely restricts the movement of the chains when high stresses are applied. Another factor results from the presence of fillers is the change in the distribution of the end-to-end distance because the fillers occupy a volume. Therefore, the chains are squeezed between fillers and the distribution of the end-to-end distance is changed. Hence, the inorganic particles influence not only the network chain mobility but also the distribution of the end-to-end distance, causing the increase in f_0/f and $d \ln \langle r^2 \rangle / dT$ values with increasing silica concentration.

Silica provides tremendous reinforcement in PDMS elastomer, but the mechanism of the reinforcement is not fully understood. A molecular interpretation of the reinforcement, in particular, is a challenging problem.

CHAPTER 4. DIMENSIONS OF POLYSTYRENE PARTICLES DEPOSITED ON MICA FROM DILUTE CYCLOHEXANE SOLUTION AT DIFFERENT TEMPERATURES

4. 1. Background

Dimensions of a single polymer chain in solvent at different temperatures depend on the structural features of the chain and the interaction between the chain and the solvent. The temperature dependence of the interaction is most significant for the polystyrene (PS) – cyclohexane (CH) system, which has been studied extensively in the past, both experimentally and theoretically [60-62]. A single PS chain in CH exhibits a rapid decrease of dimensions when the temperature is decreased below about 35°C. This phenomenon is known as the coil-globule transition. For sufficiently long PS chains, it has been shown, by using thermodynamic and statistical mechanical arguments, which the system goes through a critical transition [17]. This is the reason for the observed abrupt change in the dimensions of PS at the stated temperature. In systems that do not go through or near critical conditions as the solvent quality becomes poorer, the dimensions of the chains also decrease. However, this change takes place gradually, and a rapid ‘collapse-like’ transition or a sharp coil-globule transition is not possible.

The PS-CH system is representative in this respect. The observation of large dimensional changes in single chains at easily accessible temperatures is especially important for technological applications at the molecular scale. In the present study, we observe, by an atomic force microscope (AFM), the dimensions of the PS particles deposited and dried on mica surfaces from dilute cyclohexane solution at temperatures above, at and below the θ temperature. A strong temperature dependence of the dimensions is observed. However, AFM measurement does not indicate whether the deposited particles consist of single or several chains. Here, we interpret the results of

the measurements in terms of two different scenarios. The first scenario is based on the single chain per particle picture. This is based on the fact that the solutions from which the particles are deposited are extremely dilute, and on the assumption that individual molecules remain separated during evaporation. The second scenario is based on the several chains per particle picture. In this picture, the individual chains in solution aggregate during evaporation. The maximum possible number of chains per particle can be estimated because the upper bound of the segment density of the molecules on the surface is the bulk density. If the observed particles have bulk densities, and then the number of particles in each, i.e., the maximum possible number, may be calculated by dividing its volume by the volume of a single collapsed chain. This number turns out to be strongly dependent on temperature.

Single PS molecules deposited on mica or silicon from various solutions has previously been investigated by Qian et al. [63], Festag et al. [64], Stange et al. [65] and Zhang et al. [66] using STM, AFM and electron microscopy. Qian et al. [63] investigated the morphology of electrosprayed PS particles from solvents of different quality and the changes in morphology over long times of observation. Zhang et al. [66] used the droplet evaporation technique on a graphite surface and identified the dimensions of different molecular weight PS molecules. Stange et al. [65] studied the effects of concentration and molecular weight on discontinuous PS films on silicon surfaces. In this chapter, we present a systematic AFM analysis of the temperature dependence of dimensions of PS molecules cast from CH.

4. 2. Experimental

4. 2. 1. Materials

2×10^6 g/mol molecular weight PS, ($M_w/M_n = 1.30$), was provided from Alfa Caesar (Lot # K29J21). CH was obtained from Reidel-de Haen and used as received. A dilute solution of PS in CH, 4.6×10^{-6} g/ml, was prepared at room temperature. Concentrations lower and higher than 4.6×10^{-6} g/ml were also investigated. However, the number of particles deposited on mica was too few to allow for a rigorous analysis at lower concentrations and aggregation effects were observed at

higher concentrations [64]. The optimum concentration of 4.6×10^{-6} g/ml was therefore used throughout all measurements.

4. 2. 2. Sample preparation

All specimens were prepared by depositing a drop of the solution onto freshly cleaved mica surfaces. Approximately 1 cm^2 area from the top layer of mica was peeled by using scotch tape to make a fresh, clean, and flat surface. Equal volumes of polymer solution, approximately $40 \mu\text{l}$, were deposited on the freshly cleaved mica by a micropipette. The deposition was carried out immediately following the cleavage to avoid oxidation of the mica surface. The solutions were deposited on mica at 25, 35, 50, and 80°C . The mica substrate and the polymer solution were left to dry in an oven for 24 hours at the temperature of deposition. The samples were then transferred to a desiccator under low vacuum. Humidity was controlled and kept under 40 % inside the desiccator. All samples were prepared at least three times. The highest temperature, 80°C is close to the boiling temperature of CH. In order to investigate possible anomalous effects at such a high temperature, several experiments were also carried out around 70°C . No anomalous results were observed.

4. 2. 3. AFM imaging

Tapping mode in air AFM (Nanoscope IIIa, Digital Instruments) imaging was carried out with oxide sharpened Si tips. Dimensions of the adsorbed molecules were measured at room temperature by using bearing analysis and section analysis options of the Nanoscope software. In addition to humidity control, the head of the AFM was flushed with liquid N_2 before the start of the measurement [67]. AFM images were recorded in the height and phase modes without any image processing except flattening and plane fitting. Comparing at least two images of different samples verified the reproducibility of the images. More than 230 data were collected from three different reproducible images for each temperature value. At least 50 particles were examined for obtaining height and diameter distributions at each temperature. Several freshly cleaved mica surfaces, as well as mica surfaces on which pure cyclohexane was deposited and evaporated, were studied under the AFM in order to distinguish between PS particles and possible impurities on the surface. The freshly cleaved mica showed no structure within the length scales of our observations ($0.5 -$

500 nm). On surfaces onto which, pure CH was deposited and evaporated, we observed occasional spherical particles. However, the number of these particles was very small, and their dimensions were approximately an order of magnitude smaller than the smallest PS particles observed at 25°C.

Two sources of uncertainty may be affecting the observations. First, particles observed with the microscope may contain CH bound to PS although the samples remain in the oven for 24 hours. Second, the dimensions of the particles may be somewhat overestimated by the AFM due to tip geometry, known as tip convolution. To obtain the actual diameter of the particles, the radius of the tip and the particle should be taken into account. The corrected particle radius is estimated by Festag et al. [64], assuming the tip and the particle as hemispheres, according to the expression

$$r_{\text{particle}} = [r_{\text{tip}}^2 + r_{\text{observed}}^2]^{1/2} - r_{\text{tip}} \quad (1)$$

It should be stressed that whether or not an observed particle consists of a single chain cannot be directly inferred from the AFM measurements. To understand if the observed particles consist of single chains, observations were also made on particles obtained from solutions with concentrations of 10^{-8} g/ml, at which the particles are expected to consist of single chains. These measurements indicated that the dimensions of the particles observed at extremely low concentrations agree with a statistically significant portion of the distribution of sizes observed at higher concentrations.

4. 3. Results of measurements

Four AFM images of PS molecules on mica surfaces are shown in Figure 4.1, obtained at four temperatures, 25, 35, 50 and 80°C. The shapes of the particles are round and symmetric except those obtained at 35 °C. As the temperature increases, the dimensions (height, diameter and volume) of the particles increase and their number density per unit area decreases. There are 172-particles/ $25 \mu\text{m}^2$ in the image of the 25 °C samples whereas the number of particles decreases in the order 149, 102, and 28 as the temperature increases. All of the particles are well separated from each other as can be seen from the AFM images of Figure 4.1.

A drop of polymer solution, approximately 10 μl in volume and with a concentration of 10^{-8} g/ml, spreads out in the form of a circular region when deposited on mica. The diameter of the circular region diminishes gradually as the solvent evaporates. After complete evaporation of the solvent, areas of $4 \mu\text{m}^2$ were scanned in the region initially occupied by the drop. Resulting images show that the polymer molecules move towards the perimeter of the drop as the solvent evaporates. The number of polymer molecules per unit area was markedly less at the center of the drop than at the perimeter, as can be seen from Figure 4.2. This observation is in agreement with the recent theoretical predictions of Deegan et al [68].

The dimensions of the particles were examined as height, diameter, and volume. To determine the diameter, the principle axes of the particles were determined in a 2-dimensional view. The major and the minor horizontal distances, d_1 and d_2 , respectively, were measured for each particle, and the diameter d was evaluated according to the expression $d = [d_1 \times d_2]^{1/2}$. The height of each particle was taken as the vertical distance between the plane of the mica and the highest point of protrusion above the smooth plane of mica. The volume of the particle above the smooth mica plane was determined using the bearing volume analysis options of Nanoscope III software. Results of measurements of the PS particles at four different temperatures are presented in the Table 4.1. The diameter values in the fourth column are corrected according to eq. 1. The height values in the fifth column are given in the form of a range of values owing to the uncertainties resulting from the smallness of the height values.

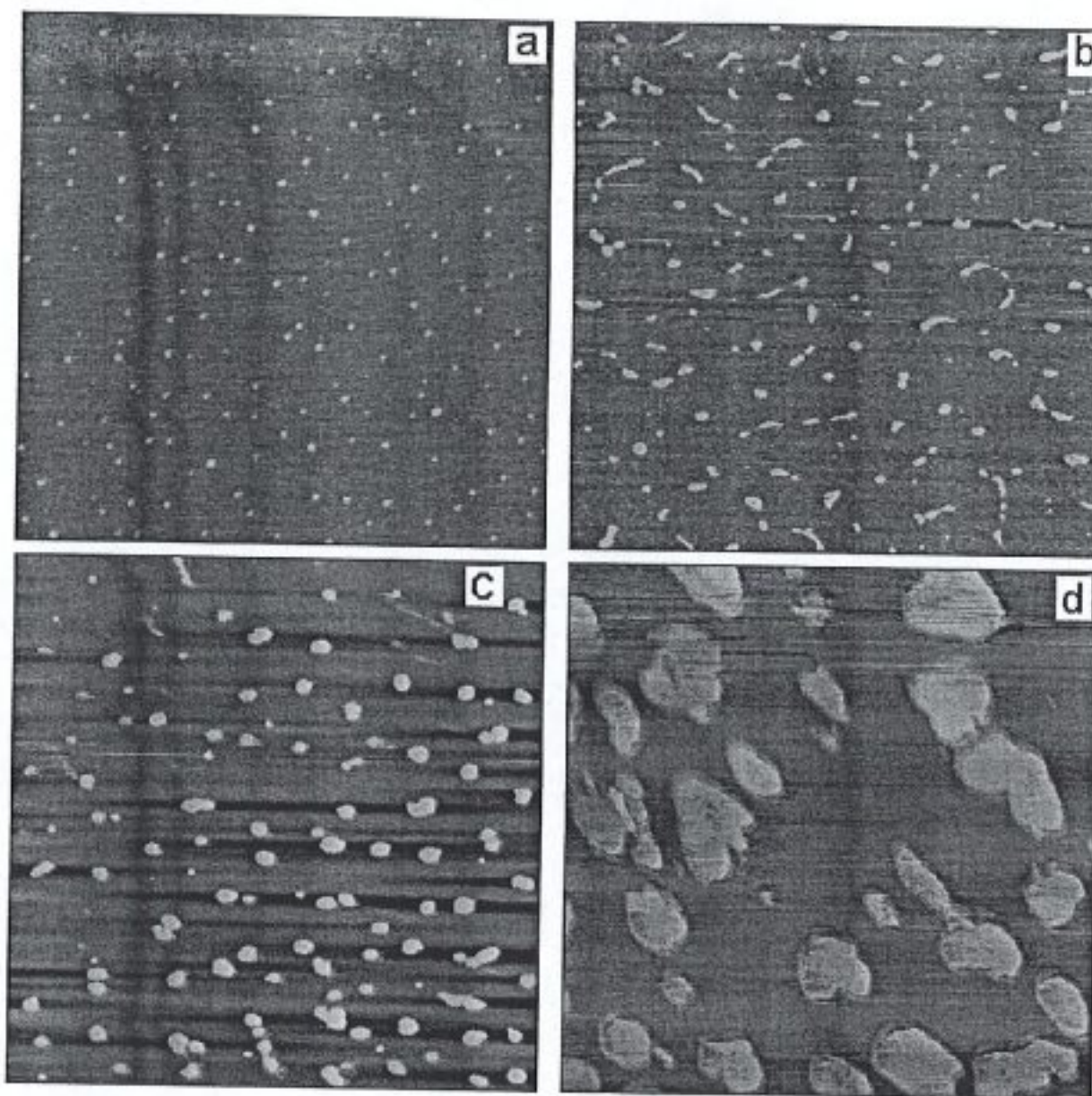


Figure 4.1. AFM images of polystyrene particles deposited from a very dilute solution of PS in CH onto a mica substrate at (a) 25 °C (b) 35°C (c) 50 °C (d) 80 °C. All images have 5 x 5 μm^2 scan area.

Table 4.1. Experimentally measured particle dimensions on mica at four different temperatures.

T °C	Volume (Dry, on mica) nm^3	Diameter (measured) nm	Diameter (corrected) nm	Height (Dry, on mica) nm
25	4000	65	52	1.0-1.5
35	11,000	70	57	2.5-3.0
50	50,000	136	122	4.0-4.5
80	125,000	506	491	0.5-1.0

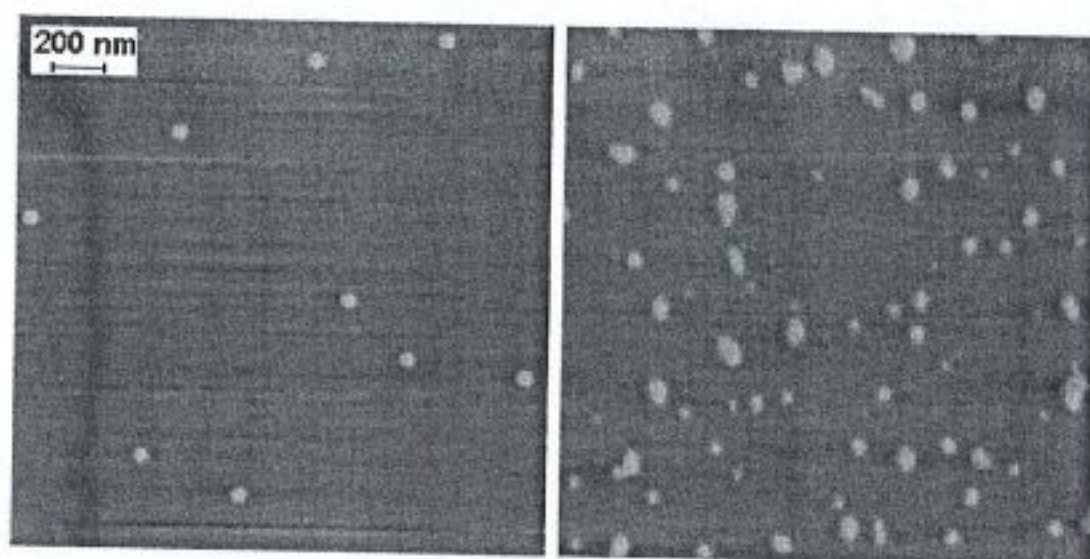


Figure 4.2. AFM height images captured from (a) center (b) perimeter of the drop after solvent evaporation. Images have $2 \times 2 \mu\text{m}^2$ scan area.

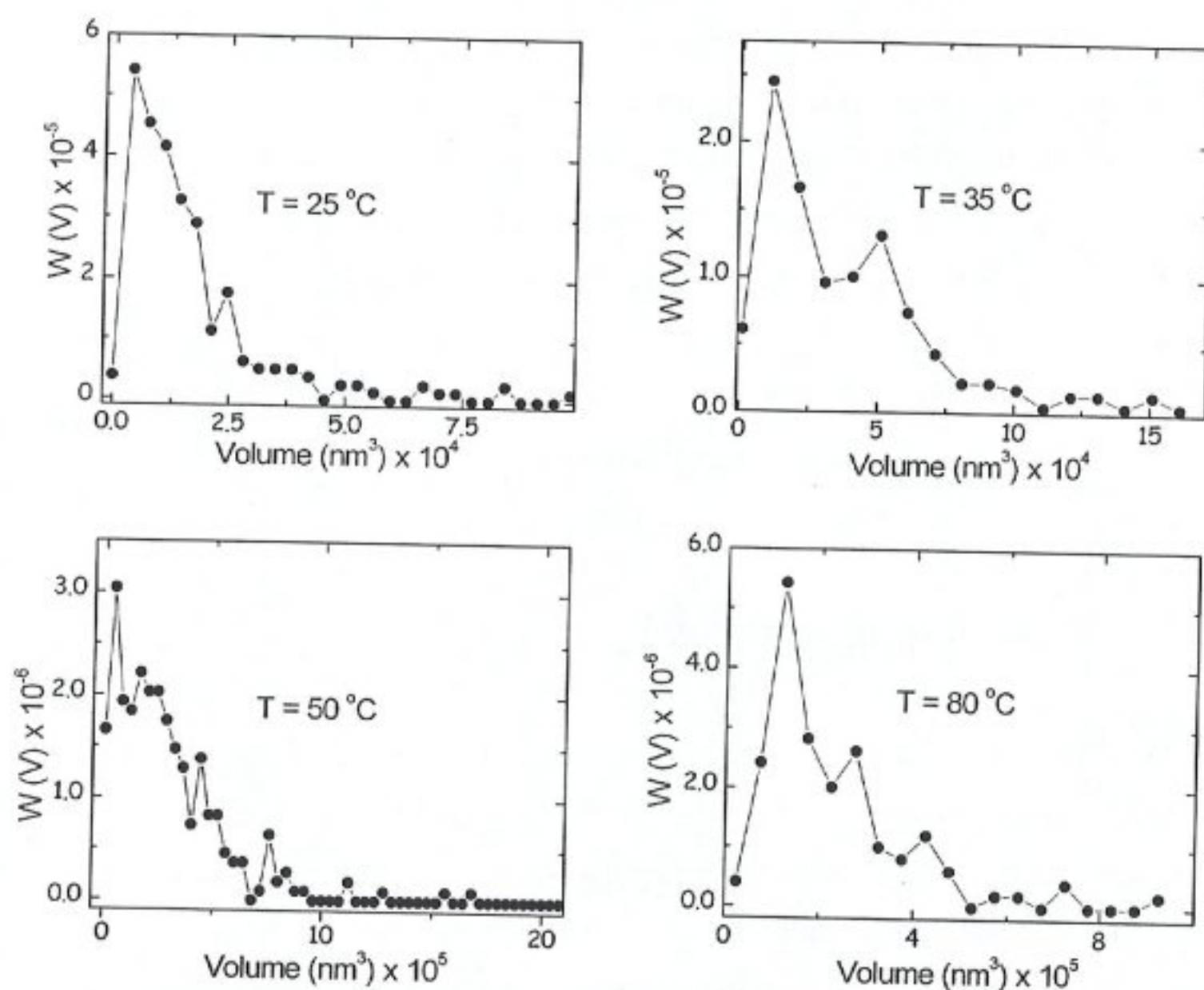


Figure 4.3. Volume distributions of polystyrene particles at 25°C , 35°C , 50°C , 80°C . Bin sizes are 3500, 10000, 40000, and 50000 nm^3 , respectively.

The distributions of the measured volumes are presented in Figures 4.3 for the four temperatures. The filled circles represent experimental data, and the curves through the points are drawn to guide the eye. The ordinate represents the distribution

of the observed volumes, normalized to unity. A striking feature of the curves is that the volumes are distributed over a wide range of values at all temperatures and that all of the distributions are strongly skewed, with a long tail towards larger values of the volume.

The volume of the single globular polymer molecule can be calculated from its bulk density (1.05 g/cm^3) [64,66]. For the molecular weight of $2 \times 10^6 \text{ g/mol}$, this volume is 3200 nm^3 . This value is close to the peak value of the distribution in Figure 4.3 at room temperature. Considering that the chains are already in the globular state in solution at 25°C , we may conclude that their deposition and subsequent drying does not further affect their dimensions. The larger volumes observed in the distribution of Figure 4.3 may be mainly due to two reasons. Either there may be more than one chain in the larger particles observed, or, the particles may consist of single chains which were not globular in the CH solution and remained non-globular during drying. AFM measurements cannot differentiate between these two cases. Similar arguments apply to chains deposited at higher temperatures, shown in Figures 4.3.

To further elaborate on the effects of the numbers of chains in a particle, we study the problem in terms of two limiting scenarios:

4. 3. 1. The single chain per particle scenario

The concentrations of solutions used in the present study are sufficiently low to ensure that the individual chains in the solution are well separated from each other. If the chains also remain well separated during deposition on the mica surface and during subsequent evaporation, then the observed particles should predominantly contain single PS molecules each. In this case the segmental density in the measured volume is low which is essentially an envelope enclosing the total space needed to contain the chain.

4. 3. 2. Several chains per particle scenario

If the attractive intermolecular forces during evaporation are dominant, several single chains may adhere together to form a particle having clusters of single chains. In the extreme case that the clusters formed in this manner have segmental densities

equating to the bulk density, then the number of molecules in each cluster may be estimated as the ratio of the observed volume to the volume of a single globular chain. The width of the distributions in Figure 4.3 depends strongly on temperature as may be verified from a comparison of abscissa values.

Table 4.2. Maximum possible number of chains in a particle on mica at four different temperatures.

T °C	Observed dry volume (nm ³)	Number of chains per particle
25	4,000	1
35	11,000	3
50	50,000	13
80	125,000	32

The distributions of diameters are presented in Figure 4.4 for the four temperatures. The points represent experimental data, and the lines are drawn to guide the eye. The distributions for 25°C and 35°C are sharply peaked and are approximately the same. The distributions for 50°C and 80°C are wider, the latter showing a significant degree of dispersion about the mean value.

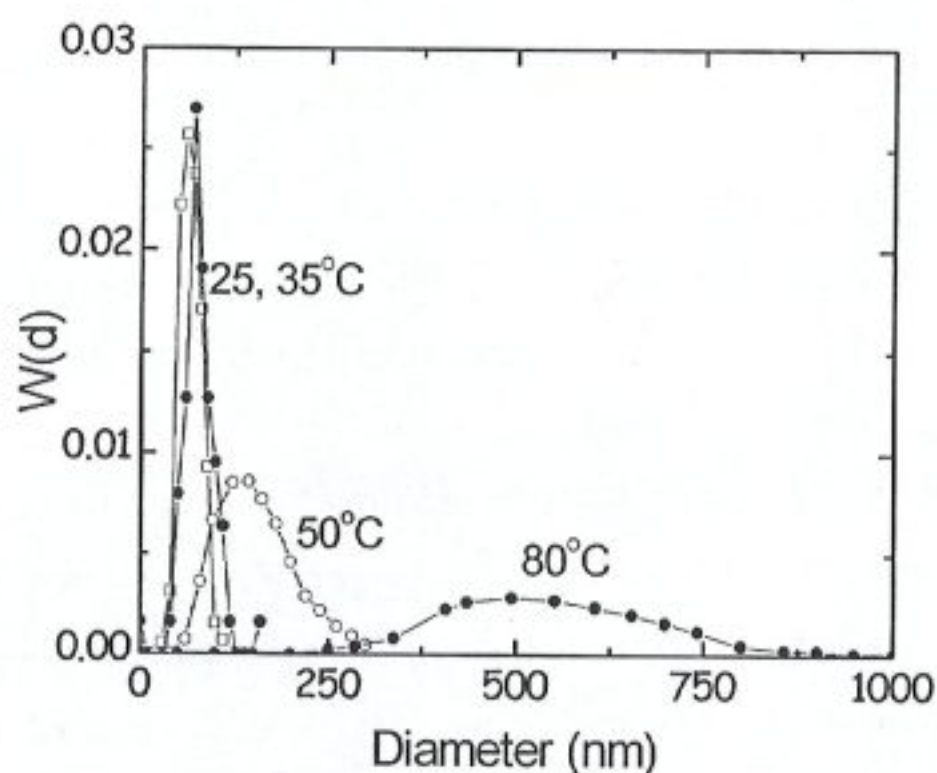


Figure 4.4. Diameter distribution of polystyrene particles at 25, 35, 50, and 80°C.

The distributions of heights are presented in Figure 4.5. The points represent experimental data, and the curves are drawn to guide the eye. The curve through the points for $T = 25^\circ\text{C}$ is drawn heavier in order to differentiate it from the curve for 80°C . The height values at 80°C are low due to extensive spreading of the molecules on the mica surface. Otherwise, the features of the height distributions parallel those for diameter distributions, as evident from the comparison of Figures 4.7 and 4.8.

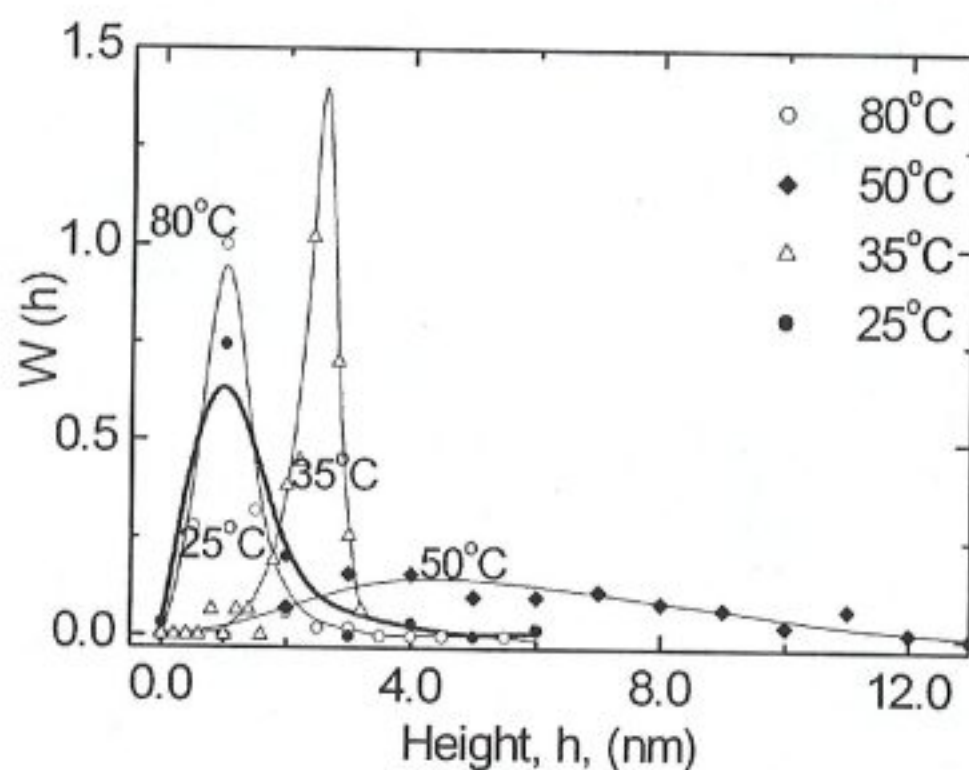


Figure 4.5. Height distribution of polystyrene particles at 25, 35, 50, and 80°C .

4. 3. 3. Morphology of PS structures - Round versus Flat

Above 35°C , the temperature of the substrate on which the solution is deposited strongly affects the shape of the particles. If, during deposition, the mica is at room temperature and the solution is at 50°C , then the diameter of the resulting particle is small and its height is large. This is shown in Figure 4.6 (a). Figure 4.6 (b), on the other hand, shows that a flat particle is obtained if both mica and the solution are at 50°C . The two images shown in Figure 4.6 are obtained separately by section analysis and then combined. In order to fit the two shapes into the same figure, the horizontal scale of the flat particle is reduced ten-fold and the vertical scale is expanded ten-fold relative to that of the round one.

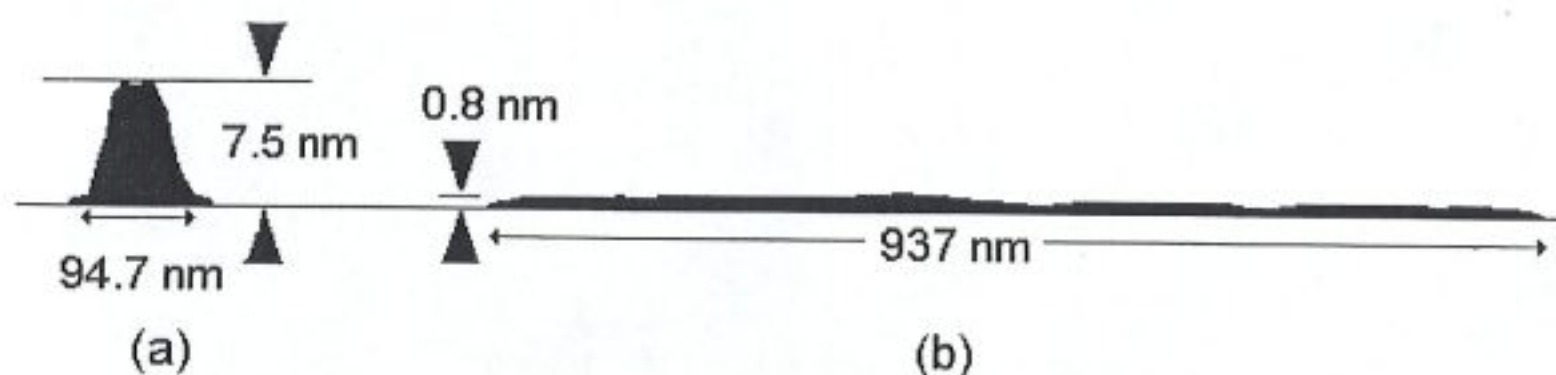


Figure 4.6. Section analysis of two different morphologies of PS (a) round (b) flat.

4.3.4. Conformational change of PS chains in coil-to-globule transition

The kinetics of collapse and conformational change of the PS chain during transition were investigated by quenching the dilute polystyrene solution from theta temperature to 28 °C [61]. An abrupt temperature change induces the transition from θ coil to compact globule. Figure 4.7(a) taken from literature shows the hydrodynamic radius of PS chain as a function of time. The change in the hydrodynamic radius with time clearly exhibits the existence of a two stage process. The PS solution in cyclohexane was quenched from 35°C to 28°C at a concentration of 8.7×10^{-6} g/ml. Initially, temperature was at 35°C, the conformation of chain was θ coil which occupied a large volume. The final equilibrium state was a compact globule at 28°C. The chain occupied the smallest amount of volume. However, at the intermediate stage, the conformation of the chain resembled a sausage of collapsed blobs. The diameter of the sausage increased and its length decreased with further collapse. Figure 4.7(b) illustrates our AFM result of PS particles cast from dilute solution at 35°C onto freshly cleaved mica at room temperature. The solution was quenched at the mica surface. While the solvent evaporated and the particles were adsorbed to the mica, a fraction of particles found time for transition (compact globule) whereas the remaining ones could not perform transition during this time period (θ coil and sausage structure). The particles on the AFM image appear a mix of the four conformations as proposed by the theory and the light scattering experiment results. The image contains small and large spherical particles corresponding to the compact globule and θ coil, respectively. Particles other than spherical ones are the sausage-like structures called crumpled globules.

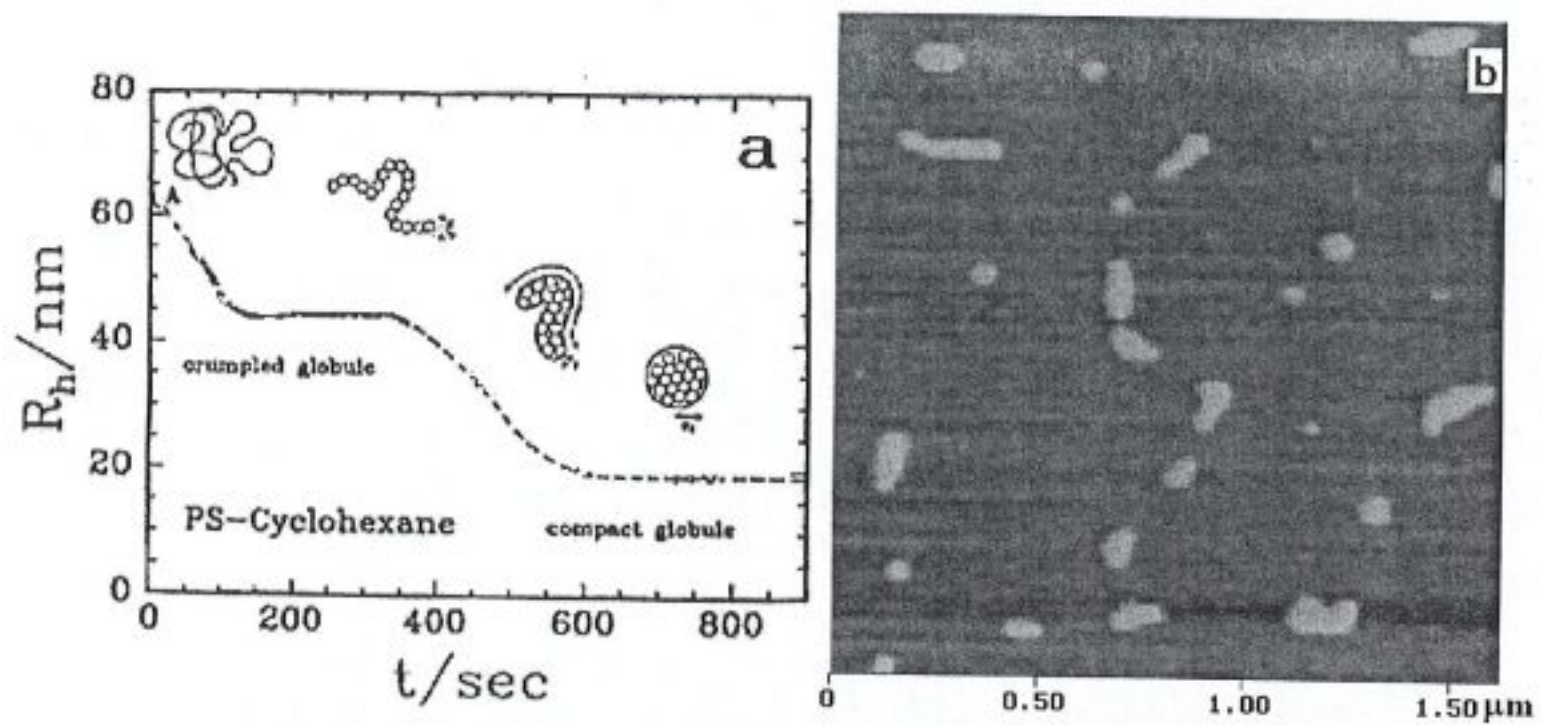


Figure 4.7. a) Time dependence of hydrodynamic radius of a single polystyrene chain in cyclohexane during the transition [61] b) AFM image of polystyrene chain deposit on mica from cyclohexane at 35 °C.

Appendix I. Calculation of degree of end-linking and modulus from swelling data

The elastic equation of state for an affine network is

$$\sigma = \frac{\rho RT}{M_c} (\alpha - \alpha^{-2}) \quad (\text{A-1})$$

where σ is the stress, ρ is the density of dry chains, R is the gas constant, T is the absolute temperature, M_c is the molecular weight of chains between two cross-links, and α is the extension ratio. For small deformations, Eq. (A-1) takes the form $\sigma = 3E\varepsilon$, where ε is the strain, and the modulus of elasticity is related to M_c as

$$E = 3 \frac{\rho RT}{M_c} \quad (\text{A-2})$$

Alternatively, M_c may be obtained by swelling from the expression [49]

$$M_c = - \frac{\rho V_1 v_{2c}^{2/3} v_2^{1/3}}{\ln(1 - v_2) + \chi v_2^2 + v_2} \quad (\text{A-3})$$

where $v_2 = 1/q_c$ is the volume fraction of polymer, and χ is the polymer-solvent interaction parameter. v_{2c} is the volume fraction of polymer during the formation of the polymer, which is not constant throughout the cross-linking stage in the present experiments. An average value of 0.5 is estimated for v_{2c} which is used in Eq. (A-3) for the evaluation of M_c . The network is assumed to obey the affine model because the chains are expected to be highly constrained due to the presence of the rigid filler particles. In Eq. (A-3), the concentration dependence of the χ parameter is important. For toluene at 25°C it is taken as [69]

$$\chi = 0.48 + 0.38 v_2 \quad (\text{A-4})$$

for toluene-PDMS, and as

$$\chi = 0.49 + 0.36 v_2 \quad (\text{A-5})$$

for benzene-PDMS [70].

CHAPTER 5. CONCLUSION

Synthesis and characterization of polymeric systems at the nanoscale were examined. The processing parameters and characterization techniques were identified and studied in detail. Based on the results, the following conclusions can be drawn:

i) Polyacrylonitrile based nanofibers were metallized with two transition metals, palladium and silver. Nanofibers were obtained by the electrospinning technique, an easy, fast, and economical process. The main advantage of electrospinning is to obtain ultrathin fibers, producing very high surface area to volume ratio films. Metallization of the nanofibers makes them conductive and reflective, the desired properties in the technology of sensors, solar energy converters, and light weight mirrors. Electrospun film as a template provides a large surface area for metals as well. The primary application of the transition metals in chemistry is as a catalyst in organic reactions. Palladium containing nanofibers were investigated in terms of their catalytic activity in the hydrogenation of unsaturated alcohols. Electrospun film with palladium exhibited 4.5 times higher catalytic activity than the alumina-supported (standard), along with 100% selectivity. From the industrial aspect, both electrospinning and metal deposition are low temperature solution processing techniques. The nanosized polymer-metal composite was obtained without heat energy consumption and without using any sophisticated equipment. The presented techniques are economical and efficient. For further studies, metallized polyacrylonitrile nanofibers can be post-processed into metallized carbon nanofibers, which are expected to exhibit unusual electronic and mechanical properties.

ii) Entropy is the determinant factor in polymer elasticity. PDMS, one of the most popular rubber-type material, shows extensive elasticity. Since the mechanical properties of the PDMS network is poor, fumed silica particles were introduced into these networks as a reinforcing agent. The elastic modulus of the network which was filled with 5 wt% silica was ten times that of the unfilled network. The ratio of the energetic contribution to the total elastic force as a function of silica content was determined by performing thermoelasticity experiments, which additionally provide the temperature coefficient of the chains. Results of experiments show that the energetic component of the force and temperature coefficient of the chains increase with silica content. The

increase of f_e/f ratio and temperature coefficient is a consequence of elastomer layers close to the filler surface. Large surface area fillers provide a high number of particles and, accordingly, a large surface area of layers. Varying the thermoelastic behaviour of the networks upon introducing 1 wt% filler implies that nanosized additives are cost effective and material efficient ways to enhance the properties of materials.

iii) Morphology and dimensions of amorphous polystyrene particles at dry state were studied by AFM with molecular resolution. Amorphous polystyrene molecules in CH were separated from each other when the concentration was on the order of 10^{-6} g/ml at room temperature. The average dimensions of a single chain on mica is as follows: 1 nm in height, 40 nm in diameter and 3500 nm^3 in volume. In theory, long polystyrene chains in CH collapse when the temperature is lowered from 50°C to 25°C . The solutions were kept at desired temperature and deposited on mica after the solution came into equilibrium. The measurements were performed after the solvent evaporation. A gradual dimensional change in polystyrene particles was observed in our experiments. It is to be noted that the size of the chain used in this study was not sufficiently large for the single chain to exhibit a discrete transition from the coil to globular shape at 35°C . Such a discrete transition would be obtained for ten times longer chains.

REFERENCES

- [1] Kenneth J. Klabunde, *Nanoscale Materials in Chemistry*, 2001, USA, Wiley.
- [2] Richard Feynman, *Six easy Pieces*, Penguin Science, 1995
- [3] Allivisatos, A.P. "Semiconductor Clusters, Nanocrystals, and Quantum Dots" *Science* 271 (1996), 933-937.
- [4] Feynman, R.P. (1960) *A lecture in engineering science*. In California Institute of Technology February edn.
- [5] Edelstein, A.S., Cammarata R.C. "Nanomaterials: Synthesis, Properties, and Applications" The Institute of Physics (London).
- [6] Kroto, H.W., Heath J.R., O'Brien S.C., Curl R.F and Smalley R.E "C₆₀: Buckminsterfullerene", *Nature* (1985), 318, 162-163.
- [7] Iijima, S., "Helical microtubules of graphitic carbon" *Nature* (1991), 354, 56-59.
- [8] Balkwill, D. L., Maratea D., and Blakemore R. P. "Ultrastructure of a magnetotactic spirillum", *J. Bacteriol.* 141, (1980) 1399-1403.
- [9] Frankel, R.B., Blakemore, R.P., and Wolfe, R.S., "Magnetite in Freshwater Magnetic Bacteria" *Science* 203, (1979) 1355-1359.
- [10] Meldrum, F.C., Heywood, B.R., Mann, S., Frankel, R.B., and Bazylinski, D.A., *Proc. Roy. Soc. Lond. B* (1993) 251, "Magnetotactic Bacteria at Cal Poly" 237.
- [11] Christoffer, J., Dissertation: " Novel routes to metal nanoparticle" Helsinki University of Technology (2003), Department of Chemistry.
- [12] Demir, M.M., Yilgor, E., Yilgor, I., Erman, B. "Electrospinning of polyurethane fibers", *Polymer* (2002), 43, 3303-3309.
- [13] Arrighi, V., Higgins, J.S., Burgess, A.N. and Floudas, G. "Local dynamics of poly(dimethyl siloxane) in the presence of reinforcing filler particles" *Polymer* (1998), (25) 39, 6369-6376.
- [14] Litvinov, W.M., Barthel, H., Weis, J. "Structure of a PDMS Layer Grafted onto a Silica Surface Studied by Means of DSC and Solid-State NMR" *Macromolecules* (2002), 35, 4356-4361.
- [15] Gussoni, M., Greco, F., Mapelli, M., Vezzoli, A., Ranucci, E., Ferruti, P., Zetta L. "Elastomeric Polymers. 2. NMR and NMR Imaging Characterization of Cross-Linked PDMS" *Macromolecules* (2002), 35, 1722-1729.
- [16] Berriot, J., Lequeux, F., Monnerie, L., Montes, H., Long, D., Sotta, P. "Filler-elastomer interaction in model filled rubbers, a ¹H NMR study" *Journal of Non-Crystalline Solids* (2002);

307-310, 719-724.

[17] Erman, B., Flory, P.J. "Critical Phenomena and Transition in Swollen Polymer Networks and in Linear Macromolecules" *Macromolecules* (1986), 19, 2342-2353

[18] Kiriya, A., Gorodskaya, G., Minko, S., Stamm, M., Tsitilianis, C. "Single Molecules and Associates of Heteroarm Star Copolymer Visualized by Atomic Force Microscopy" *Macromolecules* (2003); 36, 8704-8711.

[19] Chu, B., Ying, Q., Grosberg, A.Y. "Two-Stage Kinetics of Single-Chain Collapse. Polystyrene in Cyclohexane" *Macromolecules* (1995), 28, 180-189.

[20] Yoshimura, M., Han, K.S., Suchanek, W. "Soft Solution Processing: Low energy Direct Fabrication of Advanced Inorganic Materials" *Bulletin Korean Chemical Society* (1999), 20(8), 875-878.

[21] Yonezawa, T., Imamura, K., Kimizuka, N. "Direct Preparation and Size Control of Palladium Nanoparticle Hydrosols by Water-Soluble Isocyanide Ligands" *Langmuir* (2001), 17, 4701-4703.

[22] Bönnemann, H., Brijoux, W., Brinkmann R. *Journal of Molecular Catalysis* "Preparation, Characterization, and Application of Fine Metal Particles and Metal Colloids Using Hydrotiorganoborates" (1994), 86, 129-134.

[23] Horswell, S., Schiffrin, D.J. *Journal of the American Chemical Society* "Alkyl Isocyanide-Derivatized Platinum Nanoparticles" (1999), 121, 5573-5578.

[24] Itoh, H., Naka, K., Chujo, Y. *Polymer Bulletin* "Synthesis of palladium clusters with surface initiator for polymerization of 2-methyl-2-oxazoline" (2001), 46, 357-362.

[25] Hirai, H., Yakaru, N. I., Seta, Y., Hodosima, S. "Characterization of palladium nanoparticles protected with polymer as a hydrogenation catalyst" *Reactive Functional Polymers* (1998), 37, 121-131.

[26] Doshi, J., Reneker, D. H. "Electrospinning Process and Applications of Electrospun Fibers" *Journal of Electrostatics* (1995), 35, 151-159.

[27] Li, Y.D., Li, L.Q., Liano, H. W., Wang, H. R. "Preparation of pure nickel, cobalt, nickel-cobalt and nickel-copper alloys by hydrothermal reduction" *Journal of Materials Chemistry* (1999), 9, 2675-2679.

[28] Gui, Z., Fan, R., Mo, W., Chen, X., Yan, L., Hu, Yuan. "Synthesis and characterization of reduced transition metal oxides and nanophase metals with hydrazine in aqueous solution"

Materials Research Bulletin (2003), 38, 169-176; Wonterghem, J.van; Morup, S., Koch, C. J., Wells, S. *Nature* (1986), 322, 622-625.

[29] Bronstein, L.M., Sidorov, S. N., Gourkova, A.Y., Valetsky, P.M., Hartmann, J., Bruelmann, M., Cölfen, H., Antonietti, M. "Interaction of metal compounds with 'double-hydrophilic' block

- copolymers in aqueous medium and metal colloid formation " *Inorganica Chimia Acta* (1998), 280, 348-354.
- [30] Sidorov, S.N., Bronstein, L.M., Valetsky, P.M., Hartmann, J., Cölfen, H., Schnablegger, H., Antonietti, M. "Stabilization of metal nanoparticles in aqueous medium by polyethyleneoxide-polyethyleneimine block copolymers" *Journal of Colloidal and Interface Science* (1999) 212, 197-211.
- [31] Hedden, R.C., Bauer, B.J., Smith, A.P., Gröhn, F., Amis, E. "Templating of inorganic nanoparticles by PAMAM/PEG dendrimer-star polymers" *Polymer* (2002), 43, 5473-5481.
- [32] Willis, M., Brace, G., "Palladium catalysed enamine synthesis from vinyl triflates" *Tetrahedron Letters* (2002), 43, 9085-9088.
- [33] Basu, B., Jha, S., Midra, N.K., Bhuiyan, M. H. "Palladium-catalysed amination of halopyridines on a KF-alumina surface" *Tetrahedron Letters* (2002), 43, 7967-7969.
- [34] Ledaux, M., Vieira R., Pham-Huu, C., Keller, N. "New catalytic phenomena on nanostructured (fibers and tubes) catalysts" *Journal of Catalysis* (2003), article in press.
- [35] Jia, H., Zhu, G., Vugrinovich, B., Kataphinan, W., Reneker, D. H., Wang, P., "Enzyme-carrying polymeric nanofibers prepared via electrospinning for use as unique biocatalysts" *Biotechnol. Prog.* (2002), 18, 1027-1032.
- [36] Sulman, E., Bodrova Y., Matveeva V. et.al. "Hydrogenation of dehydrolinalool with novel catalyst derived from Pd colloids stabilized in micelle cores of polystyrene-poly-4-vinylpyridine block copolymers" -*Applied catalysis A-General* (1999), 176, 75-81.
- [37] Bronstein, L., Chernyshov, D., Volkov, I., Ezernitskaya, M., Valetsky, P., Matveeva, V., Sulman, E. *Journal of Catalysis* "Structure and Properties of Bimetallic Colloids Formed in Polystyrene-*block*-Poly-4-vinylpyridine Micelles: Catalytic Behavior in Selective Hydrogenation of Dehydrolinalool" (2000), 196, 302-314.
- [38] Cotton, F.A., Wilkonson, G., Gaus, P.L. *Basic Inorganic Chemistry*, 3rd ed.; John Wiley&Sons: New york, 1995; p 404.
- [39] Cullity B.D, *Elements of X-ray diffraction*, 2nd ed.; Addison-Wesley; Massachusetts, 1978; p. 284.
- [40] Spatz, J.P.; Roescher, A.; Möller, M. "Gold nanoparticles in micellar poly(styrene)-*b*-poly(ethylene oxide) films-size and interparticle distance control in monoparticulate films" *Advanced Materials* (1996), 8, 337-341.
- [41] Forster, J.F.; Keane, L. "Nanoparticle-metallopolymer assemblies: charge percolation and redox particles" *Journal of Electroanalytical Chemistry* (2003) 554-555, 345-354.
- [42] Koura, N. and Kubota, A., "Electroless Plating of Silver" *Kinzoku Hyoumen Gijutsu* (1985), 36(5), 182-190.

- [43] Butenko, A.N., Savenkov, A.S., "Modified silver catalyst for oxidative conversion of methanol to formaldehyde" *Russ J Appl Chem* (2000), 73 (11), 1942-1945.
- [44] Monnier, J.R., Medlin, J.W., Barteau, M.A. "Use of Oxygen-18 to Determine Kinetics of Butadiene Epoxidation over Cs-Promoted, Ag Catalysts" *Journal of Catalysis* (2001), 203 (2), 362-368.
- [45] Smith, B., *Infrared spectral interpretation: a systematic approach* Boca Raton, Florida; London: CRC Press, c1999.
- [46] Osman, M.A., Atallah, A., Müller, M., Suter U.W. "Reinforcement of poly(dimethylsiloxane) networks by mica flakes" *Polymer* (2001); 42, 6545-6556.
- [47] Yuan, W.Q., Mark, J.E. "Reinforcement of poly(dimethylsiloxane) networks by blended and *in-situ* generated silica fillers having various sizes, size distributions, and modified surfaces" *Macromol. Chem. Phys.* (1999); 200, 206-220.
- [48] Breiner, J.M., Mark, J.E. "Preparation, structure, growth mechanisms and properties of siloxane composites containing silica, titania or mixed silica-titania phases" *Polymer* (1998); 39(22), 5483- 5493
- [49] Mark, J.E., Erman, B. *Rubberlike Elasticity A Molecular Primer*, New York: Wiley Interscience, 1988; p. 61.
- [50] Erman, B., Mark, J.E. *Structures and properties of rubberlike networks*, Oxford: Oxford University Press, (1997).
- [51] Cosgrove, T., Roberts, C., Garasanin, T., Schmidt, G.R., Gordon, V.G. "NMR Spin-Spin Relaxation Studies of Silicate-Filled Low Molecular Weight Poly(dimethylsiloxane)s" *Langmuir* (2002), 18, 10080-10085.
- [52] Galanti, A.V., Sperling, L.H. "Relationship Between Thermoelasticity and Reinforcement in Elastomers: Silica Filled Silicone Elastomers" *Poly. Eng. Sci.* (1970),10(3), 177.
- [53] Shackelford, J.F. *Introduction to Materials Science For Engineers*, 5th ed. New Jersey: Prentice] Hall Inc, 2000; p. 802 and 808.
- [54] Brandrup, J., Immergut, E.H., Grulke, E.A. *Polymer Handbook Fourth Edition*, V-168.
- [55] Ciferri, A., Hove, C.A., Flory, P.J. "Stress-Temperature Coefficients of Polymer Networks and the Conformational Energy of Polymer Chains" *J. Am. Chem. Soc.* (1961); 83: 1015.
- [56] Flory P.J., Hove C.A., Ciferri A.. *J. Poly. Sci.* (1959);34:337.
- [57] Flory P.J., Ciferri A., Hove C.A. *J. Poly. Sci.* (1960);45:235.
- [58] Flory, P.J. *Statistical Mechanics of Chain Molecules*; New York: Interscience,1969: p. 39.
- [59] Mark JE. *Macromol. Rev.* 1976;11:135.

- [60] Yu, J., Wang, Z., Chu, B. "Kinetic study of coil-to-globule transition" *Macromolecules* (1992), 25, 1618-1620.
- [61] Chu, B., Ying, Q., Grosberg, A. Yu. "Two-Stage Kinetics of Single-Chain Collapse. Polystyrene in Cyclohexane" *Macromolecules*, (1995), 28, 180-189.
- [62] Chu, B., Ying, Q. "Single-Chain Expansion from the Collapsed Globule of Polystyrene in Cyclohexane to the θ -Coil" *Macromolecules* (1996), 29, 1824-1826.
- [63] Qian, R., Shen, J., Bei, N., Zhu, C., Wang, X. "Morphological observations of single-chain glassy polystyrene by means of tapping mode atomic force microscopy" *Macromolecular Chemistry and Physics* (1996), 187, 2165-2174.
- [64] Festag, R., Alexandratos S.D., Cook D.K., Joy D.C., Annis B., Wunderlich B. "Single- and Few-Chain Polystyrene Particles by Electrospray" *Macromolecules* (1997), 30, 6238-6242.
- [65] Stange, T.G., Mathew, R., Evans, D.F.; Hendricson, W.A. "Scanning tunneling microscopy and atomic force microscopy characterization of polystyrene spin-coated onto silicon surfaces" *Langmuir* (1992), 8, 920-926.
- [66] Zhang, L.S.; Manke, C.W.; Ng, K.Y.S. "Scanning Tunneling Microscopy of Discontinuous Polystyrene Films Adsorbed on Graphite" *Macromolecules* (1995), 28, 7386-7393.
- [67] Morris, V.J., Kirby, A.R., Gunning, A.P. *Atomic Force Microscopy for Biologist*, 1st ed.; Imperial College Press, 1999, p 79.
- [68] Deegan, R.D., Olgica, B., DuPont, T.F.; Huber, G.; Nagel, S.R.; Witten, T.A. "Capillary flow as the cause of ring stains from dried liquid drops" *Nature* (1997), 389, 827-829.
- [69] Schneider, A., Schuld, N., Bercea, M., Wolf, B.A. "On what terms and why the thermodynamic properties of polymer solutions depend on chain length up to the melt" *J. Polym. Sci. Part B: Polym. Phys.* in press.
- [70] Flory, P.J., Shih, H. "Thermodynamics of Solutions of Poly(dimethylsiloxane) in Benzene, Cyclohexane, and Chlorobenzene" *Macromolecules* (1972), 5, 761.

REFERENCES

- [1] Kenneth J. Klabunde, *Nanoscale Materials in Chemistry*, 2001, USA, Wiley.
- [2] Richard Feynman, *Six easy Pieces*, Penguin Science, 1995
- [3] Allivisatos, A.P. "Semiconductor Clusters, Nanocrystals, and Quantum Dots" *Science* 271 (1996), 933-937.
- [4] Feynman, R.P. (1960) *A lecture in engineering science*. In California Institute of Technology February edn.
- [5] Edelstein, A.S., Cammarata R.C. "Nanomaterials: Synthesis, Properties, and Applications" The Institute of Physics (London).
- [6] Kroto, H.W., Heath J.R., O'Brien S.C., Curl R.F and Smalley R.E "C60: Buckminsterfullerene", *Nature* (1985), 318, 162-163.
- [7] Iijima, S., "Helical microtubules of graphitic carbon" *Nature* (1991), 354, 56-59.
- [8] Balkwill, D. L., Maratea D., and Blakemore R. P. "Ultrastructure of a magnetotactic spirillum" , *J. Bacteriol.* 141, (1980) 1399-1403.
- [9] Frankel, R.B., Blakemore, R.P., and Wolfe, R.S., "Magnetite in Freshwater Magnetic Bacteria" *Science* 203, (1979) 1355-1359.
- [10] Meldrum, F.C., Heywood, B.R., Mann, S., Frankel, R.B., and Bazylinski, D.A., *Proc. Roy. Soc. Lond. B* (1993) 251, "Magnetotactic Bacteria at Cal Poly" 237.
- [11] Christoffer, J., Dissertation: " Novel routes to metal nanoparticle" Helsinki University of Technology (2003), Department of Chemistry.
- [12] Demir, M.M., Yilgor, E., Yilgor, I., Erman, B. "Electrospinning of polyurethane fibers", *Polymer* (2002), 43, 3303-3309.
- [13] Arrighi, V., Higgins, J.S., Burgess, A.N. and Floudas, G. "Local dynamics of poly(dimethyl siloxane) in the presence of reinforcing filler particles" *Polymer* (1998), (25) 39, 6369-6376.
- [14] Litvinov, W.M., Barthel, H., Weis, J. "Structure of a PDMS Layer Grafted onto a Silica Surface Studied by Means of DSC and Solid-State NMR" *Macromolecules* (2002), 35, 4356-4361.
- [15] Gussoni, M., Greco, F., Mapelli, M., Vezzoli, A., Ranucci, E., Ferruti, P., Zetta L. "Elastomeric Polymers. 2. NMR and NMR Imaging Characterization of Cross-Linked PDMS" *Macromolecules* (2002), 35, 1722-1729.
- [16] Berriot, J., Lequeux, F., Monnerie, L., Montes, H., Long, D., Sotta, P. "Filler-elastomer

interaction in model filled rubbers, a ^1H NMR study” *Journal of Non-Crystalline Solids* (2002); 307–310, 719-724.

[17] Erman, B., Flory, P.J. “Critical Phenomena and Transition in Swollen Polymer Networks and in Linear Macromolecules” *Macromolecules* (1986), 19, 2342-2353

[18] Kiriya, A., Gorodskaya, G., Minko, S., Stamm, M., Tsitilianis, C. “Single Molecules and Associates of Heteroarm Star Copolymer Visualized by Atomic Force Microscopy” *Macromolecules* (2003); 36, 8704-8711.

[19] Chu, B., Ying, Q., Grosberg, A.Y. “Two-Stage Kinetics of Single-Chain Collapse. Polystyrene in Cyclohexane” *Macromolecules* (1995), 28, 180-189.

[20] Yoshimura, M., Han, K.S., Suchanek, W. “Soft Solution Processing: Low energy Direct Fabrication of Advanced Inorganic Materials” *Bulletin Korean Chemical Society* (1999), 20(8), 875-878.

[21] Yonezawa, T., Imamura, K., Kimizuka, N. ”Direct Preparation and Size Control of Palladium Nanoparticle Hydrosols by Water-Soluble Isocyanide Ligands” *Langmuir* (2001), 17, 4701-4703.

[22] Bönnemann, H., Brijoux, W., Brinkmann R. *Journal of Molecular Catalysis* “Preparation, Characterization, and Application of Fine Metal Particles and Metal Colloids Using Hydrotiorganoborates” (1994), 86, 129-134.

[23] Horswell, S., Schiffrin, D.J. *Jornal of the American Chemical Society* “Alkyl Isocyanide-Derivatized Platinum Nanoparticles” (1999), 121, 5573-5578.

[24] Itoh, H., Naka, K., Chujo, Y. *Polymer Bulletin* “Synthesis of palladium clusters with surface initiator for polymerization of 2-methyl-2-oxazoline” (2001), 46, 357-362.

[25] Hirai, H., Yakaru, N. I., Seta, Y., Hodosima, S. “Characterization of palladium nanoparticles protected with polymer as a hydrogenation catalyst” *Reactive Functional Polymers* (1998), 37, 121-131.

[26] Doshi, J., Reneker, D. H. “Electrospinning Process and Applications of Electrospun Fibers” *Journal of Electrostatics* (1995), 35, 151-159.

[27] Li, Y.D., Li, L.Q., Liano, H. W., Wang, H. R. “Preparation of pure nickel, cobalt, nickel-cobalt and nickel-copper alloys by hydrothermal reduction” *Journal of Materials Chemistry* (1999), 9, 2675-2679.

[28] Gui, Z., Fan, R., Mo, W., Chen, X., Yan, L., Hu, Yuan. “Synthesis and characterization of reduced transition metal oxides and nanophase metals with hydrazine in aqueous solution” *Materials Research Bulletin* (2003), 38, 169-176; Wouterghem, J.van; Morup, S., Koch, C. J., Wells, S.

Nature (1986), 322, 622-625.

[29] Bronstein, L.M., Sidorov, S. N., Gourkova, A.Y., Valetsky, P.M., Hartmann, J., Bruelmann,

- M., Cölfen, H., Antonietti, M. "Interaction of metal compounds with 'double-hydrophilic' block copolymers in aqueous medium and metal colloid formation" *Inorganica Chimica Acta* (1998), 280, 348-354.
- [30] Sidorov, S.N., Bronstein, L.M., Valetsky, P.M., Hartmann, J., Cölfen, H., Schnablegger, H., Antonietti, M. "Stabilization of metal nanoparticles in aqueous medium by polyethyleneoxide-polyethyleneimine block copolymers" *Journal of Colloidal and Interface Science* (1999) 212, 197-211.
- [31] Hedden, R.C., Bauer, B.J., Smith, A.P., Gröhn, F., Amis, E. "Templating of inorganic nanoparticles by PAMAM/PEG dendrimer-star polymers" *Polymer* (2002), 43, 5473-5481.
- [32] Willis, M., Brace, G., "Palladium catalysed enamine synthesis from vinyl triflates" *Tetrahedron Letters* (2002), 43, 9085-9088.
- [33] Basu, B., Jha, S., Midra, N.K., Bhuiyan, M. H. "Palladium-catalysed amination of halopyridines on a KF-alumina surface" *Tetrahedron Letters* (2002), 43, 7967-7969.
- [34] Ledaux, M., Vieira R., Pham-Huu, C., Keller, N. "New catalytic phenomena on nanostructured (fibers and tubes) catalysts" *Journal of Catalysis* (2003), article in press.
- [35] Jia, H., Zhu, G., Vugrinovich, B., Kataphinan, W., Reneker, D. H., Wang, P., "Enzyme-carrying polymeric nanofibers prepared via electrospinning for use as unique biocatalysts" *Biotechnol. Prog.* (2002), 18, 1027-1032.
- [36] Sulman, E., Bodrova Y., Matveeva V. et.al. "Hydrogenation of dehydrolinalool with novel catalyst derived from Pd colloids stabilized in micelle cores of polystyrene-poly-4-vinylpyridine block copolymers" -*Applied catalysis A-General* (1999), 176, 75-81.
- [37] Bronstein, L., Chernyshov, D., Volkov, I., Ezernitskaya, M., Valetsky, P., Matveeva, V., Sulman, E. *Journal of Catalysis* "Structure and Properties of Bimetallic Colloids Formed in Polystyrene-*block*-Poly-4-vinylpyridine Micelles: Catalytic Behavior in Selective Hydrogenation of Dehydrolinalool" (2000), 196, 302-314.
- [38] Cotton, F.A., Wilkinson, G., Gaus, P.L. *Basic Inorganic Chemistry*, 3rd ed.; John Wiley&Sons: New York, 1995; p 404.
- [39] Cullity B.D, *Elements of X-ray diffraction*, 2nd ed.; Addison-Wesley: Massachusetts, 1978; p. 284.
- [40] Spatz, J.P.; Roescher, A.; Möller, M. "Gold nanoparticles in micellar poly(styrene)-*b*-poly(ethylene oxide) films-size and interparticle distance control in monodisperse films" *Advanced Materials* (1996), 8, 337-341.
- [41] Forster, J.F.; Keane, L. "Nanoparticle-metallopolymer assemblies: charge percolation and redox particles" *Journal of Electroanalytical Chemistry* (2003) 554-555, 345-354.
- [42] Koura, N. and Kubota, A., "Electroless Plating of Silver" *Kinzoku Hyoumen Gijutsu* (1985), 36

(5), 182-190.

[43] Butenko, A.N., Savenkov, A.S., "Modified silver catalyst for oxidative conversion of methanol to formaldehyde" *Russ J Appl Chem* (2000), 73 (11), 1942-1945.

[44] Monnier, J.R., Medlin, J.W., Barteau, M.A. "Use of Oxygen-18 to Determine Kinetics of Butadiene Epoxidation over Cs-Promoted, Ag Catalysts" *Journal of Catalysis* (2001), 203 (2), 362-368.

[45] Smith, B., *Infrared spectral interpretation: a systematic approach* Boca Raton, Florida; London: CRC Press, c1999.

[46] Osman, M.A., Atallah, A., Müller, M., Suter U.W. "Reinforcement of poly(dimethylsiloxane) networks by mica flakes" *Polymer* (2001); 42, 6545-6556.

[47] Yuan, W.Q., Mark, J.E. "Reinforcement of poly(dimethylsiloxane) networks by blended and *in-situ* generated silica fillers having various sizes, size distributions, and modified surfaces" *Macromol. Chem. Phys.* (1999); 200, 206-220.

[48] Breiner, J.M., Mark, J.E. "Preparation, structure, growth mechanisms and properties of siloxane composites containing silica, titania or mixed silica-titania phases" *Polymer* (1998); 39 (22), 5483- 5493

[49] Mark, J.E., Erman, B. *Rubberlike Elasticity A Molecular Primer*, New York: Wiley Interscience, 1988; p. 61.

[50] Erman, B., Mark, J.E. *Structures and properties of rubberlike networks*, Oxford: Oxford University Press, (1997).

[51] Cosgrove, T., Roberts, C., Garasanin, T., Schmidt, G.R., Gordon, V.G. "NMR Spin-Spin Relaxation Studies of Silicate-Filled Low Molecular Weight Poly(dimethylsiloxane)s" *Langmuir* (2002), 18, 10080-10085.

[52] Galanti, A.V., Sperling, L.H. "Relationship Between Thermoelasticity and Reinforcement in Elastomers: Silica Filled Silicone Elastomers" *Poly. Eng. Sci.* (1970),10(3), 177.

[53] Shackelford, J.F. *Introduction to Materials Science For Engineers*, 5th ed. New Jersey: Prentice] Hall Inc, 2000; p. 802 and 808.

[54] Brandrup, J., Immergut, E.H., Grulke, E.A. *Polymer Handbook Fourth Edition*, V-168.

[55] Ciferri, A., Hoeve, C.A., Flory, P.J. "Stress-Temperature Coefficients of Polymer Networks and the Conformational Energy of Polymer Chains" *J. Am. Chem. Soc.* (1961); 83: 1015.

[56] Flory P.J., Hoeve C.A., Ciferri A.. *J. Poly. Sci.* (1959);34:337.

[57] Flory P.J., Ciferri A., Hoeve C.A. *J. Poly. Sci.* (1960);45:235.

[58] Flory, P.J. *Statistical Mechanics of Chain Molecules*; New York: Interscience,1969: p. 39.

[59] Mark JE. *Macromol. Rev.* 1976;11:135.

[60] Yu, J., Wang, Z., Chu, B. "Kinetic study of coil-to-globule transition" *Macromolecules* (1992),

25, 1618-1620.

[61] Chu, B., Ying, Q., Grosberg, A. Yu. "Two-Stage Kinetics of Single-Chain Collapse. Polystyrene in Cyclohexane" *Macromolecules*, (1995), 28, 180-189.

[62] Chu, B., Ying, Q. "Single-Chain Expansion from the Collapsed Globule of Polystyrene in Cyclohexane to the θ -Coil" *Macromolecules* (1996), 29, 1824-1826.

[63] Qian, R., Shen, J., Bei, N., Zhu, C., Wang, X. "Morphological observations of single-chain glassy polystyrene by means of tapping mode atomic force microscopy" *Macromolecular Chemistry and Physics* (1996), 187, 2165-2174.

[64] Festag, R., Alexandratos S.D., Cook D.K., Joy D.C., Annis B., Wunderlich B. "Single- and Few-Chain Polystyrene Particles by Electrospray" *Macromolecules* (1997), 30, 6238-6242.

[65] Stange, T.G., Mathew, R., Evans, D.F.; Hendricson, W.A. "Scanning tunneling microscopy and atomic force microscopy characterization of polystyrene spin-coated onto silicon surfaces" *Langmuir* (1992), 8, 920-926.

[66] Zhang, L.S.; Manke, C.W.; Ng, K.Y.S. "Scanning Tunneling Microscopy of Discontinuous Polystyrene Films Adsorbed on Graphite" *Macromolecules* (1995), 28, 7386-7393.

[67] Morris, V.J., Kirby, A.R., Gunning, A.P. *Atomic Force Microscopy for Biologist*, 1st ed.; Imperial College Press, 1999, p 79.

[68] Deegan, R.D., Olgica, B., DuPont, T.F.; Huber, G.; Nagel, S.R.; Witten, T.A. "Capillary flow as the cause of ring stains from dried liquid drops" *Nature* (1997), 389, 827-829.

[69] Schneider, A., Schuld, N., Bercea, M., Wolf, B.A. "On what terms and why the thermodynamic properties of polymer solutions depend on chain length up to the melt" *J. Polym. Sci. Part B: Polym. Phys.* in press.

[70] Flory, P.J., Shih, H. "Thermodynamics of Solutions of Poly(dimethylsiloxane) in Benzene, Cyclohexane, and Chlorobenzene" *Macromolecules* (1972), 5, 761.